Quantitative targeted proteomics by combining microfluidics with electron microscopy

Inauguraldissertation

zur

Erlangung der Würde eines Doktors der Philosophie

Vorgelegt der

Philosophisch-Naturwissenschaftlichen Fakultät

Der Universität Basel

von

DOMINIC GISS

Aus Basel, Schweiz

Basel, Schweiz 2014

Genehmigt von der Philosophisch-Naturwissenschaftlichen Fakultät

auf Antrag von:

Prof. Dr. Henning Stahlberg, Fakultätsverantwortlicher

Prof. Dr. Roderick Lim, Koreferent

Basel, den 16.09.2014

Prof. Dr. Jörg Schibler (Dekan)

Summary

Nearly all cellular functions are dictated by proteins, thus the proteome defines the functional capacity of a cell. Protein interactions form and dissociate in order to perform specific cellular functions. These dynamic interactions are subject to stochastic fluctuations causing cell-to-cell variability within a population. The investigation of dynamic and heterogeneous multimolecular protein complexes is a hallmark of experimental systems biology. However, this aim puts demanding requirements on analytical methods used since these should provide single molecule and single cell resolution. Due to the low copy number of proteins from individual cells, the lack of amplification techniques for proteins and the small sample volumes, single-cell proteomics still challenges existing biophysical and biochemical methods and requires novel and complementary approaches.

This thesis is part of a project that seeks for a novel approach to visual proteomics that aims for the qualitative and quantitative analysis of the entire proteome from a single eukaryotic cell by transmission electron microscopy (TEM), also termed as "single-cell visual proteomics". However, the identification of all the molecular components constituting the crude cell lysate is difficult and suggests to follow a targeted proteomics approach where isolation and separation techniques are applied in combination with TEM to make protein identification comprehensible.

During the course of this thesis, a novel approach to targeted proteomics was developed and evaluated [1,2], combining microfluidic techniques with magnetic beads and photocleavable composites. The proposed method enables rapid and specific isolation of different protein complexes from a few thousand cells under close to physiological condition. The isolation method yields samples of high purity, in particular for a one-step purification method. Subsequent single particle analyses of negative stain TEM images provide averaged projection structures of the isolated target proteins. During the isolation process, the target protein complexes are immobilized and immuno-labelling techniques using electron-dense markers can be applied. This procedure allows protein-binding partners constituting a complex to be detected. Hence, the approach can provide initial information on structure and composition of weakly interacting protein complexes formed *in vivo* without applying time consuming traditional large-scale methods for protein expression and purification followed by complex hybrid techniques for analysis.

In addition, initial experiments showed that quantitative information on protein abundances can be extracted upon combining the isolation method with semi-automatic image acquisition and analysis procedures used for TEM investigations. Thereby the suitability of single particle TEM for protein quantification is reported for the first time. Consequently, the fundamentals of "quantitative TEM" were elucidated and a method for reliable and efficient concentration measurements proposed [3]. The results imply that picomolar to nanomolar ranged concentrations, typically hard to assess with traditional absorbance-based methods, can be reliably measured. Interestingly, this technique uses standard equipment readily available in many laboratories.

Our findings have proven that classical TEM grid preparation by hand can be very reproducible and of quantitative manner. This is in contradiction to the general assumption of the community that sample preparation by hand is not reproducible and therefore quantitative information may be distorted. However, the results also confirmed that classical grid preparation is disadvantaged by inefficient protein adsorption to the sample carriers, which is moreover specific to the particular protein species applied. Therefore, a prerequisite for single-cell visual proteomics is the lossless and unbiased deposition of low volume samples to TEM grids. To this end, a versatile novel approach to sample conditioning and deposition was developed and validated [4]. This microfluidic method was capable of staining minute sample volumes prior to their deposition to TEM grids and the samples produced were suitable for structural analysis by negative stain TEM. Various negative stains were tested and applied to several test samples, all of which provided very reproducible staining of excellent quality, clearly resolving membranes, filaments and soluble proteins. Furthermore, initial experiments demonstrated the feasibility of the methodology for preparing samples dedicated for mass measurements using scanning TEM.

Future developments aim to improve some of the central aspects of the developed methodologies and to implement a cryo-sample preparation routine to complement negative stain data. Ultimately, the individual processing concepts presented will be combined with a recently published method for single-cell lysis. While a global quantitative and qualitative visual analysis of the complete proteome by TEM still requires extended effort and development, the methodologies developed during the course of this thesis ensure that quantitative targeted proteomics at the single cell level is soon in the realms of possibility. Upon completion, the envisaged methodology will provide a completely new way to study the heterogeneity of large protein complexes from individual cells and thus helps to elucidate the emergence of biological functions from underlying interaction networks.

List of manuscripts included in this thesis

[1] D. Giss, S. Kemmerling, V. Dandey, H. Stahlberg & T. Braun (2014). Exploring the interactome: microfluidic isolation of proteins and interacting partners for quantitative electron microscopy. *Anal Chem*, 86(10), 4680-7.

[2] D. Giss, S. Kemmerling, V. Dandey, H. Stahlberg & T. Braun (2013). Microfluidics to isolate untagged proteins from cell extracts for visual analysis by electron microscopy. *Proceedings of the 17th International Conference on Miniaturized Systems for Chemistry and Life Sciences (MicroTAS)*, Freiburg, Germany, pp. 1785-1787, ISBN 978-0-9798064-6-9.

[3] D. Giss, H. Stahlberg & T. Braun (2014). Protein quantification by single particle transmission electron microscopy. *To be submitted to the Journal of Structural Biology.*

[4] S. Kemmerling, J. Ziegler, G. Schweighauser, S. A. Arnold, D. Giss, S. A. Mueller, P. Ringler, K. N. Goldie, N. Goedecke, A. Hierlemann, H. Stahlberg, A. Engel & T. Braun *et al.* (2012) Connecting µ-fluidics to electron microscopy. *J Struct Biol*, 177, 128-134.

Table of contents

1 Introduction

1.1 Systems biology and the challenge of biological noise

A full understanding of the emergent properties of all cellular life requires the combination of multiple systems-perspectives and cannot be deduced from simple reductionist approaches. In this context, the research field of systems biology is an integrative holistic approach that aims to obtain a complete picture of all intracellular processes with spatiotemporal resolution to understand the emergence of biological functions.[1] To this end, all the molecular elements within a cell must be identified, quantified and their interactions characterized. This requires experimental approaches that obtain data beyond the statistical average of a cell population, i.e. at the single cell level, and computational approaches to map the data to cellular functions and behaviour.

The need for single-cell analysis arises from the stochastic nature of all biomolecular processes. Biomolecules presented in low copy numbers, such as in single cells, are more affected by stochastic fluctuations, which causes pronounced variations in the molecular concentrations and activities. Consequently, this intrinsic noise leads to phenotypic diversity within a population of isogenic cells being exposed to identical environmental conditions. The occurrence of such subpopulations is important for maintaining evolution by allowing organisms to adapt better to rapid perturbations.[2] However, even if some noise, e.g. noisy gene expression, is utilized and appreciated to some extend, biological systems have to preserve functional robustness[3] and therefore various mechanisms that control intrinsic noise have evolved.[4,5]

Understanding cell-to-cell variability is a key element of systems biology and places demanding requirements on the analytical methods used in order to study cellular functions at different system-perspective levels, i.e. omic levels, with single-cell resolution. Investigating single cells is inherently connected to the need for methods to handle, control and prepare individual cells and requires analytical techniques that are suitable for data acquisition from such samples on the genome, transcriptome, proteome, metabolome and fluxome. A comprehensive overview on the individual approaches used for single-cell analysis can be found in a variety of reviews.[6-11]

1.2 The heterogeneity of multimolecular protein complexes

This thesis is dedicated to the development of methods serving single-cell proteomics; in this section, the challenges accompanying proteomic studies are elucidated in more detail.

Nearly all cellular functions are ruled by proteins, thus the proteome defines the functional capacity of a cell at a given time point. The investigation of the emergence of cellular functions directly at the proteomic level represents a central element of systems biology. A typical human cell contains $1\text{-}3\text{x}10^4$ different protein species and about $1\text{x}10^9$ proteins in total,[6,11] all of which geared to form dynamic protein-protein and protein-substrate interactions and being subject to posttranslational modifications, such as phosphorylation. The

combination of sheer complexity, broad range of protein abundances, lack of amplification techniques for proteins and small sample volumes, makes proteomic studies extremely challenging, particularly at the single cell level.

Traditional quantitative and qualitative proteomic studies are dominated by MS-based analysis strategies. MS rapidly took proteomics to the next level as it offers large-scale protein identification, characterization and quantification of biological samples.[12-14] In general, such studies analyse the sample from an ensemble of cells and thus suffer from biological noise, masking the particular response and properties of single cells. Yet, recent advances in detection sensitivity and the utilization of miniaturized systems for sample preparation, e.g. by capillary electrophoresis, ensure that MS is accessing the realms of single-cell proteomics.[15-17]

However, the characterization of multimolecular protein complexes from single cells still challenges existing biophysical and biochemical techniques. Proteins form, dissociate and re-form to conduct specific cellular functions. To efficiently resolve the vast and dynamic heterogeneity of the protein complexes formed, they must be tackled at the single molecule level and a comprehensive understanding of their role in a cell requires knowledge on their composition, structure and temporal persistence, in the context of the cell.

MS-based strategies are in general not well suited to characterize multimolecular protein complexes since information at the single molecule level is missing. Hence, complex hybrid approaches were suggested to characterize heterogeneous protein complexes formed around a central bait protein when analysed by MS.[18] These procedures rely on the combination of affinity purification, chemical crosslinking and gel electrophoresis with MS to resolve the composition and relative occurrence of the particular subcomplexes. However, such measurements are performed from bulk samples, structural information is only limited and the preservation of the fidelity of a complex can be very difficult.

Alternatively, electron microscopy techniques can be employed to characterize protein complexes at the single molecule level by an approach termed “visual proteomics”. E.g., cryo-electron tomography can provide structural information at molecular resolution of individual protein complexes in the context of nearly unperturbed single cells.[19-21] However, protein recognition is restricted to relatively large complexes[22,23] and the identification of the individual constituents in intact cells proved to be difficult in the absence of electron-dense labels.[24]

Single-cell proteomics is a challenging task, which is even impeded when dynamic, large and fragile multimolecular protein complexes are targeted. A holistic understanding on the tremendous complexity and dynamics of the proteome can only be accomplished by combining and correlating data from different techniques and exploring novel and complementary strategies for sample preparation and analysis.

1.3 Objective of this thesis and general framework

The aim of this thesis was to develop new methodologies for quantitative targeted visual proteomics of single eukaryotic cells by negative stain transmission electron microscopy (TEM).

The work presented is part of a research project that seeks for a novel integrative approach to visual proteomics of single eukaryotic cells. The basic idea was proposed in 2009 and suggested to physically lyse individual eukaryotic cells and process the entire proteome in a lossless fashion for subsequent characterization by TEM and scanning TEM (STEM).[25] The gathered information on mass and shape of the individual protein assemblies can then be linked to the proteomics data provided by alternative approaches such as electron tomography (ET), negative stain TEM, MS and various sectioning techniques used in electron microscopy.

Based on the idea outlined above a versatile novel methodology to single-cell proteomics is currently under development. This approach comprises various microfluidic modules that combine live-cell imaging and culturing of anchorage-dependent eukaryotic cells, the uptake and processing of the entire proteome from individual cells and the subsequent qualitative and quantitative analysis of the interactome employing various techniques such as STEM, quantitative TEM (qTEM), MS and reverse phase protein arrays (RPPA). A schematic representation of the proposed modular approach and a brief description of the individual modules are given in Figure 1-1. During the course of this thesis, modules d-f were developed (chapter 2, 3 and 5)[26,27] and the fundamentals for qTEM acquired (chapter 4).

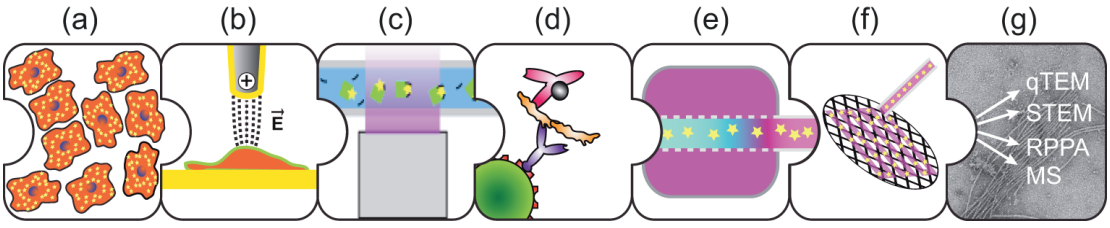

Figure 1-1: *Scheme of the modular microfluidic methodology for single-cell proteomics.* ***(a):*** *Module for cell culturing and live-cell imaging. Adherent eukaryotic cells are growing on an electrically conductive and transparent support mounted on a light microscope.* ***(b):*** *Module for single-cell lysis. A microcapillary electrode is positioned over a targeted cell to rupture the cell membrane using electric fields (electroporation), followed by the rapid aspiration of all cellular components.* ***(c):*** *Optional module for cross-linking. A light-induced generic cross-linking reaction stabilizes ultrastructures and weak interactions in protein complexes.*[28,29] ***(d):*** *Optional module for protein isolation and labelling. An affinity molecule-based approach is used to specifically isolate or label target structures from the cell lysate to reduce the complexity of the sample and thus facilitate subsequent data analysis. Alternatively a generic approach based on chromatography or electrophoresis is used to induce an order in the sample (not shown).* ***(e):*** *Optional module for sample conditioning. Microdialysis is used to specifically condition the sample for the subsequent analysis method, e.g. to negatively stain or desalt the protein solution.* ***(f):*** *Module for sample deposition. A microcapillary and rapid motorized stages are used to deposit nanoliter-sized analyte volumes to sample carriers, e.g. to TEM grids or nitrocellulose substrates.* ***(g):*** *Data acquisition by qTEM, STEM, RPPA or MS.*

Microflulidic and microcapillary based techniques are proposed to assess the picoliter ranged cell lysates. Current approaches used for single-cell processing are usually not suitable for adherent growing cell cultures or tissues as these techniques are typically operated in flow-through configurations. [30] Recently my co-workers reported on a new method to single-cell proteome studies (modules a-b) relying on electroporation and capillary techniques permitting experiments dependent on standard anchorage dependent cell cultures.[31]

Many analysis techniques, e.g., negative stain TEM, demand the protein sample to be conditioned and deposited on sample carriers prior to the analysis. Traditional protocols for TEM preparation involve blotting or washing steps and require microliters of sample volumes, thus being not well suited for single-cell lysate samples of inherent low volume and concentration, as the transfer of the analytes to the sample carriers would be very inefficient. Hence, a novel methodology was developed enabling minute volumes of protein solutions to be conditioned in microfluidic devices prior to their nearly lossless and unbiased deposition on sample carriers (modules e-f). This technique utilizes microdialysis fibers to, e.g. mix the sample with negative stain. Subsequently nanoliters of the conditioned sample are micro-patterned and dried down on the sample carriers such as TEM grids or MS targets,[32] thereby avoiding blotting or washing steps and preferential protein adsorption to the supports.

The investigation of whole cell lysates using negative stain TEM permits the detection of *de novo* protein components. Such discovery-driven experiments aim to image the entire cell lysate and subsequently qualitatively and quantitatively analyse the recorded protein structures based on image segmentation, classification of the segmented objects and correlation of the data to other methods such as STEM. However, the identification of the individual protein species in such samples is extremely challenging. Hence, hypothesis-driven experiments, where *a priori* information about a particular protein is known, will follow a simpler strategy. For example, targeted visual proteomics can be done, whereby the complexity of crude cell lysate samples is reduced employing labelling methods, e.g. utilizing electron-dense markers, or protein separation and isolation techniques. Traditional methods used for protein purification often rely on affinity and gel chromatography. Again, these methods are in general not well suited to process samples of low volumes and low concentrations such as single-cell lysates and often face difficulties with maintaining the state of protein complexes in terms of structure and architecture. Therefore, a novel methodology to targeted proteomics enabling the specific isolation and labelling of protein complexes from minute volumes of cell lysate for subsequent visual analysis in TEM was developed and evaluated (module d). This technique utilizes affinity molecules, i.e. antibodies, to bind the target proteins in the cell lysate. Protein solutions are then loaded in microcapillaries where antibodies and targets become immobilized on magnetic beads that are hold in place using magnetic field gradients. Photocleavable linkers between antibodies and beads enable convenient recovery and mild elution of isolated targets conserving structural integrity of fragile protein complexes for subsequent TEM analysis. Alternative approaches aim to induce a kind of sorting in the crude cell lysate applying capillary electrophoresis

techniques and preliminary experiments with capillary isoelectric focusing were carried out.

Hybrid approaches are required to efficiently tackle the challenging proteome, which suggests to complement the qualitative data on proteins that is routinely acquired using negative stain TEM with quantitative information. For this purpose, the suitability of single particle TEM for protein quantification (hence termed qTEM, module g) was demonstrated, to our knowledge, for the first time. Exploiting the single particle detection limit of TEM, a concept for reliable and efficient protein concentration measurements of low concentrated samples was developed, giving proteomic studies an alternative approach to MS-based protein quantification in future.

Presently, a hybrid setup that accommodates the techniques for cell culturing and lysis, protein isolation, sample conditioning and deposition is under development. Upon completion, the envisaged methodology will be an ideal tool to qualitatively and quantitatively characterize the proteome and interactome of single eukaryotic cells, and in particular, to investigate the cell-to-cell variations of the heterogeneity of large multimolecular protein assemblies, thus providing a complementary approach for obtaining a holistic dynamic picture on biological processes underlying intracellular functions.

1.4 References

[1] Aderem, A. **Systems biology: its practice and challenges.** *Cell* **121**, 511-3 (2005).

[2] Kaern, M.; Elston, T. C.; Blake, W. J.& Collins, J. J. **Stochasticity in gene expression: from theories to phenotypes.** *Nature reviews. Genetics* **6**, 451-64 (2005).

[3] Barkai, N.& Shilo, B. Z. **Variability and robustness in biomolecular systems.** *Molecular cell* **28**, 755-60 (2007).

[4] Rao, C. V.; Wolf, D. M.& Arkin, A. P. **Control, exploitation and tolerance of intracellular noise.** *Nature* **420**, 231-7 (2002).

[5] Raser, J. M.& O'Shea, E. K. **Noise in gene expression: origins, consequences, and control.** *Science* **309**, 2010-3 (2005).

[6] Fritzsch, F. S.; Dusny, C.; Frick, O.& Schmid, A. **Single-cell analysis in biotechnology, systems biology, and biocatalysis.** *Annual review of chemical and biomolecular engineering* **3**, 129-55 (2012).

[7] Wang, D.& Bodovitz, S. **Single cell analysis: the new frontier in 'omics'.** *Trends in biotechnology* **28**, 281-90 (2010).

[8] Amantonico, A.; Urban, P. L.& Zenobi, R. **Analytical techniques for single-cell metabolomics: state of the art and trends.** *Analytical and bioanalytical chemistry* **398**, 2493-504 (2010).

[9] Kalisky, T.& Quake, S. R. **Single-cell genomics.** *Nature methods* **8**, 311-4 (2011).

[10] Wu, M.& Singh, A. K. **Single-cell protein analysis.** *Current opinion in biotechnology* **23**, 83-8 (2012).

[11] Schmid, A.; Kortmann, H.; Dittrich, P. S.& Blank, L. M. **Chemical and biological single cell analysis.** *Current opinion in biotechnology* **21**, 12-20 (2010).

[12] Burkhart, J. M.; Vaudel, M.; Zahedi, R. P.; Martens, L.& Sickmann, A. **iTRAQ protein quantification: a quality-controlled workflow.** *Proteomics* **11**, 1125-34 (2011).

[13] Aebersold, R.& Mann, M. **Mass spectrometry-based proteomics.** *Nature* **422**, 198-207 (2003).

[14] Bantscheff, M.; Lemeer, S.; Savitski, M. M.& Kuster, B. **Quantitative mass spectrometry in proteomics: critical review update from 2007 to the present.** *Analytical and bioanalytical chemistry* **404**, 939-65 (2012).

[15] Rubakhin, S. S.& Sweedler, J. V. **Quantitative measurements of cell-cell signaling peptides with single-cell MALDI MS.** *Analytical chemistry* **80**, 7128-36 (2008).

[16] Rubakhin, S. S.; Romanova, E. V.; Nemes, P.& Sweedler, J. V. **Profiling metabolites and peptides in single cells.** *Nature methods* **8**, S20-9 (2011).

[17] Kleparnik, K. **Recent advances in the combination of capillary electrophoresis with mass spectrometry: from element to single-cell analysis.** *Electrophoresis* **34**, 70-85 (2013).

[18] Rudashevskaya, E. L.; Sacco, R.; Kratochwill, K.; Huber, M. L.; Gstaiger, M. *et al.* **A method to resolve the composition of heterogeneous affinity-purified protein complexes assembled around a common protein by chemical cross-linking, gel electrophoresis and mass spectrometry.** *Nature protocols* **8**, 75-97 (2013).

[19] Kukulski, W.; Schorb, M.; Welsch, S.; Picco, A.; Kaksonen, M. *et al.* **Correlated fluorescence and 3D electron microscopy with high sensitivity and spatial precision.** *J Cell Biol* **192**, 111-9 (2011).

[20] Baumeister, W. **Electron tomography: towards visualizing the molecular organization of the cytoplasm.** *Current opinion in structural biology* **12**, 679-84 (2002).

[21] Vanhecke, D.; Asano, S.; Kochovski, Z.; Fernandez-Busnadiego, R.; Schrod, N. *et al.* **Cryo-electron tomography: methodology, developments and biological applications.** *Journal of microscopy* **242**, 221-7 (2011).

[22] Bohm, J.; Frangakis, A. S.; Hegerl, R.; Nickell, S.; Typke, D. *et al.* **Toward detecting and identifying macromolecules in a cellular context: Template matching applied to electron tomograms.** *Proceedings of the National Academy of Sciences of the United States of America* **97**, 14245-14250 (2000).

[23] Beck, M.; Malmstrom, J. A.; Lange, V.; Schmidt, A.; Deutsch, E. W. *et al.* **Visual proteomics of the human pathogen Leptospira interrogans.** *Nature methods* **6**, 817-23 (2009).

[24] Bouchet-Marquis, C.; Pagratis, M.; Kirmse, R.& Hoenger, A. **Metallothionein as a clonable high-density marker for cryo-electron microscopy.** *J Struct Biol* **177**, 119-127 (2012).

[25] Engel, A. **Scanning Transmission Electron Microscopy: Biological Applications.** *Adv Imag Elect Phys* **159**, 357-386 (2009).

[26] Giss, D.; Kemmerling, S.; Dandey, V.; Stahlberg, H.& Braun, T. **Exploring the Interactome: Microfluidic Isolation of Proteins and Interacting Partners for Quantitative Analysis by Electron Microscopy.** *Analytical chemistry* **86**, 4680-4687 (2014).

[27] Kemmerling, S.; Ziegler, J.; Schweighauser, G.; Arnold, S. A.; Giss, D. *et al.* **Connecting mu-fluidics to electron microscopy.** *J Struct Biol* **177**, 128-34 (2012).

[28] Fancy, D. A.& Kodadek, T. **Chemistry for the analysis of protein-protein interactions: rapid and efficient cross-linking triggered by long wavelength light.** *Proceedings of the National Academy of Sciences of the United States of America* **96**, 6020-4 (1999).

[29] Gomes, A. F.& Gozzo, F. C. **Chemical cross-linking with a diazirine photoactivatable cross-linker investigated by MALDI- and ESI-MS/MS.** *Journal of mass spectrometry : JMS* **45**, 892-9 (2010).

[30] Yun, H.; Kim, K.& Lee, W. G. **Cell manipulation in microfluidics.** *Biofabrication* **5** (2013).

[31] Kemmerling, S.; Arnold, S. A.; Bircher, B. A.; Sauter, N.; Escobedo, C. *et al.* **Single-cell lysis for visual analysis by electron microscopy.** *Journal of structural biology* **183**, 467-473 (2013).

[32] Weidmann, S.; Kemmerling, S.; Madler, S.; Stahlberg, H.; Braun, T. *et al.* **Ionic liquids as matrices in microfluidic sample deposition for high-mass matrix-assisted laser desorption/ionization mass spectrometry.** *Eur J Mass Spectrom* **18**, 279-286 (2012).

2 Exploring the interactome: Microfluidic isolation of proteins and interacting partners for visual analysis by quantitative electron microscopy

The following section has been published in:

Analytical Chemistry 86(10), 4680-7 (2014)
(doi: 10.1021/ac4027803.)

Exploring the interactome: Microfluidic isolation of proteins and interacting partners for visual analysis by quantitative electron microscopy

Dominic Giss, Simon Kemmerling, Venkata Dandey,
Henning Stahlberg and Thomas Braun*

Center for Cellular Imaging and NanoAnalytics (C-CINA), Biozentrum,
University of Basel, Switzerland.

*Corresponding Author: Thomas.braun@unibas.ch

2.1 Abstract

Multimolecular protein complexes are important for many cellular processes. However, the stochastic nature of the cellular interactome makes the experimental detection of complex protein assemblies difficult, and quantitative analysis at the single molecule level essential. Here, we present a fast and simple microfluidic method for (i) the quantitative isolation of endogenous levels of untagged protein complexes from minute volumes of cell lysates under close to physiological conditions and (ii) the labeling of specific components constituting these complexes. The method presented uses specific antibodies that are conjugated via a photocleavable linker to magnetic beads that are trapped in microcapillaries to immobilize the target proteins. Proteins are released by photocleavage, eluted and subsequently analyzed by quantitative transmission electron microscopy at the single molecule level. Additionally, before photocleavage, immunogold can be employed to label proteins that interact with the primary target protein. Thus, the presented method provides a new way to study the interactome and, in combination with single molecule transmission electron microscopy, to structurally characterize the large, dynamic, heterogeneous multimolecular protein complexes formed.

2.2 Introduction

Systems biology aims to identify and quantify the molecular elements of biological systems, to determine the dynamic interactions between them, and to integrate the resulting information into system networks.[1] The development of these holistic models necessitates the quantitative detection of protein-interaction assemblies and their characterization in terms of stoichiometry, structure and temporal persistence. The stochastic nature of biological processes makes the analysis of these heterogeneous, multimolecular complexes at the single molecule level essential.

Many experimental strategies are used today to characterize the proteome of cells[2,3] or to define the interactome.[4,5] In these, protein complexes are often identified using hybrid approaches relying on affinity purification or immunoprecipitation in combination with chemical cross-linking[6] or gel electrophoresis[7] and mass spectrometry.[8] These methods analyze a sample from multiple cells, and quantify the average relative occurrence and composition of the available protein complexes. Due to the large number of protein copies required, these methods are generally not well suited for the analysis of heterogeneous, multimolecular protein complexes, such as the human Mediator complex,[9] transiently formed during interaction pathways. Further, although proteins interacting within a complex can be defined,[10] the structure of the entire multimolecular complex remains unknown. Yet, the structure of the entire complex has to be known to fully understand the role of the complex in the cell.

Electron microscopy can be used to image single molecules and obtain various types of structural information.[11,12] For example, cryo-electron tomography (cryo-ET) can provide information at molecular resolution for larger proteins in

unperturbed single cells.[13-15] However, *visual proteomics* by electron tomography[16] is restricted to small cells or to sections of cells (the sample diameter must be below 1 µm for cryo-ET to reach higher resolution),[17] and protein recognition is limited to relatively large protein complexes.[18,19] Further, the identification of complexes and their constituents without electron dense labels[20] in intact cells is challenging. We have recently developed a new approach to visual proteomics in which eukaryotic cells are lysed and the proteins in the lysate and membrane fragments visually analyzed by single molecule transmission electron microscopy (TEM).[21,22] Again, without the aid of electron dense labels interpretation can be ambiguous. However, in this case the cell lysate is easily accessible for labeling methods.

Here we present a fast microfluidic protein isolation method and demonstrate its use with TEM for the extraction of protein assemblies from cell lysate and their quantification. The method allows endogenous levels of untagged protein complexes to be specifically isolated from minute volumes of complex biological background, and investigated at the single molecule level. It provides initial structural information. Importantly, the approach also allows interacting partners to be identified by a labeling step, here termed interaction-labeling, and the intact complex to be visualized by TEM.

2.3 Experimental section

2.3.1 Working principle

The approach is based on antibodies (ABs) that are conjugated to a photocleavable biotin crosslinker[23] (Figure 2-1A). These conjugates interact with streptavidin-coated magnetic beads that are immobilized in microcapillaries by a magnetic trap (Figure 2-1B; Supporting Information Figure 2-7). The basic protocol is as follows: Cell lysate is mixed with biotinylated ABs against the target protein and passed over the trapped beads. Subsequently, the capillary is rinsed with buffer to wash out all unbound proteins. Finally, the immobilized target proteins are released by illuminating the capillary with UV-light at a wavelength of 365 nm to photocleave the crosslinker. Target proteins are then eluted and loaded on TEM grids (Figure 2-1C). This protocol can be extended by two variations before photocleavage and elution: (i) A labeling step using immunogold can be included to identify and localize the target proteins or their copurified interacting partners in a protein assembly; (ii) extracted proteins can be used as bait to 'fish' for potential binding partners, again followed by a labeling step.

2.3.2 Separation setup

A 250 µm inner-diameter fused silica capillary (BGB Analitik AG #TSP-250350, Switzerland) was guided through a lens tube construction cube (Thorlabs #SM1C6, Germany) so that optical components could be easily mounted, and to provide protection from UV-light (Supporting Information Figure 2-7). The outer polymer coating of the capillary was thermally removed

from a length of 1 cm-long region at the center of the cube to avoid absorbance of UV-light. Magnetic beads were trapped in the stripped region by two external permanent magnets (Supermagnete #Q-20-10-05-N, Switzerland) positioned below the capillary at the center of the cube. UV-light at 365 nm was emitted by a high power UV LED (Thorlabs #M365L2, Germany) mounted on top of the cube and guided onto the magnetic beads using collimator and focusing lenses (Thorlabs #LA1952 and #LA1131, Germany). Liquids were aspirated or dispensed via a stepper motor syringe pump (Genie Pump, Kent Scientific) from 200 µl PCR tubes mounted on an xy-stage.

2.3.3 Loading of magnetic beads

About $40*10^6$ streptavidin-coated magnetic beads with a diameter of 1 µm (corresponding to 4 µl of the beads employed; Dynabeads® MyOne™, Invitrogen #656-01, Switzerland) presented in phosphate buffered saline (PBS) were aspirated into a 250 µm inner-diameter fused silica capillary at a flow rate of 20 µl/min. An external permanent magnet positioned in close proximity below the capillary caused a plug of beads to form (Supporting Information Figure 2-7). After this bead-loading step, a second magnet was added to fully trap the plug, and the beads were rinsed with the buffer used for the subsequent experiment. In this manner, a robust, 3 - 4 mm long plug was formed and equilibrated with the required buffer.

2.3.4 Antibody biotinylation

ABs were incubated with a 10-fold molar excess of photocleavable NHS-Biotin crosslinker (Ambergen, USA) for 1.5 h at pH 8.2. After incubation, the mixture was dialyzed overnight against 2 l of PBS (phosphate buffered saline, 0.01 M phosphate buffer 0.0027 M potassium chloride and 0.137 M sodium chloride, pH 7.4, Sigma-Aldrich #P4417, Switzerland) using dialysis buttons (membranes with a 13 kDa cut-off) to remove unbound crosslinker.

2.3.5 Extraction and purification of target structures

A stock solution of apoferritin (AF) from equine spleen in 50% glycerol (Sigma-Aldrich #A3660, Switzerland) was diluted to 3 - 300 nM using baby hamster kidney (BHK) cell lysate. The AF / cell lysate mixtures were incubated for one hour on ice with biotinylated polyclonal anti-horse spleen ferritin ABs produced in rabbit (Sigma-Aldrich #F6136, Switzerland; henceforth termed anti-ferritin ABs) at 47 nM concentration. Subsequently, 2 µl of the mixture was passed over trapped magnetic beads for 15 min to immobilize target proteins on the beads. The actual incubation time of the biotinylated ABs with the streptavidin-coated beads was about 60 s on average. Finally, the capillary was rinsed with PBS to remove unbound proteins. Progress of the washing process was probed by collecting a series of eluted wash fractions and analyzing them by TEM.

To demonstrate that immobilized proteins can be used as bait for potential binding partners, 2 µl of a 1 nM solution of polyclonal anti-horse ferritin antibodies produced in goat (Lubio Science #A70-128A, Switzerland), were diluted with BHK cell lysate and passed over previously immobilized AF for 15 min. After incubation, the capillary was rinsed with PBS to completely separate trapped ABs from cell lysate. Immobilized goat anti-ferritin ABs were then labeled with 10 nm colloidal immunogold by rinsing the capillary with 2 µl of anti-goat IgG gold (Sigma-Aldrich #G5402, Switzerland) diluted 1:10 in 0.1% BSA (Sigma-Aldrich #A3294, Switzerland), for 15 min.

To extract endogenous 26S proteasome, HEK293 cell lysate was incubated with biotinylated polyclonal anti-20S proteasome ABs from rabbit (Merck Millipore #ST1053) for 120 min on ice. 4 µl of the mixture, corresponding to the lysate of about forty thousand cells, were then passed over immobilized magnetic beads during a time period of 15 min. Washing steps were carried out with HEPES buffer (25 mM HEPES-KOH, pH 7.4; 5 mM $MgCl_2$ and 10% glycerol).

The isolation of endogenous TCP-1 ring complex (TRiC) from HEK293 cell lysate was performed using biotinylated monoclonal anti-CCT epsilon ABs (Pierce Antibodies #MA1-82643) and HEPES buffer (20 mM HEPES-KOH, pH 7.4; 5 mM $MgCl_2$; 50 mM NaCl and 10% glycerol).

2.3.6 Recovery of target structures

Immobilized target proteins were released from the magnetic beads by illuminating the plug in the capillary with UV-light for 10 min to cleave photocleavable biotin. Photocleavable biotin shows maximal absorbance around 270 nm, but still has distinct absorbance at 365 nm, the wavelength emitted by the UV LED employed. After cleavage, analytes were eluted in 3 - 6 µl of buffer and collected.

2.3.7 Washing procedure

After each incubation step, the capillary was rinsed with buffer (PBS or HEPES buffer, depending on the experiment) to separate unbound from immobilized proteins. Depending on the applied cell lysate concentration, the immobilized beads were washed for 5 - 25 min at 20 - 40 µl/min flow rates. After an experiment, the magnetic beads were discarded by pressurizing the capillary. The latter was then extensively washed with double-distilled H20, 70% EtOH and 0.1 M NaOH.

2.3.8 Cell preparation

Adherent baby hamster kidney fibroblasts (BHK21; ECACC 85011433) and 293 cell line human embryonic kidney cells (HEK293; ECACC 85120602) were cultured in polystyrene T75-flasks containing 30 ml DHI-5 medium (see below) for BHK cells and 10 ml culture medium (see below) for HEK293 cells, at 37 °C and 5% carbon dioxide. To split the cells, the medium was removed and the flask

was washed with 10 ml of 37 °C warm PBS w/o calcium and magnesium (Dulbecco's phosphate buffered saline, Sigma-Aldrich #D8537, Switzerland). To detach the cells, 3 ml of trypsin-EDTA solution (0.05% trypsin 0.53 mM EDTA, Invitrogen #25300-054, Switzerland) were added and drained before the cells were incubated at 37 °C for 5 min. The detached cells were diluted with 10 ml of 37 °C warm medium and homogenized using a pipette. For BHK cells, 0.5 ml of the homogenized cell suspension and 30 ml of fresh medium were returned to the flask for further cultivation. For HEK293 cells, 1 ml of the homogenized cell suspension and 9 ml of fresh medium were used. The rest of the cell suspension was washed twice with PBS and concentrated to a final cell concentration of 1000 cells/µl for BHK cells or 10000 cells/µl for HEK cells using PBS or HEPES buffer (depending on the experiment). In both cases, cells in 0.5 ml of the suspension were then physically lysed by sonication for 30 - 60 s using a tip sonicator while cooling. The fresh lysates were either directly used for experiments or aliquoted and stored at -80 °C.

DHI-5 medium is a 1:1:2 mixture of DME (Dulbecco's modified Eagles medium, Sigma-Aldrich #D6171, Switzerland), HamF12 (Nutrient mixture F-12Ham, Sigma-Aldrich #N8641, Switzerland), and IMDM (Iscove's modified Dulbecco's medium, Sigma-Aldrich # I3390, Switzerland) media, supplemented with 5% FCS (Fetal calf serum, Sigma-Aldrich #E7524, Switzerland) and complemented with non essential amino acids (MEM non-essential amino acid solution, Sigma-Aldrich #M7145, Switzerland), L -glutamine (L -glutamine solution, Sigma-Aldrich #G7513, Switzerland), and vitamins (RPMI1640 vitamins solution, Sigma-Aldrich #R7256, Switzerland).

For HEK293 cells the culture medium was EMEM (Eagle’s minimal essential medium, Sigma-Aldrich #M2279, Switzerland) supplemented with 10% FCS and complemented with nonessential amino acids and L–glutamine.

2.3.9 TEM grid preparation

Immediately after elution, 3 µl of the eluted analytes were incubated for 90 s on glow-discharged carbon coated copper TEM grids (200 mesh). After a blotting step, grids were washed five times for 12 s on double-distilled H20 and negatively stained on two 4.5 µl drops of 2% uranylacetate. After every incubation and the final washing step, excess liquid was removed using blotting paper.

2.3.10 Image acquisition and processing

Automated image acquisition was done on a FEI T12 operated at 100 kV using the Leginon 2.1 (incl. in Myami 2.1) software.[24] The images were recorded on a Gatan 2k x 2k CCD camera. A semi-automatic image acquisition routine was used for the quantitative analysis of analytes (Figure 2-2): First, five squares of the TEM grid were manually selected for analysis. Then, a mesh consisting of 35 sub-squares was created within every square, and 11 images per sub-square were automatically acquired at 12000x magnification (pixelsize: 0.8725 nm, defocus: 0.8 - 1.4 µm, dose: 22 - 35 electrons/$Å^2$). Thereby about 12% of the area of a

particular square was imaged. Subsequently, using the 1925 images collected per grid, target proteins were identified by their visual appearance in negative stain, and counted. This was done manually and/or using the Appion 2.1 (incl. in Myami 2.1) software[25] in combination with a template picking routine.[26] Note, that ABs often linked targets to form multi-protein complexes. In this case, every target unit was counted individually.

Manual TEM was carried out on a Philips CM10 operated at 80 kV. The images were recorded on a 2k x 2k CCD camera (Olympus SIS, Münster, Germany). For 2D class averages, images were acquired at 130000x nominal magnification (pixelsize: 0.37 nm, defocus: 0.1 – 0.3 µm. Particles were picked manually using EMAN2 software package,[27] classified and averaged using the e2refine2d algorithm.

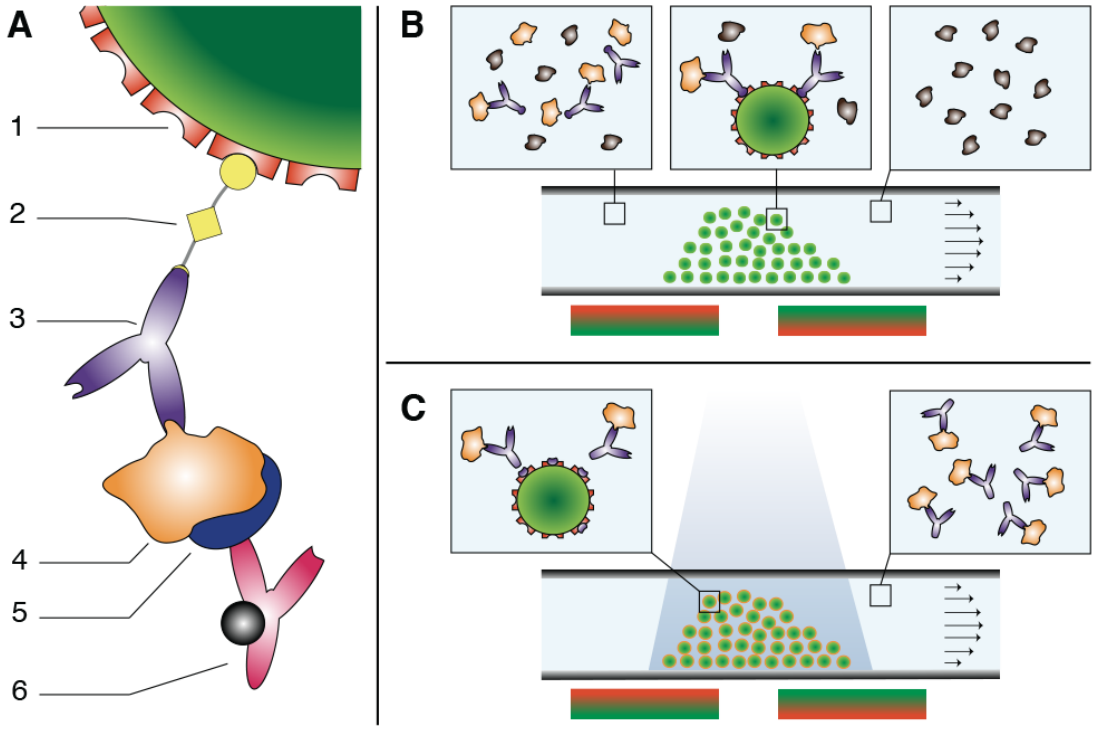

Figure 2-1: *Principle of the microfluidic affinity isolation method. (**A**) AB-biotin conjugates bound to a streptavidin-coated magnetic bead. 1: Streptavidin-coated magnetic bead of 1 µm in diameter; 2: photocleavable NHS-Biotin crosslinker; 3: AB against the target protein; 4: target protein; 5: protein binding partner (optional); 6: immuno-gold labeled AB against the binding partner. (**B**) Affinity extraction. Streptavidin-coated magnetic beads are trapped in a microcapillary (inner diameter of 250 µm) using two external magnets positioned underneath the capillary. After loading, the capillary is rinsed with sample solution that was previously incubated with biotinylated ABs against the target structure. The capillary and beads are then washed to remove other proteins; ABs and their targets remain immobilized. Optionally, the capillary can next be rinsed with potential binding partners of the target structures and/or with immuno-gold ABs to label immobilized target proteins or their interacting partners. (**C**) Photocleavage and elution. Target structures are recovered by illuminating the beads with UV-light at a wavelength of 365 nm and eluting the released AB-target protein complexes. Downstream applications such as TEM analysis follow.*

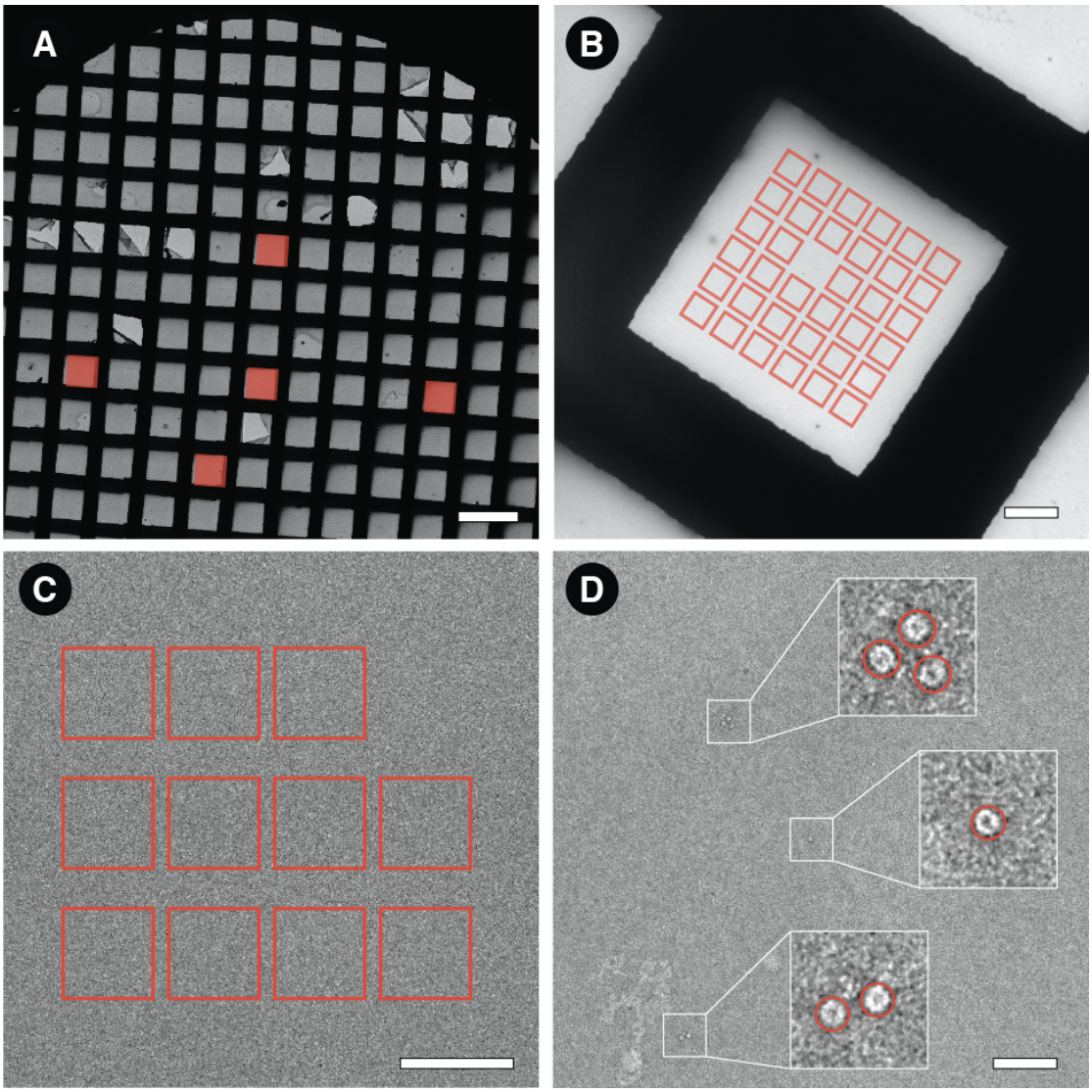

Figure 2-2: *Semi-automatic TEM procedure for image acquisition and data-analysis. (**A**) Step 1: Manual selection of five squares of a TEM grid. (**B**) Step 2: The procedure targets 35 sub-squares per grid square. (**C**) Step 3: 11 images are recorded per sub-square. (**D**) Step 4: Image processing. Particles of interest are detected by their visual appearance in negative stain on the total of 1925 images per grid either manually or automatically using a template, and counted; each AF was counted as one particle, regardless of whether it was associated with other AFs or not. Scale bars, 200 µm (**A**), 20 µm (**B**), 2 µm (**C**) and 200 nm (**D**).*

2.4 Results and discussion

We have developed a quantitative method that enables the fast and specific extraction and recovery of target proteins from minute volumes of cell lysate without the need for genetic engineering to introduce affinity tags. Samples are deposited on TEM grids and examined at the single molecule level by quantitative TEM (qTEM), which also delivers structural information by single particle analysis. Our method also allows potential binding partners to be detected and analyzed. These interaction partners either copurify with the primary target protein or can be "fished" from complex samples using a previously isolated protein as bait. Immunogold labeling both aids protein identification and localizes specific proteins in the extracted multimolecular complexes.

To quantitatively assess the method, we complemented the crude cell lysate obtained from sonicated BHK cells with known amounts of AF as target protein and incubated this lysate with biotinylated anti-ferritin ABs. 2 µl of the mixture (total amount of AF, 6 - 600 fmol, depending on the experiment) were passed over previously immobilized magnetic beads during a time period of 15 min, followed by 200 µl of PBS during a time period of 10 min. Photolysis was carried out for 10 min after this washing step, and the released AF-AB complexes were eluted in 6 µl of PBS for TEM analysis. The excess of streptavidin-coated magnetic beads offered ample binding surface for the biotinylated ABs; as expected control experiments showed that using more beads did not improve extraction efficiencies.

An example of the isolation process is shown in Figure 2-3. The first wash fractions after the immobilization step contained BHK cell lysate and some non-extracted AF (Figure 2-3B), recognizable by its typical ring-shaped projection (compare Supporting Information Figure 2-8). Most of the unbound proteins were removed by the washing procedure (Figure 2-3C). AF-AB complexes were recovered after the subsequent photocleavage step (Figure 2-3D). The clean background in this image documents the very low concentration of contaminants on the TEM grids. Proteins that were nonspecifically bound to the beads were not released by the photocleavage step (compare Figure 2-3D and Supporting Information Figure 2-9).

We performed qTEM to analyze the results of the isolation experiments. A semi-automatic, TEM image acquisition and data analysis procedure was developed for this (Figure 2-2). Thereby, 1925 images were recorded from defined regions of each TEM grid and the target proteins were detected by their visual appearance and counted, allowing the total amount of recovered protein to be measured. Running a series of experiments as described above with concentrations of the target protein AF ranging from 3 - 300 nM and an AB concentration of 47 nM, yielded the signal transfer function (SiTF, Figure 2-4 and Supporting Information Figure 2-10) of the method for AF. This quantitative measurement reflects the AB-antigen binding curve (Figure 2-4). Using the Hill equation for non-cooperative binding to extract the *apparent* dissociation constant K_d of the AB-AF interaction from the recorded data, gave an apparent K_d of 12 nM. Control experiments showed that the SiTF of AF to TEM grids depends linearly on the applied concentration of AF (Supporting Information Figure 2-

11). These experiments show, that the AB binding characteristics dominates the SiTF of the presented isolation method.

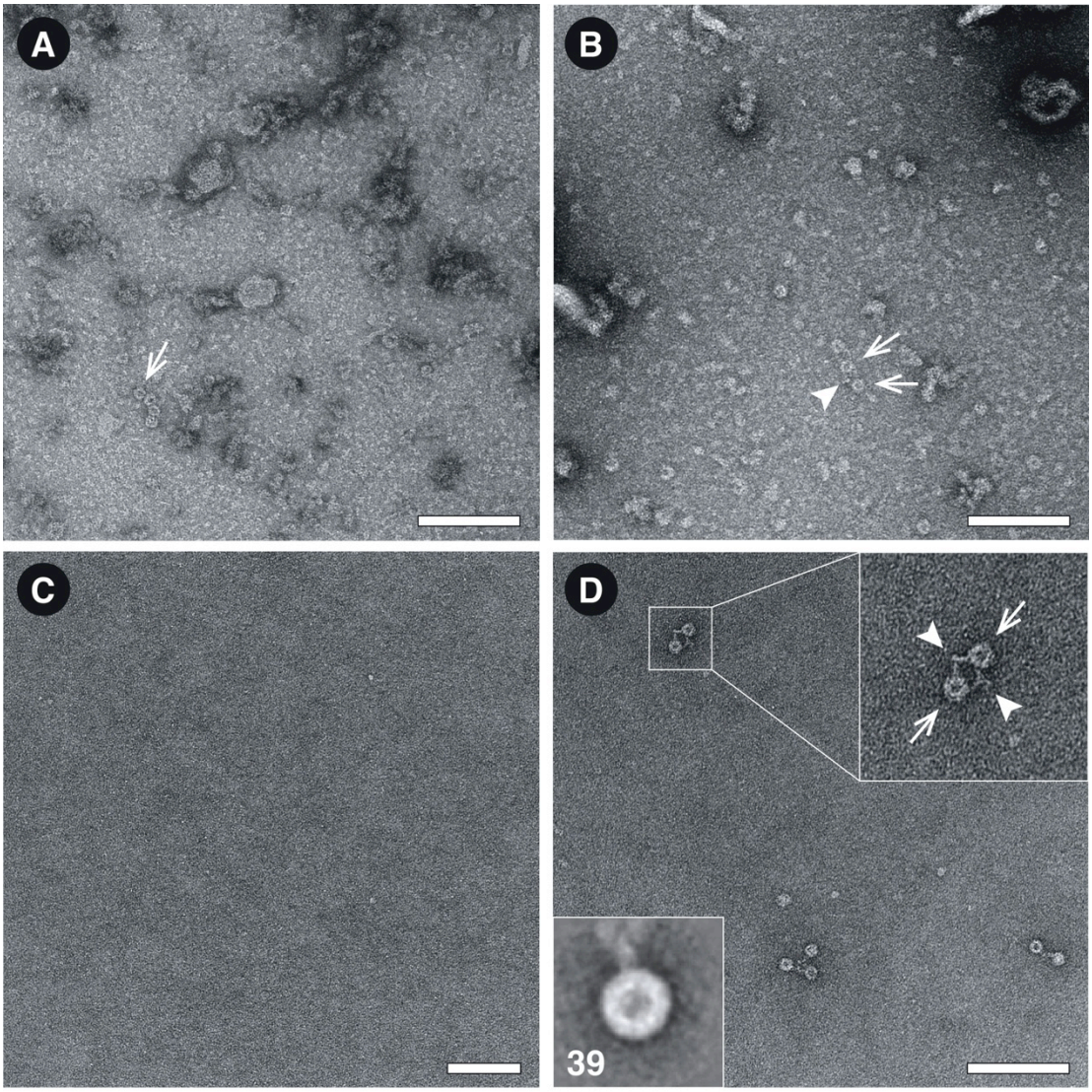

Figure 2-3: *Affinity extraction and recovery of apoferritin. (**A**) The initial cell lysate / 30 nM AF (arrow) mixture. The mixture was incubated with biotinylated anti-ferritin ABs (47 nM) and passed over streptavidin-coated magnetic beads immobilized by a magnetic trap in a microcapillary, and the capillary was subsequently washed with buffer. (**B**) First wash fractions document that crude cell lysate does not obstruct the capillary and that not every single AF (arrow) – AB (arrowhead) complex was extracted. (**C**) Last wash fraction, confirming that unbound proteins were removed by the washing process. (**D**) Eluate after photocleavage of the crosslinker showing recovered AF (arrow) – AB (arrowhead) complexes; these have been cleanly isolated from the cell lysate. Inset: 2D class average (bottom left, number of averaged particles) of recovered AF with visible AB attached. Scale bars, 100 nm.*

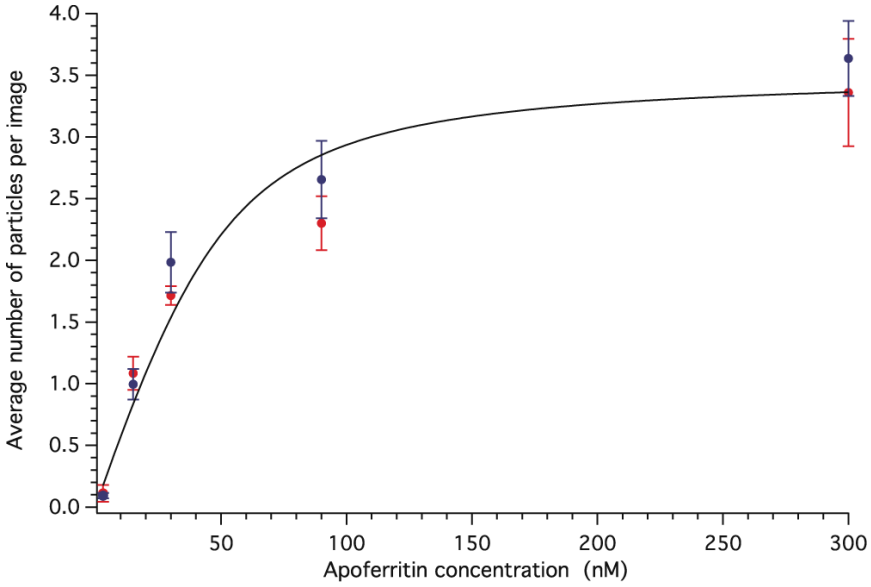

Figure 2-4: *Signal transfer function of the microfluidic affinity isolation method for AF determined by qTEM. To quantitatively assess the response of the developed method, we processed different concentrations of AF, ranging from 3 - 300 nM, using a constant amount of anti-ferritin ABs (47 nM). Two TEM grids were prepared for every experiment (red and blue symbols). In a semi-automatic manner, 1925 images were collected per grid (385 per selected grid square), and AF was detected by its visual appearance in negative stain and counted (see Figure 2-2). The average number of AF particles per image (PPI) for the particular grid is shown. Error bars represent the standard deviation of the average PPIs of the five probed grid squares of the parent grid. The data reflects the AB-antigen binding curve for an increasing antigen concentration, which was modeled (black line) using Hill's equation.*

We used HEK293 cell lysate to demonstrate the extraction and recovery of endogenous levels of protein complexes from cell extract by our one-step isolation method. In these experiments, we added biotinylated anti-20S proteasome ABs to the cell lysate to bind endogenous 26S proteasomes and processed the lysate of about forty thousand HEK293 cells suspended in HEPES buffer. The protocol was similar to that described for AF. A typical experiment, starting with the lysis of cells and ending with the isolated target protein on TEM grids, took approximately 160 min, including an AB-target protein incubation step of two hours. As depicted in Figure 2-5, the method enabled us to isolate intact 26S proteasomes comprised of a 20S core complex and two weakly interacting 19S regulatory units from cell extract, as well as 20S proteasomes lacking one or both of the 19S regulatory complexes. The isolation of fully assembled 26S proteasomes, which are sensitive to buffer conditions (Supporting Information Figure 2-12), clearly demonstrates that complexes formed by weakly interacting proteins can be isolated by the proposed method. Furthermore, using biotinylated anti-CCT ABs, we isolated endogenous levels of TRiC (Figure 2-5D). Note, that the application of unspecific ABs (or no ABs at all) did not result in the isolation of target proteins.

The proteasomes and TRiC can be visually identified in negative stain TEM images due to their characteristic size and shape. The average structures calculated by single particle analysis are in excellent agreement with previously

reported models[28-30] and 2D class averages of purified 20S proteasomes (Supporting Information Figure 2-13). Sometimes, ABs are visibly attached to the proteins, therefore we can be confident that the isolated particles are indeed the target protein complexes and that the corresponding structural analysis is relevant.

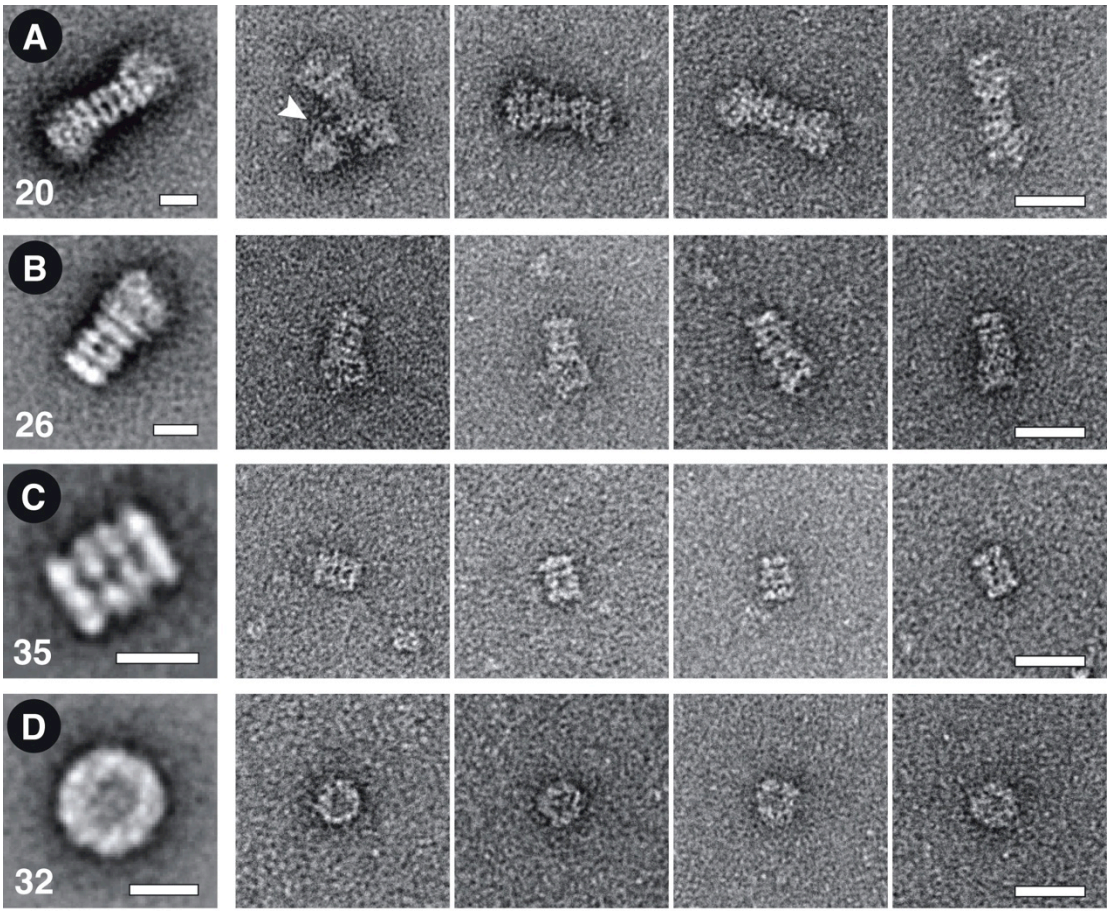

Figure 2-5: *Isolation of endogenous protein complexes. HEK293 cell lysate was incubated with biotinylated anti-20S proteasome ABs (**A**, **B**, **C**) or biotinylated anti-CCT ABs, respectively (**D**). The lysate of about forty thousand cells was then passed over trapped streptavidin-coated magnetic beads to extract target complexes, which were subsequently recovered by photocleavage and transferred onto TEM grids. Left panels: Representative 2D class averages of isolated target structures (bottom left, number of averaged). Scale bar, 10 nm. Right panels: Gallery of negatively stained particles. Scale bar, 25 nm. (**A**) 26S proteasomes composed of two regulatory 19S particles and the 20S core proteasome. In rare cases, we found complexes linked by ABs (arrowhead). (**B**) Partially disassembled proteasomes, lacking one of the regulatory 19S particles. (**C**) Side view of isolated 20S core particles. (**D**) TRiC. Typical ring-shaped top views, 16 nm in diameter, are visible.*

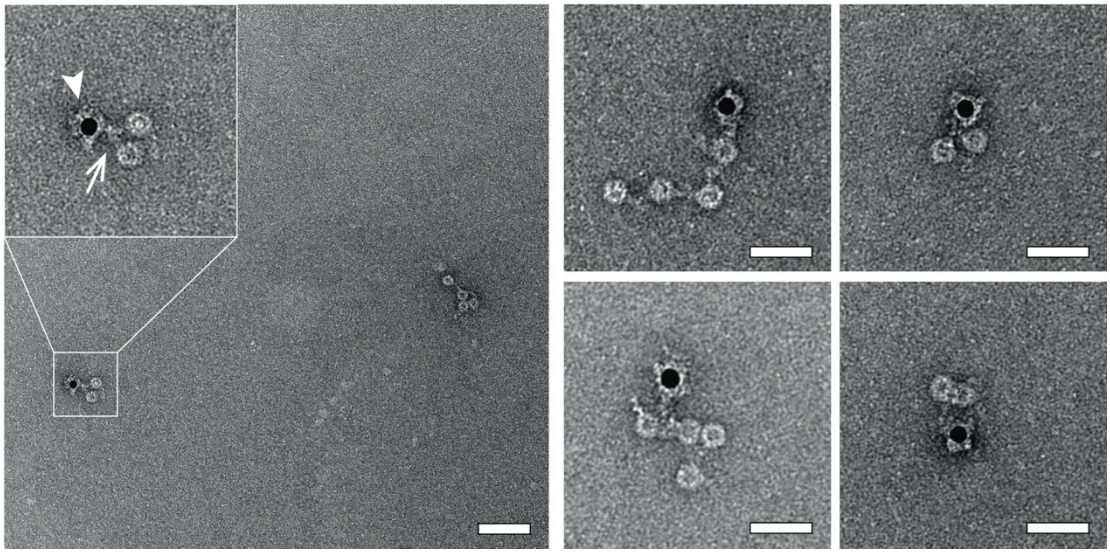

Figure 2-6: *The detection of extracted protein binding partners by interaction-labeling. AF in a mixture of cell lysate and biotinylated anti-ferritin ABs was immobilized on the streptavidin coated magnetic beads, where it acted as bait protein. In a second step, the capillary was then rinsed with goat anti-ferritin ABs (arrow) supplied in cell lysate to mimic potential binding partners. In a third step, the capillary was rinsed with anti-goat colloidal gold (10 nm, arrowhead) to label the fished goat anti-ferritin ABs and, thus, facilitate the detection of established interactions by TEM. The complexes were recovered by photocleavage and transferred onto TEM grids. The black spots on the images are gold particles labeling the goat anti-ferritin ABs. Scale bars, 50 nm.*

Additionaly, immunogold markers can be used to unambiguously detect specific proteins and localize them within a complex. Exploiting this, we used immobilized target proteins to fish for potential binding partners and identified them by gold tags (Figure 2-1A). As a proof of concept, AF was mixed with BHK cell lysate and biotinylated rabbit anti-ferritin ABs and immobilized on magnetic beads as described above. To mimic binding partners, the capillary was subsequently flushed for 15 min with a total of 2 µl of 1 nM goat anti-ferritin AB solution in BHK cell lysate. After washing, the capillary was rinsed for 15 min with 2 µl of anti-goat colloidal gold to label established protein complexes. Photolysis and the elution of AF-AB complexes for TEM analysis followed. As shown in Figure 2-6, the approach allows (i) binding partners (arrow) to be fished and recovered from complex backgrounds, and (ii) identified by an attached immunogold label (arrowhead). In our studies, we did not detect any cross-reactivity between anti-goat immunogold and rabbit ABs or AF.

The presented method uses functionalized magnetic beads to form bead plugs in microcapillaries by magnetic trapping. This approach significantly reduces the diffusion path length required for protein binding and offers a massive increase in the available binding surface compared to, for instance, functionalized capillary walls. The technique provides a fast and convenient way to process of sub-microliter volume samples. Important for future high-throughput applications, the immobilization or release of beads can be easily tuned by adjusting the applied magnetic field gradient, enabling their rapid exchange.[31]

The use of photocleavable linkers allows sample recovery under mild conditions that conserve the structural integrity of proteins. It is not necessary to

use relatively harsh methods such as boiling the beads, treatment with low pH buffers, or changing the salt concentration, all of which might affect the structural integrity of target proteins or lead to disassembly of protein complexes. Indeed, the photocleavage employed is carried out at a wavelength of 365 nm, which is not significantly absorbed by most protein targets and therefore does not interfere with their structures or the complexes formed. Moreover, finite element simulations estimate that the UV-light induced temperature rise experienced by capillaries and buffers is lower than 0.6 °C (Supporting Information Figure 2-14). Elution by photocleavage is more specific than traditional chemical procedures and serves as a second "purification" step; proteins that are nonspecifically bound to the immobilized beads or the capillary surface are not released (Supporting Information Figure 2-9). This explains the low contaminant concentration in the eluates, as indicated by the almost perfectly clean background of the TEM images (Figure 2-3D, Figure 2-5 and Figure 2-6). The purity of the eluates facilitates qTEM and structural analysis of the individual complexes. Furthermore, we have demonstrated that weak interacting protein complexes, such as the regulatory 19S and the 20S core particle forming a 26S proteasome, survive the isolation procedure (Figure 2-5A&B).

Quantitative TEM showed that the amount of recovered target protein depends on the initial concentration of the protein in the cell extract (Figure 2-4). Once the respective SiTF of a target protein has been calibrated (Figure 2-4 and Supporting Information Figure 2-10 and Figure 2-11), absolute quantities can be measured. To our knowledge, this is the first time where the feasibility of single molecule qTEM for protein quantification has been demonstrated. As shown in Figure 2-4, the SiTF of protein is dominated by the antibody-antigen binding curve, which also allows the apparent binding constant to be determined. Further, the method provides reproducible results; the resulting particle concentrations on two TEM grids prepared with the same sample differ by maximally 15% (peak-to-peak). The measurement variations of other methods used for protein quantification, e.g., reverse phase protein arrays, are comparable.[32]

As indicated in Supporting Information Figure 2-10, the SiTF of the presented isolation method depends on four main factors. Future improvements to their experimental aspects will result in more target proteins being isolated and detected: First, the use of smaller affinity molecules with only one binding site and higher binding constants, such as DARPins,[33] nanobodies[34,35] or aptamers[36] instead of ABs should increase the extraction efficiency of target structures. Second, the use of techniques enabling a much more efficient transfer of proteins onto TEM grids, such as the "sample writing" procedure that we described in Kemmerling et al.,[22] will significantly increase the concentration of particles on TEM grids. Third, new camera types[37] will allow isolated particles to be imaged faster with a massively improved signal-to-noise ratio and counted more accurately. Fourth, improved algorithms for particle detection will allow the analysis of larger data sets with better precision. Together, this will make the image acquisition and/or quantitative analysis less time consuming and improve the sensitivity and detection limits of the technique. However, already now the method presented can be applied to collect

enough images of well-distributed particles to calculate class averages of the isolated target structures (Figure 2-3 and Figure 2-5). The presence of ABs did not interfere with 2D class averaging (Supporting Information Figure 2-12). Class averages can aid protein identification and provide initial structural information. Further, if their signal is not averaged out (inset Figure 2-3D), bound ABs revealed in the average can be used to localize specific subunits in a complex.[30]

Figure 2-6 demonstrates the detection of extracted protein binding partners by immunogold labeling. In general, two problems must be overcome to detect binding partners by immunotagging: First, specific and efficient labeling must be achieved. Second, unbound label must be removed, or ways to discriminate between label specifically bound to the protein and label randomly adsorbed to the TEM grid must be found. The method presented provides an elegant and efficient way to remove unspecific label before elution of the protein complexes and TEM grid preparation, thus avoiding hurdle two.

2.5 Conclusions

We have presented a fast, one-step affinity isolation method for the quantitative extraction of endogenous levels of protein from complex samples without significant contaminants. Furthermore, protein-protein interactions can be probed and interacting partners labeled for subsequent structural analysis at the single molecule level by qTEM. This allows the composition, conformation and the structure of individual protein assemblies to be investigated. Moreover, quantitative conclusions can be drawn, since relative or even absolute quantification of protein levels can be achieved. This will allow the study of, e.g., pulse chase experiments inducing changes in protein complexes such as inflammasomes,[38] not only on a functional and structural but also on a quantitative level. We foresee that in combination with novel grid preparation techniques, the use of single binding site affinity proteins and new class of detectors in electron microscopy, this methodology will facilitate the processing of single cell extracts by “lyse and spread” visual proteomics[21,22,39] and ultimately will offer a completely new way to study the interaction networks of protein complexes in individual cells.

2.6 Supporting Information

2.6.1 Photograph of the experimental setup

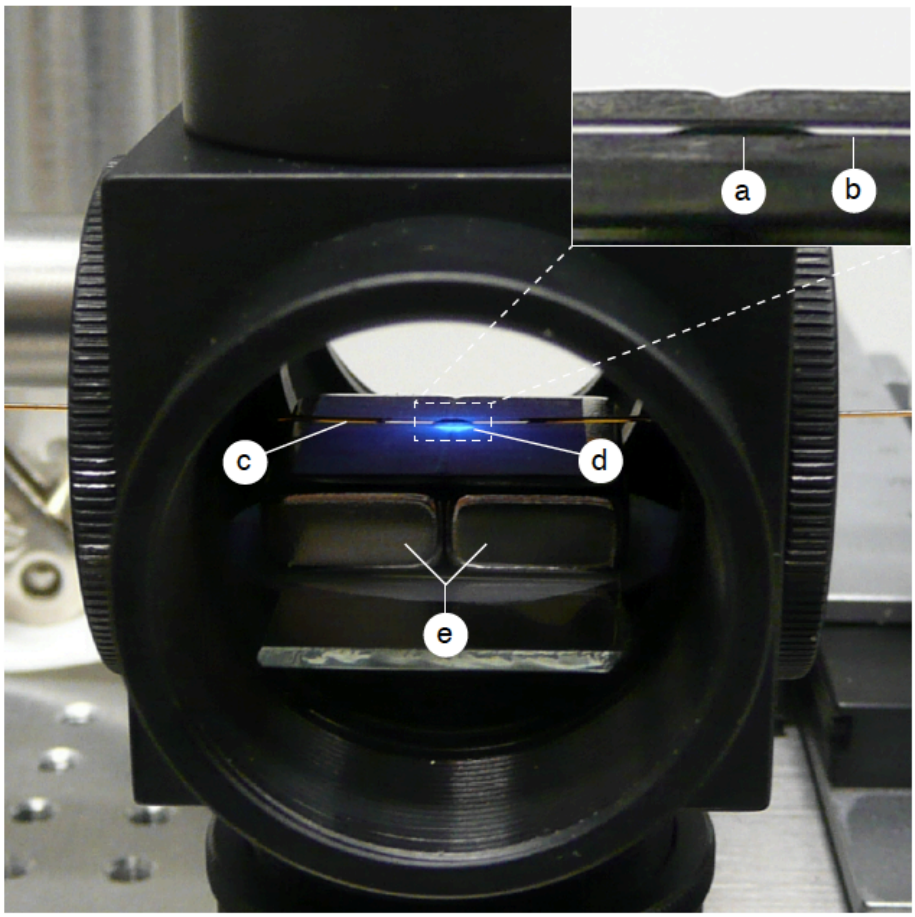

Figure 2-7: *Photograph of the experimental setup and higher magnification photograph of a magnetic bead plug (inset). A fused silica capillary (c) with an inner diameter of 250 µm was guided through a lens tube construction cube. The outer polymer coating of the capillary was removed (b) over a length of 1 cm at the center of the cube to optimize the illumination conditions. About 40*10⁶ magnetic beads (a) with a diameter of 1 µm were captured at the center of the cube by a magnetic trap consisting of two permanent magnets (e). Typically a bead plug with a length of 3 - 4 mm was created. UV-light with a wavelength of 365 nm emitted by a high power UV LED mounted on top of the cube was guided onto the capillary (d).*

2.6.2 Electron micrograph and 2D class averages of apoferritin

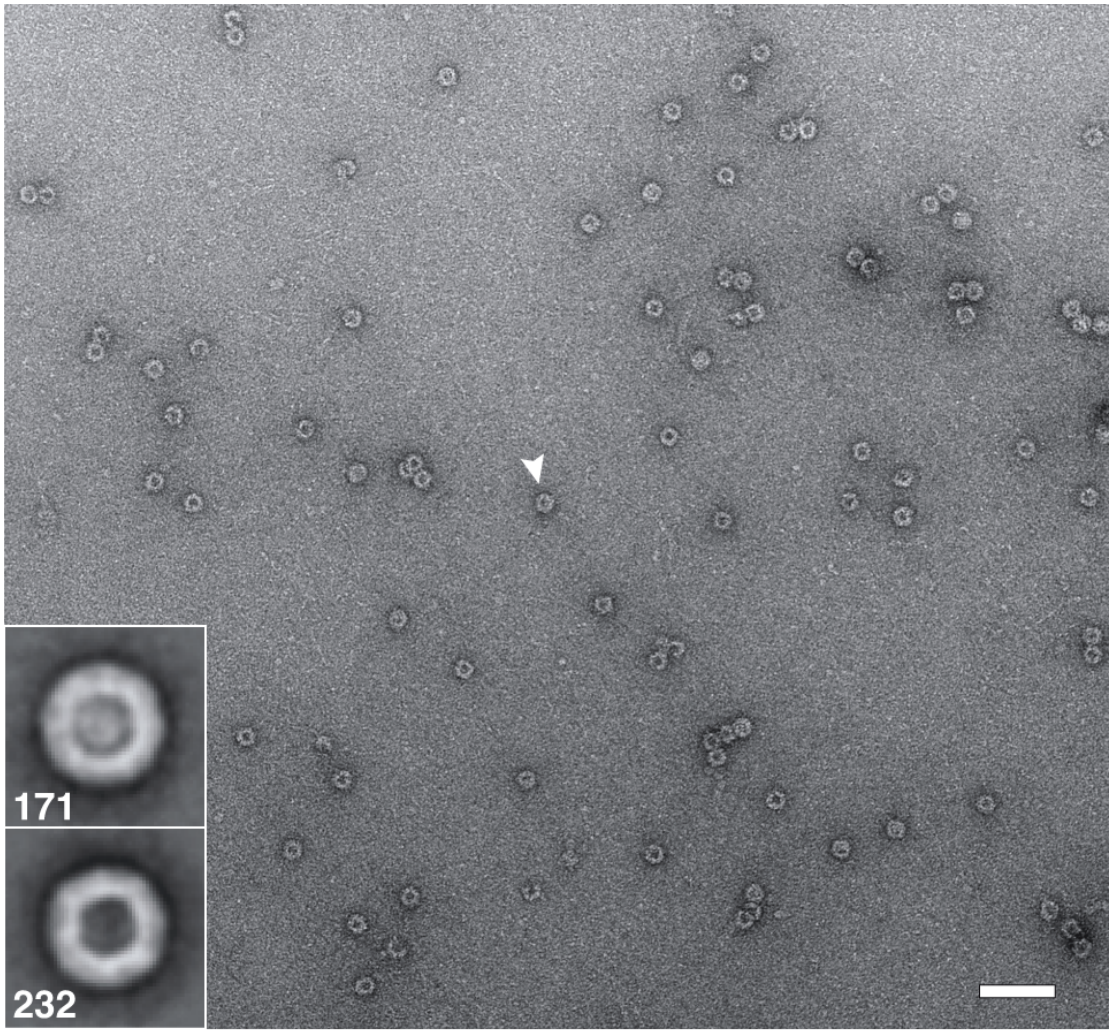

Figure 2-8: *Negative stain transmission electron microscopy (TEM) of apoferritin (AF). A TEM grid was prepared applying a 200 nM solution of AF in PBS, negatively stained and imaged in the TEM. Ring-shaped projections (arrowhead) about 15 nm in diameter typical of AF (molecular weight, 443 kDa) are visible. Insets show representative 2D class averages (bottom left, number of averaged particles). Scale bar, 50 nm.*

2.6.3 Electron micrograph of nonspecifically bound proteins

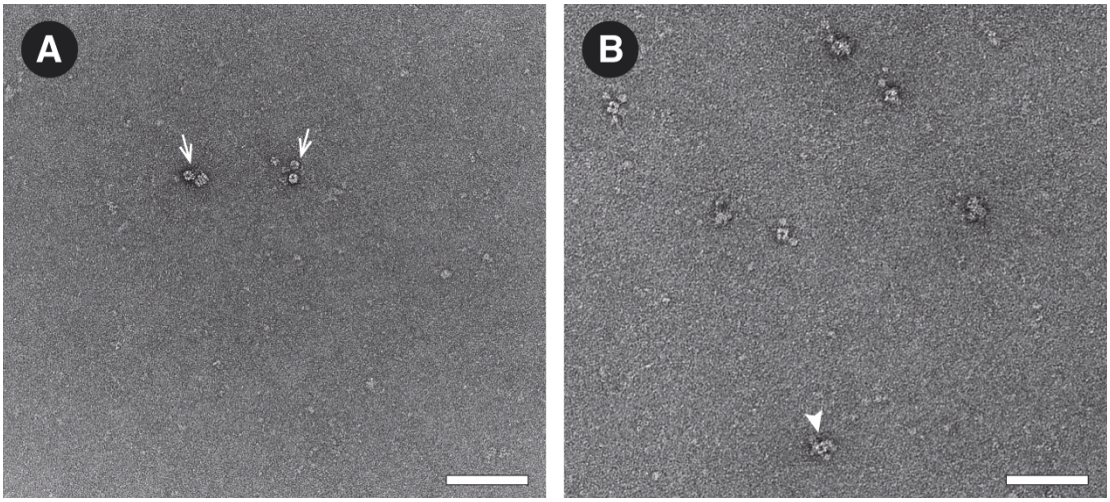

Figure 2-9: *Negative stain electron micrograph of isolated 20S proteasomes (**A**) and nonspecifically bound protein (**B**). The 20S proteasomes of about one hundred thousand HEK293 cells were extracted and recovered using the presented approach. After photocleavage and elution of the released protein complexes (arrows, isolated 20S proteasome conjugates), the trapped beads were rinsed with 4 µl of PBS complemented with 0.5 mM biotin (Sigma-Aldrich #B4501, Switzerland) to competitively release proteins that were nonspecifically bound to the beads or the fused silica surface of the capillary walls. After 5 min incubation, 6 µl of liquid was eluted and used to prepare TEM grids. The eluate contained a lot of protein, which must have been nonspecifically bound to the surfaces. In particular, we observed structures (arrowhead) that strongly resembled pyruvate dehydrogenase complexes.*[40]

The results indicate that the elution by photocleavage acts as a second purification step, since such high concentrations of nonspecifically bound protein were never observed in the experiments. Scale bar, 100 nm.

2.6.4 Factors determining the signal transfer function of the method presented

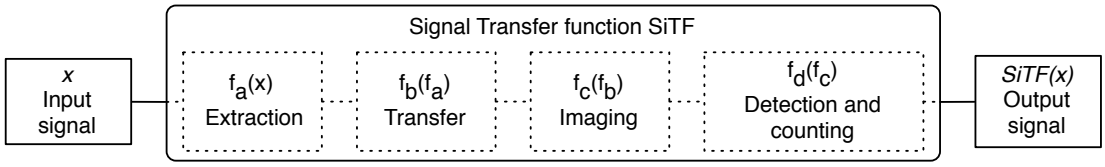

Figure 2-10: *Factors determining the signal transfer function (SiTF) of the presented isolation method. The SiTF correlates the input signal x with the output signal SiTF(x). An example is presented in Figure 2-4, where the initial concentration of apoferritin (AF) particles (input signal) is correlated to the number of recovered AF particles (output signal). The individual factors influencing the SiTF are indicated in dotted boxes (f_a-f_d). f_a: The extraction efficiency is mainly predetermined by the affinity of the antibody (AB) to the target protein, but also includes the binding efficiency of the ABs to the magnetic beads and the photocleavage efficiency. Note that the binding of ABs to the beads is expected to be very efficient due to the strong biotin-streptavidin interaction and the ample binding surface offered by the bead-plug. Furthermore, the AB concentration is a constant throughout the experiments. In general, $f_a(x)$ is a non linear function. If no extraction step is performed, $f_a(x)/x=1$ and the SiTF is determined by the transfer, imaging and detection efficiency alone. f_b: Transfer efficiency of the extracted protein to the transmission electron microscopy (TEM) grid. f_c: Imaging efficiency, i.e., how well the imaging procedure documents the eluted sample (see Figure 2-2). f_d: Detection and counting efficiency, i.e., how reliably the target protein is recognized and counted.*

*Note, that control experiments, where no extraction step was performed and target proteins were directly adsorbed to TEM grids, revealed that SiTF(x)=k*x, with constant k, for a large dynamic range (Supporting Information Figure 2-11).*

2.6.5 Signal transfer function of apoferritin to TEM grids

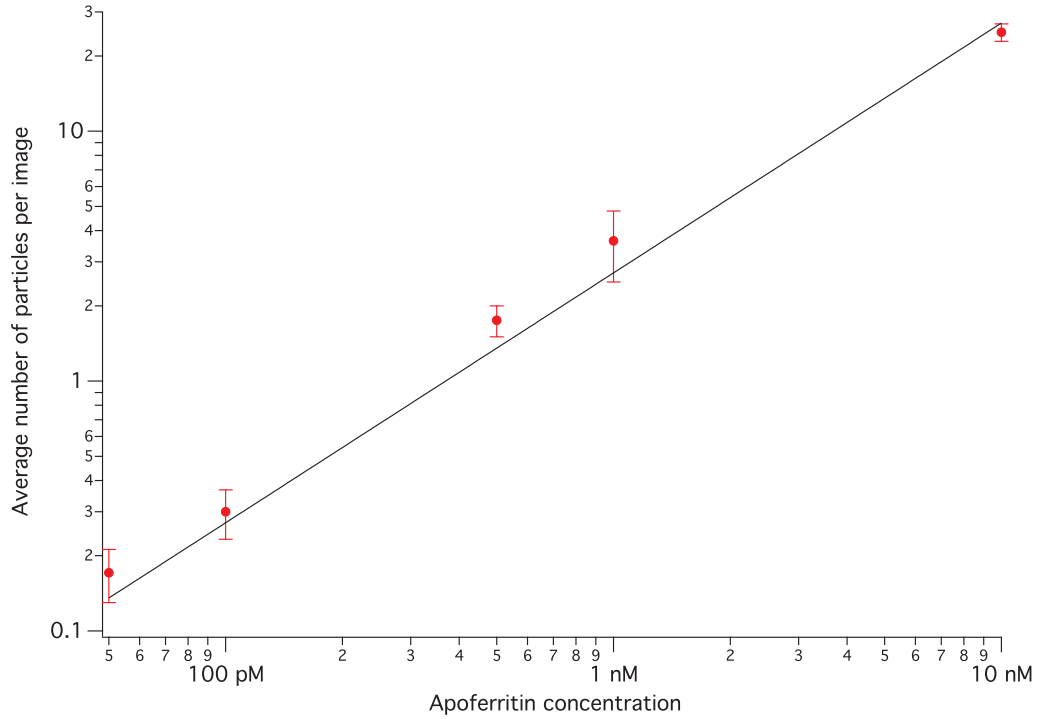

Figure 2-11: *Signal transfer function (SiTF) of apoferritin (AF) particles to transmission electron microscopy (TEM) grids. We performed quantitative TEM (Figure 2-2) of TEM grids prepared with different concentrations of AF (input signal), ranging from 50 pM – 10 nM, to measure the amount of AF particles being adsorbed on the particular TEM grids. Here, the average number of AF particles per recorded image (PPI) for the grid preparations is shown as output signal (red dots). Error bars represent the standard deviation of the average PPIs of the five probed grid squares of the parent grid.*

The data documents that the SiTF function of AF particles to TEM grids is linear (black line: linear fit without offset) if no extraction step is performed ($(f_a(x)/x=1$; see Supporting Information Figure 2-10).

2.6.6 Isolation of endogenous 20S proteasome in PBS buffer

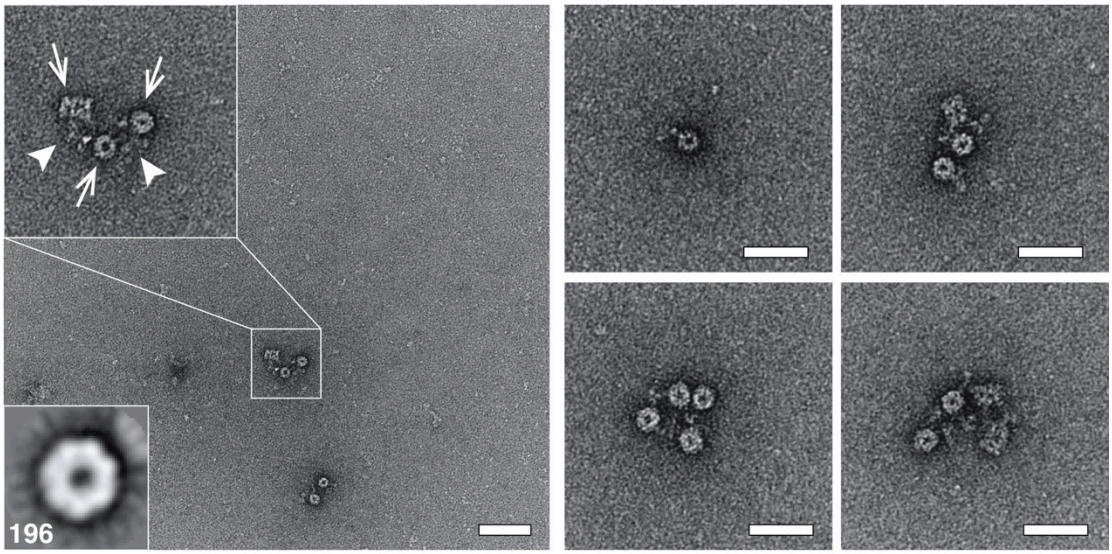

Figure 2-12: *Isolation of endogenous 20S proteasome in PBS buffer. HEK293 cell lysate was incubated with biotinylated anti-20S proteasome antibodies (ABs). The lysate of about twenty thousand cells diluted in PBS buffer was then passed over trapped streptavidin coated magnetic beads to extract 20S proteasome, which was subsequently recovered by photocleavage and transferred onto TEM grids. Both ring-like top views and rectangular side views of the isolated 20S proteasome (arrows) are visible on the images; ABs (arrowhead) can be clearly distinguished and often link 20S proteasomes. The 2D class averages calculated (inset; bottom left, number of averaged particles) were comparable to those of purified proteasomes (Supporting Information Figure 2-13), indicating, that the presence of ABs did not interfere with 2D averaging. Note, that PBS has a higher ionic strength than HEPES buffer, which can destabilize protein-protein interactions such as the 20S-19S proteasome interaction. Indeed, we experienced that the regulatory 19S particles rarely copurify with the 20S core proteasome if PBS was used instead of HEPES (compare to Figure 2-5A&B). Scale bars, 50 nm.*

2.6.7 Electron micrograph and 2D class averages of 20S proteasomes

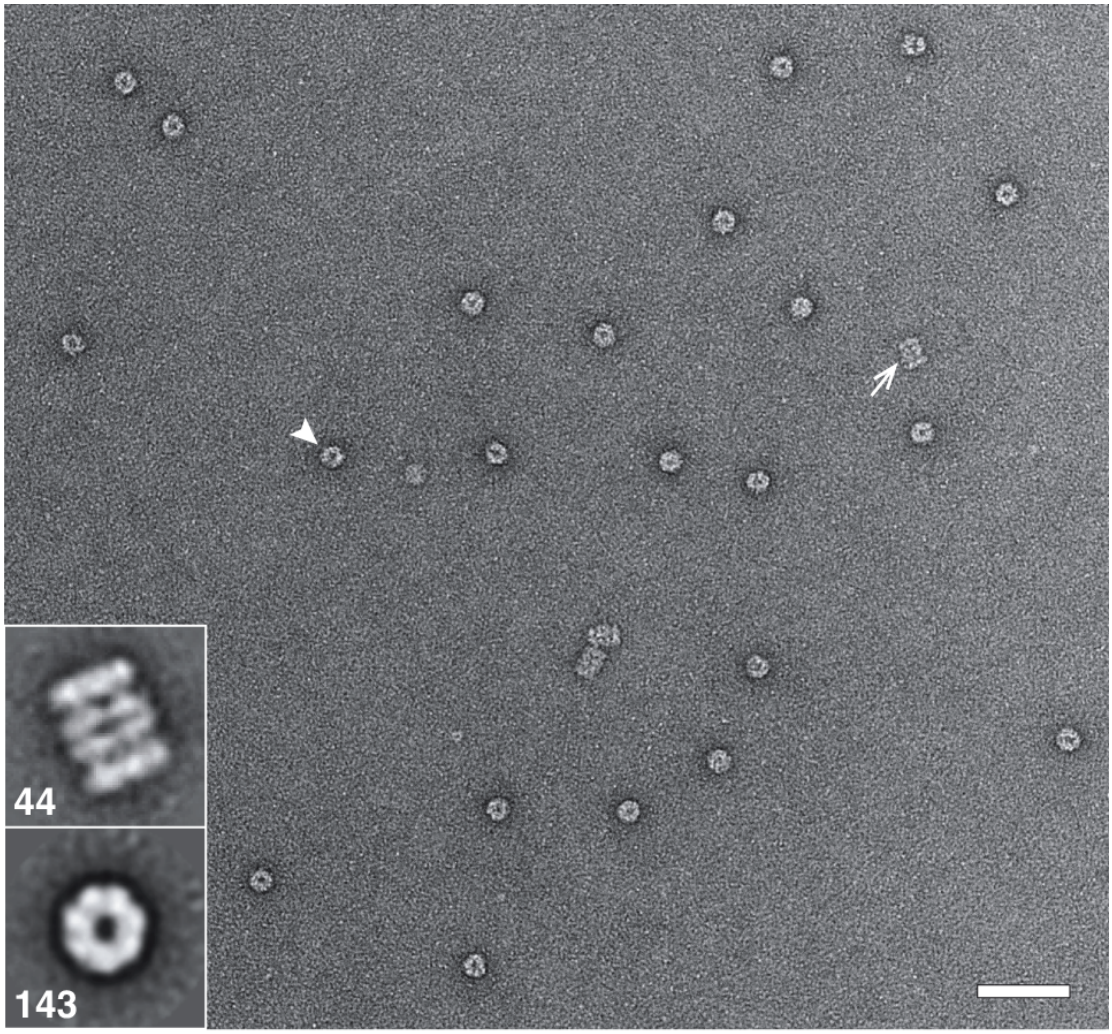

Figure 2-13: *Negative stain transmission electron microscopy (TEM) of purified 20S proteasomes. A TEM grid was prepared by applying a 30 nM solution of purified human 20S proteasomes (Enzo Life Sciences #BML-PW8720) in PBS and imaged by TEM. Ring-shaped top views (arrowhead, 11 nm in diameter) and rectangular side views (arrow, 15 nm in length) are visible. Structural details, such as the seven-fold symmetry, can be distinguished in the calculated 2D class average (inset; bottom left, number of averaged particles). Scale bar, 50 nm.*

2.6.8 COMSOL simulation of temperature rise in capillary and buffer

(A)

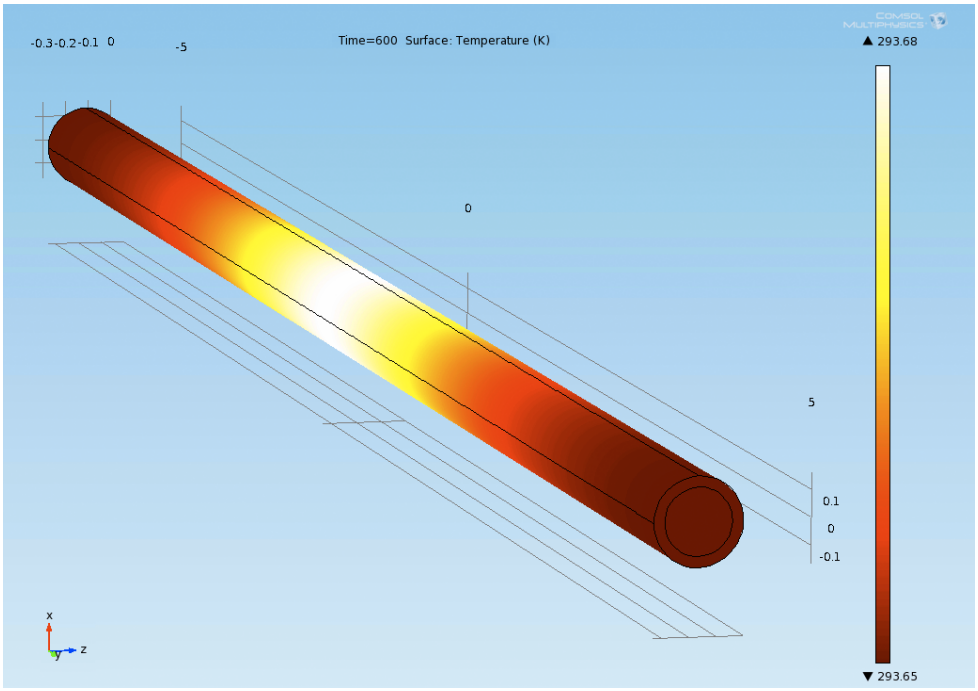

(B)

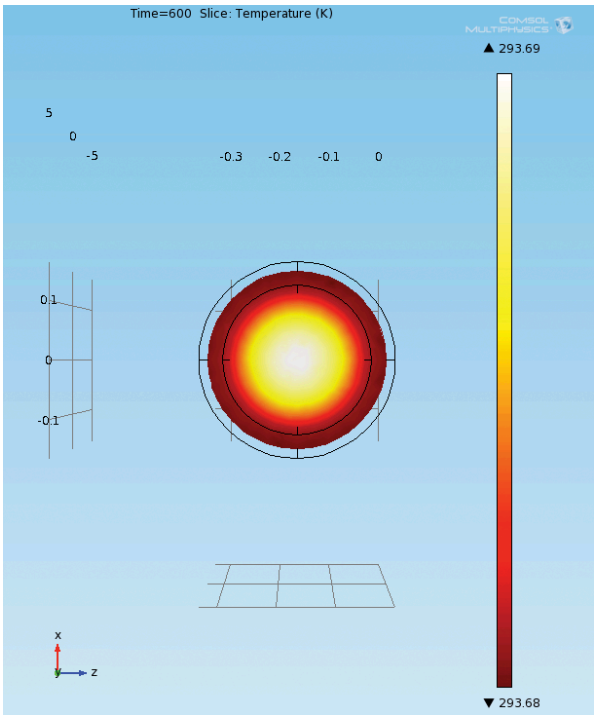

Figure 2-14: *Finite element simulations using COMSOL Multiphysics were performed to simulate the time dependent temperature rise induced in a fused silica capillary filled with PBS buffer by an incident UV-light beam with a wavelength of 365 nm. The capillary was represented by a 10 mm long, hollow cylinder with an inner diameter of 250 µm and a wall thickness of 40 µm. The heat transfer model in COMSOL was used for modeling. The body*

heat load within the liquid was calculated as described in Yang et al.[41] The following assumptions were made to simplify the model: (i) the reflectivity of the fused silica is zero, (ii) there is no heat exchange with the environment and (iii) the input power of the beam does not decay due to absorption by the illuminated material. Further, the body heat load in the fused silica was neglected, as this material is almost transparent for wavelengths between 200 nm and 1 µm.[42] An absorption coefficient of 0.0016/cm, similar to that of water, was used for PBS buffer.[43] Other material properties used in the simulation were from the COMSOL material library. The incident UV-beam was set in the z-direction and represented by a 2D-Gaussian distribution in the xy-plane with an input power of 110 mW (in the experimental setup only about 25% of the emitted 440 mW UV-light is guided to the capillary). The modeled beam dimensions (σ_x: 0.3 mm, σ_y: 0.4 mm) were smaller than the apparent dimensions (elliptical shape, 4 mm long and 3 mm wide). The initial temperature was set as 293.15 K (room temperature).

Figure 2-14A shows the surface temperature of the fused silica tubing after 10 min illumination. Figure 2-14B illustrates the temperature rise at the central cross-section of the capillary. The results show that the temperature rise is maximally about 0.6 K in the fused silica capillary and the liquid. However, several of the assumptions made in the model would be a worst-case scenario. Therefore, the results obtained strongly indicate that, for the experimental setup, there is no UV-light induced temperature rise in the fused silica or the PBS buffer that could affect proteins.

2.7 References

[1] Aderem, A. **Systems biology: its practice and challenges.** *Cell* **121**, 511-3 (2005).

[2] Fields, S.& Song, O. **A novel genetic system to detect protein-protein interactions.** *Nature* **340**, 245-6 (1989).

[3] Walther, T. C.& Mann, M. **Mass spectrometry-based proteomics in cell biology.** *Journal of Cell Biology* **190**, 491-500 (2010).

[4] Uzoma, I.& Zhu, H. **Interactome mapping: using protein microarray technology to reconstruct diverse protein networks.** *Genomics Proteomics Bioinformatics* **11**, 18-28 (2013).

[5] Vidal, M.; Cusick, M. E.& Barabasi, A. L. **Interactome networks and human disease.** *Cell* **144**, 986-98 (2011).

[6] Klockenbusch, C.& Kast, J. **Optimization of formaldehyde cross-linking for protein interaction analysis of non-tagged integrin beta1.** *J Biomed Biotechnol* **2010**, 927585 (2010).

[7] Rudashevskaya, E. L.; Sacco, R.; Kratochwill, K.; Huber, M. L.; Gstaiger, M. *et al.* **A method to resolve the composition of heterogeneous affinity-purified protein complexes assembled around a common protein by chemical cross-linking, gel electrophoresis and mass spectrometry.** *Nature protocols* **8**, 75-97 (2013).

[8] Stengel, F.; Aebersold, R.& Robinson, C. V. **Joining forces: integrating proteomics and cross-linking with the mass spectrometry of intact complexes.** *Molecular & cellular proteomics : MCP* **11**, R111 014027 (2012).

[9] Taatjes, D. J. **The human Mediator complex: a versatile, genome-wide regulator of transcription.** *Trends in biochemical sciences* **35**, 315-22 (2010).

[10] Krogan, N. J.; Cagney, G.; Yu, H.; Zhong, G.; Guo, X. *et al.* **Global landscape of protein complexes in the yeast Saccharomyces cerevisiae.** *Nature* **440**, 637-43 (2006).

[11] Koster, A. J.& Klumperman, J. **Electron microscopy in cell biology: integrating structure and function.** *Nature reviews. Molecular cell biology* **Suppl**, SS6-10 (2003).

[12] Kourkoutis, L. F.; Plitzko, J. M.& Baumeister, W. **Electron Microscopy of Biological Materials at the Nanometer Scale.** *Annu Rev Mater Res* **42**, 33-58 (2012).

[13] Kukulski, W.; Schorb, M.; Welsch, S.; Picco, A.; Kaksonen, M. *et al.* **Correlated fluorescence and 3D electron microscopy with high sensitivity and spatial precision.** *J Cell Biol* **192**, 111-9 (2011).

[14] Baumeister, W. **Electron tomography: towards visualizing the molecular organization of the cytoplasm.** *Current opinion in structural biology* **12**, 679-84 (2002).

[15] Vanhecke, D.; Asano, S.; Kochovski, Z.; Fernandez-Busnadiego, R.; Schrod, N. *et al.* **Cryo-electron tomography: methodology, developments and biological applications.** *Journal of microscopy* **242**, 221-7 (2011).

[16] Nickell, S.; Kofler, C.; Leis, A. P.& Baumeister, W. **A visual approach to proteomics.** *Nature reviews. Molecular cell biology* **7**, 225-30 (2006).

[17] Leis, A.; Rockel, B.; Andrees, L.& Baumeister, W. **Visualizing cells at the nanoscale.** *Trends in biochemical sciences* **34**, 60-70 (2009).

[18] Bohm, J.; Frangakis, A. S.; Hegerl, R.; Nickell, S.; Typke, D. *et al.* **Toward detecting and identifying macromolecules in a cellular context: Template matching applied to electron tomograms.** *Proceedings of the National Academy of Sciences of the United States of America* **97**, 14245-14250 (2000).

[19] Beck, M.; Malmstrom, J. A.; Lange, V.; Schmidt, A.; Deutsch, E. W. *et al.* **Visual proteomics of the human pathogen Leptospira interrogans.** *Nature methods* **6**, 817-23 (2009).

[20] Bouchet-Marquis, C.; Pagratis, M.; Kirmse, R.& Hoenger, A. **Metallothionein as a clonable high-density marker for cryo-electron microscopy.** *J Struct Biol* **177**, 119-127 (2012).

[21] Kemmerling, S.; Arnold, S. A.; Bircher, B. A.; Sauter, N.; Escobedo, C. *et al.* **Single-cell lysis for visual analysis by electron microscopy.** *J Struct Biol* (2013).

[22] Kemmerling, S.; Ziegler, J.; Schweighauser, G.; Arnold, S. A.; Giss, D. *et al.* **Connecting mu-fluidics to electron microscopy.** *J Struct Biol* **177**, 128-34 (2012).

[23] Lim, M.& Rothschild, K. J. **Photocleavage-based affinity purification and printing of cell-free expressed proteins: application to proteome microarrays.** *Analytical Biochemistry* **383**, 103-15 (2008).

[24] Suloway, C.; Pulokas, J.; Fellmann, D.; Cheng, A.; Guerra, F. *et al.* **Automated molecular microscopy: the new Leginon system.** *J Struct Biol* **151**, 41-60 (2005).

[25] Lander, G. C.; Stagg, S. M.; Voss, N. R.; Cheng, A.; Fellmann, D. *et al.* **Appion: an integrated, database-driven pipeline to facilitate EM image processing.** *J Struct Biol* **166**, 95-102 (2009).

[26] Roseman, A. M. **FindEM--a fast, efficient program for automatic selection of particles from electron micrographs.** *J Struct Biol* **145**, 91-9 (2004).

[27] Tang, G.; Peng, L.; Baldwin, P. R.; Mann, D. S.; Jiang, W. *et al.* **EMAN2: An extensible image processing suite for electron microscopy.** *J Struct Biol* **157**, 38-46 (2007).

[28] Bremer, A.; Henn, C.; Engel, A.; Baumeister, W.& Aebi, U. **Has Negative Staining Still a Place in Biomacromolecular Electron-Microscopy.** *Ultramicroscopy* **46**, 85-111 (1992).

[29] da Fonseca, P. C.& Morris, E. P. **Structure of the human 26S proteasome: subunit radial displacements open the gate into the proteolytic core.** *The Journal of biological chemistry* **283**, 23305-14 (2008).

[30] Martin-Benito, J.; Grantham, J.; Boskovic, J.; Brackley, K. I.; Carrascosa, J. L. *et al.* **The inter-ring arrangement of the cytosolic chaperonin CCT.** *Embo Rep* **8**, 252-257 (2007).

[31] Ramadan, Q.& Gijs, M. A. **Simultaneous sample washing and concentration using a "trapping-and-releasing" mechanism of magnetic beads on a microfluidic chip.** *The Analyst* **136**, 1157-66 (2011).

[32] O'Mahony, F. C.; Nanda, J.; Laird, A.; Mullen, P.; Caldwell, H. *et al.* **The use of reverse phase protein arrays (RPPA) to explore protein expression variation within individual renal cell cancers.** *Journal of visualized experiments : JoVE* (2013).

[33] Binz, H. K.; Stumpp, M. T.; Forrer, P.; Amstutz, P.& Pluckthun, A. **Designing repeat proteins: well-expressed, soluble and stable proteins from combinatorial libraries of consensus ankyrin repeat proteins.** *J Mol Biol* **332**, 489-503 (2003).

[34] Cortez-Retamozo, V.; Backmann, N.; Senter, P. D.; Wernery, U.; De Baetselier, P. *et al.* **Efficient cancer therapy with a nanobody-based conjugate.** *Cancer Research* **64**, 2853-2857 (2004).

[35] Conrath, K. E.; Lauwereys, M.; Galleni, M.; Matagne, A.; Frere, J. M. *et al.* **beta-lactamase inhibitors derived from single-domain antibody fragments elicited in the Camelidae.** *Antimicrobial Agents and Chemotherapy* **45**, 2807-2812 (2001).

[36] Ellington, A. D.& Szostak, J. W. **Invitro Selection of Rna Molecules That Bind Specific Ligands.** *Nature* **346**, 818-822 (1990).

[37] Li, X. M.; Mooney, P.; Zheng, S.; Booth, C. R.; Braunfeld, M. B. *et al.* **Electron counting and beam-induced motion correction enable near-atomic-resolution single-particle cryo-EM.** *Nature methods* **10**, 584-+ (2013).

[38] Broz, P.& Monack, D. M. **Molecular mechanisms of inflammasome activation during microbial infections.** *Immunol Rev* **243**, 174-190 (2011).

[39] Engel, A. In *Springer Series Chem*, 2010, pp 417-431.

[40] Yu, X.; Hiromasa, Y.; Tsen, H.; Stoops, J. K.; Roche, T. E. *et al.* **Structures of the human pyruvate dehydrogenase complex cores: a highly conserved catalytic center with flexible N-terminal domains.** *Structure* **16**, 104-14 (2008).

[41] Yang, S. T.; Matthews, M. J.; Elhadj, S.; Cooke, D.; Guss, G. M. *et al.* **Comparing the use of mid-infrared versus far-infrared lasers for mitigating damage growth on fused silica.** *Applied Optics* **49**, 2606-2616 (2010).

[42] Kitamura, R.; Pilon, L.& Jonasz, M. **Optical constants of silica glass from extreme ultraviolet to far infrared at near room temperature.** *Appl Opt* **46**, 8118-33 (2007).

[43] Hale, G. M.& Querry, M. R. **Optical-Constants of Water in 200-Nm to 200-Mum Wavelength Region.** *Applied Optics* **12**, 555-563 (1973).

3 Microfluidics to isolate untagged proteins from cell extracts for visual analysis by electron microscopy

The following section has been published in:

Proceedings of the 17th International Conference on Miniaturized Systems for Chemistry and Life Sciences (MicroTAS), Germany, 2013

pp. 1785-1787, ISBN 978-0-9798064-6-9

Microfluidics to isolate untagged proteins from cell extracts for visual analysis by electron microscopy

Dominic Giss, Simon Kemmerling, Venkata Dandey,

Henning Stahlberg and Thomas Braun*

Center for Cellular Imaging and NanoAnalytics (C-CINA), Biozentrum,

University of Basel, Switzerland.

*Corresponding Author: Thomas.braun@unibas.ch

Keywords: Microfluidics, Magnetic Beads, Photocleavage, Proteomics, Electron Microscopy

3.1 Abstract

A simple microfluidic method for the isolation and analysis of endogenous levels of untagged protein complexes from minute amounts of cell lysate is presented. The method is based on antibodies (ABs) that are conjugated via a photocleavable linker to magnetic beads being trapped in microcapillaries by magnetic field gradients. Target proteins can be released together with their trapping ABs by photocleavage for their subsequent analysis, e.g., by transmission electron microscopy (TEM). The advantages of elution by photocleavage over classical methods are: (i) Mild recovery of proteins without changing the physiological environment and, (ii) nonspecifically adsorbed proteins are only minimally eluted.

3.2 Introduction

The investigation of multimolecular protein complexes in terms of their architecture, conformation, structure and temporal persistence is a key element of experimental systems biology. However, to date, the instrumentation for the analysis of these complexes is still poorly developed, in particular, the isolation and subsequent analysis of such complexes. Several obstacles must be overcome for these studies, e.g., the quaternary structure of these protein assemblies must be maintained and, due to the heterogeneous composition of these complexes, the analysis should be performed at single molecule level. Here we present a fast and simple microfluidic method for the isolation of large multimolecular protein complexes from cell lysate and the subsequent visual analysis of the assemblies at the single molecule level by TEM. The method allows the isolation under mild and physiological conditions and exhibits only minimal background contamination.

3.3 Functional principle

Streptavidin coated magnetic beads were trapped in a fused silica capillary by two external magnets (Figure 3-1A&B). ABs, conjugated to photocleavable biotin crosslinkers, were mixed with cell lysate to bind the target protein and then immobilized on the trapped streptavidin-beads. Subsequent washing of the capillary separated the immobilized target structures from other contaminants (Figure 3-1B). Recovery of proteins was achieved by illumination of the capillary with UV-light (Figure 3-1C) followed by elution of proteins for analysis, e.g., by TEM.

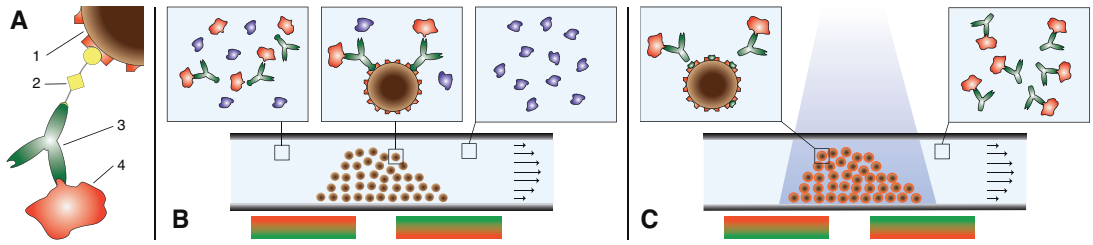

Figure 3-1: *Working principle of the method.* ***A****: Scheme of the composite material used for protein extraction. (1) Streptavidin coated magnetic bead; (2) photocleavable NHS-Biotin crosslinker; (3) antibody against target structure; (4) target structure.* ***B****: Affinity extraction of protein-antibody conjugates.* ***C****: Recovery of immobilized target proteins by photocleavage.*

3.4 Experimental

ABs were biotinylated by incubating with a 10-fold molar excess of photocleavable NHS-biotin crosslinker (Ambergen, USA) for 1.5 h at pH 8.2. The reaction mixture (50 µl) was then dialyzed over night against 2 l of PBS using dialysis buttons (13 kDa cut-off) to remove unbound crosslinker. HEK293 cells were lysed using a tip sonicator and diluted to a concentration of 10000 - 35000 cells / µl. A 250 µm inner-diameter fused silica capillary (BGB Analitik AG #TSP-250350, Switzerland) was guided through a lens tube construction cube (Thorlabs #SM1C6, Germany) providing protection from UV-light and easy mounting of optical components (Figure 3-2A). About $40*10^6$ streptavidin coated magnetic beads (Dynabeads® MyOne™, Invitrogen #656-01, Switzerland) of 1 µm diameter were loaded into the capillary at a flow rate of 20 µl/min and captured in the center of the cube by a magnetic trap consisting of two external permanent magnets (Supermagnete #Q-20-10-05-N, Switzerland). Typically, a bead plug with a length of 3 – 4 mm was created (Figure 3-2B&C). UV-light at 365 nm wavelength was emitted by a high power UV LED (Thorlabs #M365L2, Germany) mounted on top of the cube and focused onto the magnetic beads. To bind the target protein, biotinylated ABs against target structures were incubated for one hour with cell lysate. 2 µl of the AB / cell lysate mixture was flown over the trapped beads for 15 min. Thereby ABs could bind to the beads for ~ 60 s. After the affinity extraction step, the capillary was rinsed with 200 µl of buffer at flow rates of 20 – 40 µl/min to separate unbound proteins from immobilized targets. Immobilized proteins were released by illumination of the capillary for 10 min and recovered by subsequent elution of released targets in 6 – 8 µl of buffer. The eluted protein was then transferred onto TEM sample carriers and analyzed by TEM.

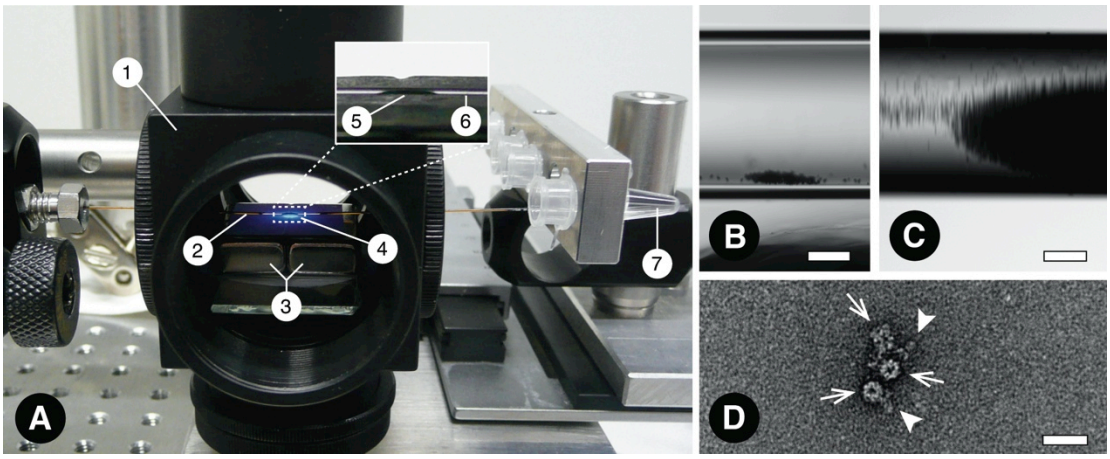

***Figure 3-2**: **A**: Experimental setup used for the experiments. Inset: higher magnification showing a magnetic bead plug. (1) Lens tube construction tube; (2) fused silica capillary (250 µm ID); (3) permanent magnets, building a magnetic trap; (4) UV-light of 365 nm wavelength, focused onto the magnetic bead plug; (5) magnetic bead plug of 3 – 4 mm length; (6) capillary without outer polymer coating; (7) sample container mounted on x,y-stage. **B and C**: The formation of a bead plug by a magnetic trap, built by the magnetic field gradient of a permanent magnet. Scale bars, 50 µm. **D**: Negative stain electron micrograph of endogenous 20S proteasome (arrow; anti-20S proteasome antibody, triangle) that was isolated from HEK293 cell lysate. Scale bar, 25 nm.*

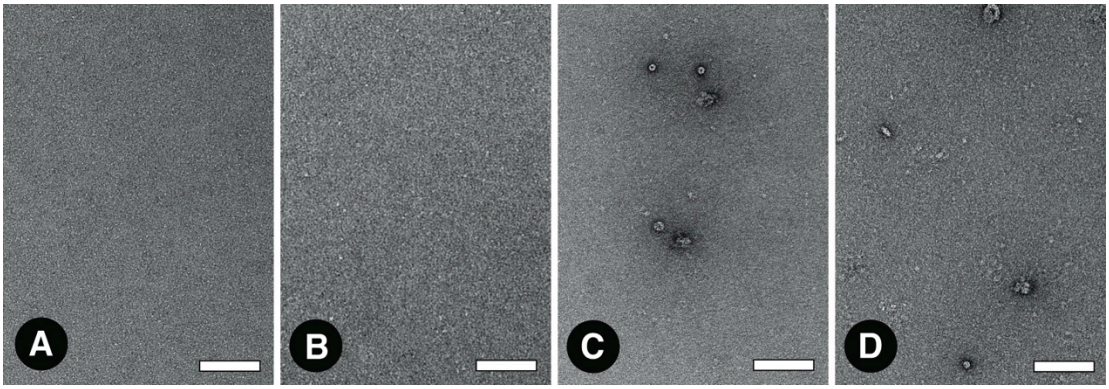

***Figure 3-3:** Comparison of contaminant background of photocleavage and competitive elution by biotin and imidazole. 3 µl of the lysate of approximately 105 cells were incubated for 15 min on a magnetic bead plug (Fig 2). Subsequently, different elution procedures were studied by TEM. **A:** Negative control using PBS buffer. **B:** Eluate obtained in PBS by illumination of the beads for 10 min with UV-light. **C:** Eluate obtained by rinsing the beads for 5 min with 0.5 mM biotin in PBS buffer. **D:** Eluate obtained by rinsing the beads for 5 min with 500 mM imidazole in PBS buffer. Scale bars, 100 nm.*

3.5 Results and discussion

The method enabled the isolation of endogenous levels of 20S proteasomes from twenty thousand HEK293 cells (Figure 3-2D). The concentration of contaminants in the resulting eluates was extremely low, as indicated by the clean background observed in TEM preparations. The recovery of immobilized proteins by photocleavage is more specific than classical chemical procedures, e.g., by competitive elution. Proteins that are nonspecifically bound to the beads or the capillary surface are not significantly released during the photocleavage

step (Figure 3-3). However, the change in the buffer conditions during elution with biotin or imidazole, both often used for competitive elution, significantly released contaminants from the beads and the microcapillary surface.

Time series varying the illumination time for the "photoelution" showed a saturation behavior and the amount of recovered protein only slightly increased beyond 10 min of illumination (Figure 3-4). Subsequent competitive elution after 10 min of illumination, e.g. by biotin solutions, did not release more target protein. We estimate the overall isolation efficiency of the method to be around 10 – 20%.

Finite element simulations estimate the UV-light induced temperature rise in the fused silica capillary and liquid to be lower than 0.6 K for 10 min of illumination, which usually does not affect protein structures. The elution by photocleavage enables mild and unperturbed recovery of proteins conserving their structural integrity since physiological conditions can be easily maintained and proteins usually do not absorb at the wavelength employed for photocleavage.

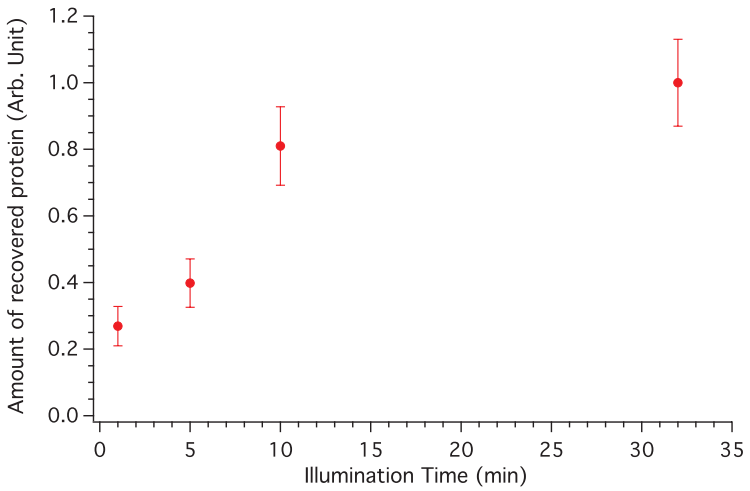

Figure 3-4: *Effect of illumination time on the recovery of protein. Equal quantities of magnetic beads, coated with biotinylated anti-ferritin AB-apoferritin conjugates, were loaded (Fig 2) and illuminated for different time periods. The amount of eluted conjugates was analyzed employing quantitative TEM. The average amount of recovered particles is shown. Error bars represent the standard deviation illustrating the distribution on the particular TEM sample carrier.*

3.6 Conclusion

The method presented combines magnetic beads being trapped in microcapillaries, with the usage of photocleavable crosslinkers, for unperturbed and specific recovery of target structures. Nonspecifically bound proteins are eluted only at minimal concentrations. This is crucial in microfluidics exhibiting high surface to volume ratios and the visual analysis by TEM. Using TEM, the resulting eluates can be investigated for the composition, conformation and the structure of individual protein assemblies. In future, the presented method will be combined with our new microfluidic sample deposition technique for TEM[1] and a method for the lysis of single cells.[2] The former technique enables a very efficient transfer of proteins onto TEM sample carriers, which will significantly

lower the detection limit of the presented method, offering the potential even the lysates of single cells to be processed.

3.7 References

[1] Kemmerling, S.; Ziegler, J.; Schweighauser, G.; Arnold, S. A.; Giss, D. *et al.* **Connecting mu-fluidics to electron microscopy.** *J Struct Biol* **177**, 128-34 (2012).

[2] Kemmerling, S.; Arnold, S. A.; Bircher, B. A.; Sauter, N.; Escobedo, C. *et al.* **Single-cell lysis for visual analysis by electron microscopy.** *J Struct Biol* **183**, 467-73 (2013).

4 Protein quantification by single particle transmission electron microscopy

The following section has been formatted for submission to The Journal of Structural Biology:

Protein quantification by single particle transmission electron microscopy

Dominic Giss, Henning Stahlberg and Thomas Braun*

Center for Cellular Imaging and NanoAnalytics (C-CINA), Biozentrum, University of Basel, Switzerland.

*Corresponding Author: Thomas.braun@unibas.ch

Keywords: Protein Quantification, Electron Microscopy, Quantitative Proteomics

4.1 Abstract

Protein quantification is important to many biological fields, but notoriously difficult to achieve. We propose the use of single particle transmission electron microscopy (TEM) to directly count individual protein complexes and thereby determine the concentration of protein solutions. We provide a workflow for the efficient and reliable measurement of particle densities on TEM grids, and show that the number of protein complexes detected linearly depends on the sample concentration over a large range. Importantly, this technique requires only minimal amounts of protein in the femtomol range and utilizes standard experimental equipment readily available in many laboratories. We envisage its use for quantitative proteomics of complex biological samples.

4.2 Introduction

Protein quantification is a fundamental requirement in many biological and biomedical experiments. Classical methods measure optical densities at high protein concentrations, respectively, require the use of dyes or radioactive labels. To date, the gold standard methods for quantitative proteomics are mass spectroscopy[1] and two-dimensional gel electrophoresis.[2,3] However, these methods are in general not well suited to resolve the abundances of large multimolecular protein complexes and their particular subcomplexes transiently and dynamically formed. Hence, such complexes must be characterized by a technique capable of analysing single molecules.

Single particle transmission electron microscopy (TEM) is such a technique, and we recently developed the methodology required to exploit it for qualitative proteomics.[4] It was demonstrated that proteins and membrane fragments present in the lysate of a single cell can characterized by negative stain TEM. This long-established electron microscopy technique delivers structural information at a resolution of ~20 Å.[5,6] The challenge is now to complement the gathered qualitative information with quantitative data by measuring the respective occurrences of the individual proteins on the TEM grid. This has two hurdles. First, identification of a particular protein species in the complex mixture present in whole cell lysates is difficult. Second, the extent to which a particular protein adsorbs to the TEM grid surface and how this relates to the actual concentration in the cell is generally not known. These issues might explain why, to our knowledge, to date there is not a single publication on quantitative proteomics by negative stain, single particle TEM. Though this technique has been successfully used to determine the concentration of relatively large purified biomolecules, such as viruses.[7] In these studies, the adsorption issue was overcome by adding a known concentration of a reference particle with similar adsorption characteristics to the viruses to the sample. To eliminate the first hurdle, we recently developed a quantitative isolation method[8] to reduce the complexity of biological samples. Thereby, we were able to measure the particle density on the TEM grids using negative stain single particle TEM in combination with a semi-automatic imaging routine, and relate this measurement to the actual protein concentration opening the way for quantitative measurements.

Here we elaborate on the fundamental aspects of protein quantification by negative stain single particle TEM, and propose a workflow for the reliable and efficient measurement of protein concentrations using standard equipment readily available in many laboratories.

4.3 Principle, methods and proof-of-concept

The proposed method to measure the concentration of a protein solution using negative stain single particle TEM is illustrated in Figure 4-1. First, a protein solution of unknown concentration is applied to carbon-coated TEM grids. Some of the proteins adsorb to the carbon surface, the amount depending on the physiochemical properties of the protein, its concentration and the TEM grid preparation protocol. Second, the average particle density on the grid is measured by recording TEM images at various positions and detecting the particles on the acquired images. Here a compromise between measurement accuracy and efficiency must be found. We propose a workflow that determines the number of images to be collected depending on the applied protein concentration and the demanded measurement accuracy. Third, the measured average particle density can be directly compared to measurements preformed with other protein concentrations to reveal relative changes in protein levels.. Absolute quantification of protein concentrations can be achieved once the respective transfer function for each protein is known, i.e. after a calibration has been made.

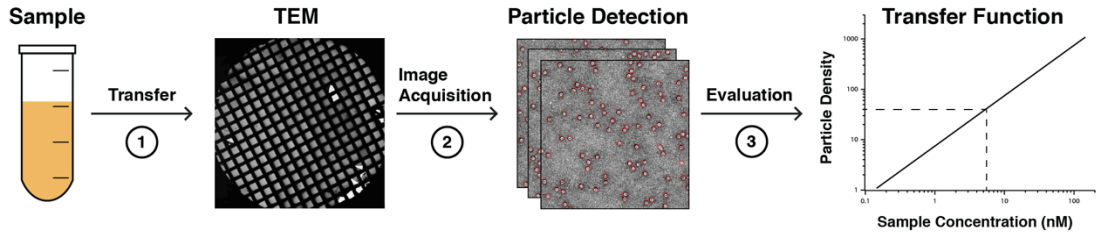

Figure 4-1*: Protein quantification by (negative stain) single particle TEM.* ***Step 1:*** *Sample solution of unknown protein concentration is applied to a TEM grid.* ***Step 2:*** *The particle density on the TEM grid is measured by collecting images at a series of positions and subsequent image processing, i.e, particles are detected, classified according to shape (mixed samples only) and counted.* ***Step 3:*** *The measured particle density is used to determine relative sample concentrations or absolute concentrations if the respective transfer function for the particular protein is known.*

4.3.1 Methods

To validate the proposed approach, we prepared TEM grids by applying solutions of 20S proteasomes at various concentrations and measured the average particle densities on the grids to study the transfer functions of the protein. The basic protocols were as follows:

A stock solution of purified 20S proteasomes (#BML-PW8720-0050, Enzo Life Sciences) was diluted to concentrations ranging from 0.18 nM to 180 nM in PBS. Three TEM grids were prepared by a standardized protocol for each concentration: 3.5 µl of the protein solution were incubated for 90 s on glow-

discharged carbon-coated 200-mesh copper TEM grids. Subsequently, the grids were washed five times for 12 s on double-distilled H_20 and negatively stained on two 4.5 µl drops of 2% uranylacetate for 3 and 15 s, respectively. After every incubation and washing step, excess liquid was removed using blotting paper. To investigate the transfer function of other proteins, we prepared one grid per concentration of apoferritin (0.05 – 100 nM, diluted in PBS, Sigma-Aldrich #A3660, Switzerland) and *Cerura* biliprotein (CBP, 2.6 – 128 nM, diluted in PBS, kindly provided by H. Kayser, Institut für Allgemeine Zoologie und Endokrinologie, Universität Ulm, Germany).[9]

The prepared TEM grids were systematically imaged (Figure 4-2) on an FEI T12 electron microscope operated at 100 kV using the Leginon 2.1 software.[10] Images were recorded on a Gatan 2k x 2k CCD camera employing a semi-automatic image acquisition routine (Figure 4-2). Up to 30 squares per grid were manually targeted, followed by the automatic acquisition of 16 – 400 images per square (depending on the particle concentration, as discussed later) at 12000x magnification (pixelsize: 0.8725 nm, defocus: 1.0 - 1.8 µm, dose: 22 - 35 electrons/$Å^2$). Note that the magnification was kept constant for all experiments. Subsequently, the particles were identified by their visual appearance in negative stain, and counted using the Appion 2.1 software[11] in combination with a template picking routine.[12] Finally, the average particle density for a grid particular square and for the entire grid was calculated employing custom-made Python scripts. For simplicity images recorded at 12000x magnification are termed 'standard images', the area imaged being the unit area used to calculate particle densities. The particle density is the number of detected particles per imaged area and the average particle density the average number of particles per standard image (PPI) of a grid square (square average) or an entire grid (grid average).

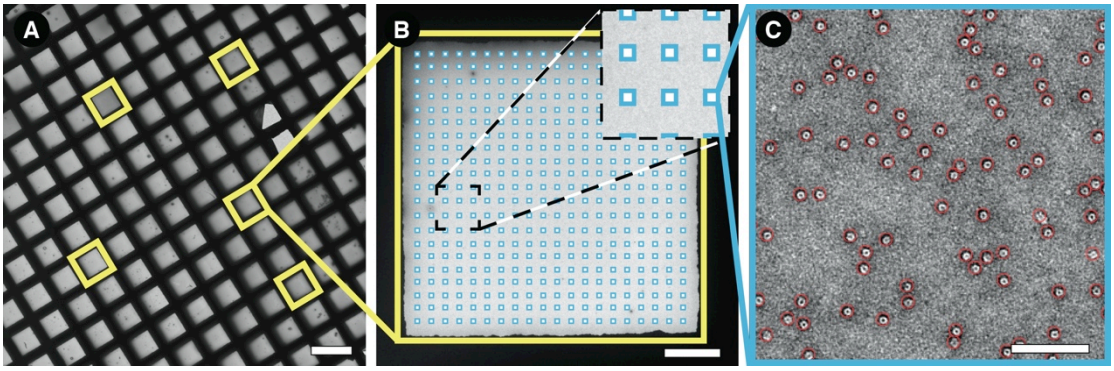

Figure 4-2: *Data acquisition.* ***A:*** *Carbon-coated 200-mesh copper TEM grid. The yellow frames mark five randomly selected squares.* ***B:*** *Overview of a square. The blue frames mark the positions of the images acquired, in this example 20 rows of 20 images. Inset: 3x enlarged region.* ***C:*** *Acquired image. Red circles highlight detected particles. The number of particles detected on one of these images (termed standard images) is defined as the particle density. For practical reasons we refer to the particle density as the number of "particles per (standard) image" or PPI. The terms "square average" and "grid average" denote the average number of particles per image for a particular square or grid, respectively. Scale bars, 150 µm (**A**), 15 µm (**B**) and 200 nm (**C**).*

4.3.2 Determining the number of images to be collected

To evaluate how many standard images must be collected per grid to perform efficient but still precise measurements of particle densities, we analyzed the particle distribution on a single square of a grid for different applied concentrations of 20S proteasomes. A histogram of the different PPIs measured for standard images recorded at multiple positions within the grid square, is shown in Figure 4-3A. The values have a normal distribution for high applied concentrations of 20S proteasome, and a Poisson distribution for low concentrations. The collected standard images were also used to determine how the square average depends on the number of standard images recorded and averaged, for a range of applied sample concentrations (Figure 4-3B). First, all standard-image PPIs were averaged to obtain the 'true' square average. Random subsets containing different numbers of collected images were then created. For each subset, the PPIs were averaged and the mean relative error of the average value with respect to the 'true' square average was calculated.[13] Generally, the higher the applied sample concentration the lower the number of standard images required to achieve a given accuracy. In subsequent measurements, the number of images collected per square was adjusted so that the expected error was less than 6%.

In a second step, we investigated how particles are distributed across the entire grid, by probing a total of 30 randomly selected squares of a grid prepared by applying a high concentration of 20S proteasomes. The measured square averages are shown in Figure 4-3C. The same 30 squares were used to calculate the grid average, and to investigate the dependence of the mean relative error of the grid average on the number of squares (Figure 4-3D). Based on these findings, we decided to acquire data from five squares per grid for subsequent measurements; expected error less than 6%.

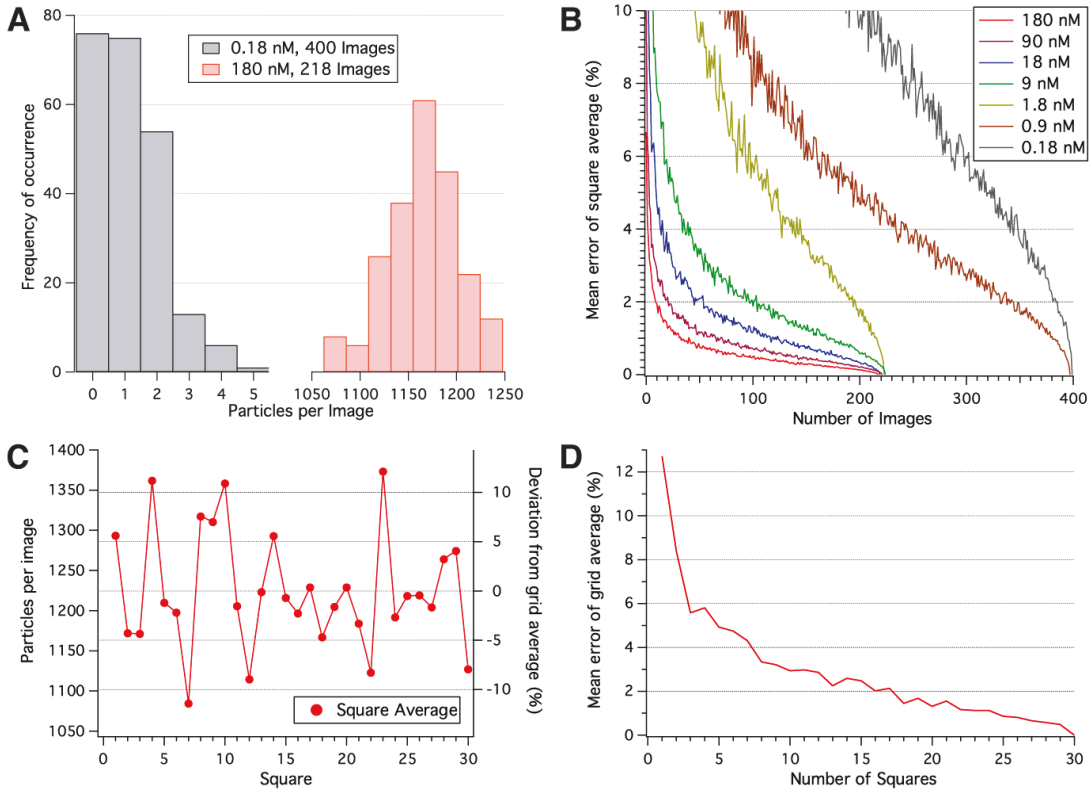

Figure 4-3: *Data requirements, accuracy and reproducibility.* ***A:*** *Histogram showing the occurrence of a particular PPI within a grid square.* ***B:*** *Dependence of the mean error of the square average at 95.4% confidence on the number of standard images averaged for a range of applied sample concentrations.* ***C:*** *Average particle density on 30 randomly selected squares of a grid prepared using a 180 nM 20S proteasome solution.* ***D:*** *Dependence of the mean error of the grid average at 95.4% confidence on the number of squares averaged; applied sample concentration of 180 nM.*

4.3.3 The deviation of particle densities over several grids

We investigated the deviations of measured particle densities over several grids prepared with the same sample solution to assess the reproducibility of our measurement approach and the grid preparation protocol. To this end, we collected data from three grids per 20S proteasome concentration. Based on the findings presented in Figures 4-3B&D, we probed five squares per grid and collected between 16 and 400 images per square, to calculate the respective grid averages (Figure 4-4). Independent of the applied sample concentration, the particle concentration over grids prepared with the same sample concentration differed by 8% on average (5%). Note that for a particular sample concentration we always prepared three grids consecutively within minutes. For the 180 nM solution of proteasomes, two grids were prepared 16 hours after the first grid, which resulted in significantly lower particle densities on these grid explaining the high peak-to-peak deviation. We attribute this effect to a decrease of the protein concentration in the sample vial caused by nonspecific adsorption of protein to the vial walls incurred during the 16 hours of storage.

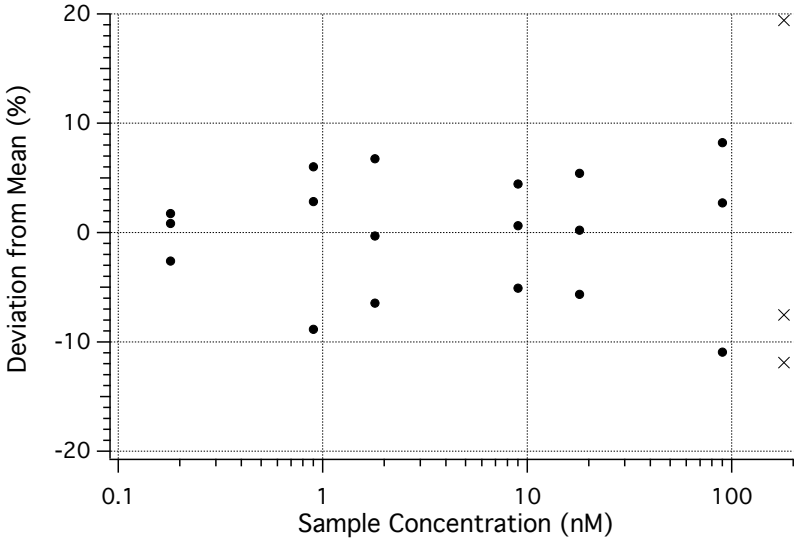

Figure 4-4: *Relative deviations of particle densities over three grids prepared using the same 20S proteasome sample. Seven different sample concentrations were investigated. Five squares were always probed per grid, and the number of standard images recorded per square was matched to the concentration of the applied sample (Figure 4-3B). The three grids examined for a given applied sample concentration were prepared within minutes, resulting in particle densities that differed by 8% on average (dots) and 18% peak-to-peak. For the 180 nM concentration (crosses) two grids were prepared 16 hours after the first grid, in both cases resulting in lower particle densities.*

4.3.4 The transfer function of different proteins

We measured particle densities on grids prepared with different proteins at various concentrations to investigate their transfer functions (Figure 4-5). For the 20S proteasome, the average of three grids per concentration is shown, and a linear response was measured over three orders of magnitude (0.18 – 180 nM, 0.63 fmol to 630 fmol in the 3.5 µl of solution applied to the grid). Deviations from this linear behaviour are mainly attributed to pipetting errors incurred during sample dilution. It is unlikely that deviations are exclusively caused by measurement inaccuracies, since particle densities were measured and averaged from three grid preparations per sample and measurement and grid preparation protocols were shown to be very reproducible (Figure 4-3 and 4-4). A similar transfer function to that of 20S proteasomes was found for apoferritin. Note that the apoferritin data consists of measurements we reported in Giss *et al*. 2014[8] complemented with novel concentration measurements. For CBP we experienced a saturation of particle concentrations starting between 1000 and 2000 PPI. This non-linear behaviour is due to the limited binding surface on the grid, which starts to become saturated at high sample concentrations. For a particle density of 2000 PPI, 13% of the carbon surface is covered with CBP.

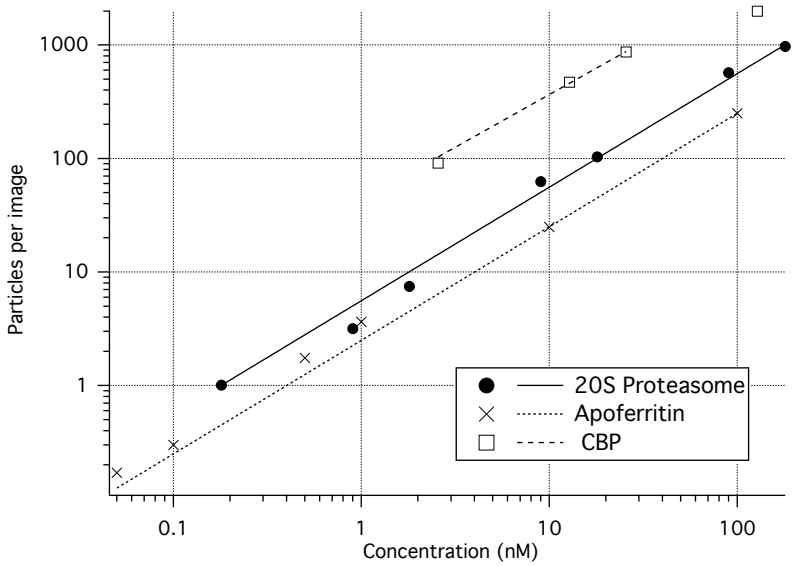

Figure 4-5: *Transfer function for 20S proteasome, apoferritin and CBP. The data indicates that the amount of particles transferred to a TEM grid depends linearly on the applied sample concentration over several orders of magnitude (lines: linear fit without offset). For high concentrations, i.e. between 1000 and 2000 PPI, the grid surface starts to be saturated (13% coverage of surface) and marks the upper limit of the linear range.*

4.4 Discussion and conclusions

We have developed a method for the efficient and reliable measurement of protein concentrations by negative stain single particle TEM. In order to minimize the amount of data required, we proposed a workflow that determines the number of images to be collected based on the applied sample concentration and the demanded accuracy (Figure 4-3). The lower the concentration of the applied sample the lower the particle density on the grid and the more standard images have to be acquired to perform accurate concentration measurements. Thus, automated image acquisition can drastically accelerate data acquisition; in particular for low concentrated samples were hundreds of standard images are required. However, automation is not a necessity for sample concentrations resulting in particle densities of 100 - 1000 PPI, since only ten standard images are needed per square to achieve accurate results (Figure 4-3B).

As illustrated in Figure 4-4, grids prepared with the same sample solution exhibit particle densities that differed 8% on average. This finding documents the reproducibility of the measurement approach and of the grid preparation protocol. The maximal particle concentration difference was found to be about 18%, which is comparable to the measurement accuracy of other methods used for protein quantification.[14]

As seen in Figure 4-5, the number of particles adsorbed to TEM grids depends linearly on the applied sample concentration over several orders of magnitude. This linear response allows the relative quantification of protein concentrations, i.e., the measured particle density on a grid can be related to another measurement made for the same protein, e.g. at another time point in the cell-cycle. Furthermore, our findings indicate that absolute quantification can be

achieved if a simple calibration is carried out using a known concentration of the particular protein species. In our hands, for the given grid preparation protocol the presented method allowed the straightforward measurement of protein concentrations ranging from 50 pM to 200 nM. Such low concentrations are typically difficult to assess by absorbance-based methods. Importantly, the amount of protein used for concentration determination is in the low femtomol range.

We experienced that the amount of protein adsorbed to the carbon surface at a given protein concentration differed for every protein (Figure 4-5). Applying 3.5 µl of a 100 nM protein solution to the grid resulted in particle densities of about 700 PPI for the 20S proteasome and about 250 PPI for apoferritin, corresponding to transfer efficiencies of about 0.6% and 0.25%. These variations will relate to the surface properties of the protein and the support surface and how well they are matched, being influenced by factors such as buffer, temperature and protein concentration itself. Retaining the same protocols throughout, allowed reproducible grids to be prepared. Alterations to a particular grid preparation protocol might distort quantitative information and imped data interpretation. However, the above numbers highlight the potential of novel grid preparation techniques that enable a much more efficient, ideally loss-less, transfer of proteins to TEM grids.[15,16] Such preparation techniques deposit only minute sample volumes in the nanoliter range to a TEM grid, thereby avoiding blotting and washing steps and preferential adsorption of proteins to the support surface. As a consequence, protein species will exhibit identical transfer efficiencies enabling to directly compare their particle densities on the grid without the need for calibrations.

Concentration measurements of mixed protein solutions are typically hard to assess using traditional methods. After the implementation of an additional image-processing step where detected particles are classified, the presented method will be capable of measuring concentrations of protein solutions containing various protein species. The feasibility of the method for mixed samples is determined by the accuracy at which particles can be distinguished.

The method presented opens the way for quantitative measurements of low concentrated proteins using negative stain single particle TEM. Such measurements can be performed without special requirements. We envisage that in the long run, the abundance of proteins presented in single cell lysates can be quantitated, thereby complementing structural information and thus, enabling a completely new way of performing qualitative and quantitative proteomics.

4.5 References

[1] Bantscheff, M.; Schirle, M.; Sweetman, G.; Rick, J.& Kuster, B. **Quantitative mass spectrometry in proteomics: a critical review.** *Analytical and Bioanalytical Chemistry* **389**, 1017-31 (2007).

[2] Ong, S. E.& Mann, M. **Mass spectrometry-based proteomics turns quantitative.** *Nat Chem Biol* **1**, 252-262 (2005).

[3] Bantscheff, M.; Lemeer, S.; Savitski, M. M.& Kuster, B. **Quantitative mass spectrometry in proteomics: critical review update from 2007 to the present.** *Analytical and bioanalytical chemistry* **404**, 939-65 (2012).

[4] Kemmerling, S.; Arnold, S. A.; Bircher, B. A.; Sauter, N.; Escobedo, C. *et al.* **Single-cell lysis for visual analysis by electron microscopy.** *J Struct Biol* **183**, 467-73 (2013).

[5] Bremer, A.; Henn, C.; Engel, A.; Baumeister, W.& Aebi, U. **Has Negative Staining Still a Place in Biomacromolecular Electron-Microscopy.** *Ultramicroscopy* **46**, 85-111 (1992).

[6] Ohi, M.; Li, Y.; Cheng, Y.& Walz, T. **Negative Staining and Image Classification - Powerful Tools in Modern Electron Microscopy.** *Biological procedures online* **6**, 23-34 (2004).

[7] Ferris, M. M.; Stoffel, C. L.; Maurer, T. T.& Rowlen, K. L. **Quantitative intercomparison of transmission electron microscopy, flow cytometry, and epifluorescence microscopy for nanometric particle analysis.** *Anal Biochem* **304**, 249-256 (2002).

[8] Giss, D.; Kemmerling, S.; Dandey, V.; Stahlberg, H.& Braun, T. **Exploring the Interactome: Microfluidic Isolation of Proteins and Interacting Partners for Quantitative Analysis by Electron Microscopy.** *Anal Chem* **86**, 4680-4687 (2014).

[9] Kayser, H.; Mann, K.; Machaidze, G.; Nimtz, M.; Ringler, P. *et al.* **Isolation, Characterisation and Molecular Imaging of a High-Molecular-Weight Insect Biliprotein, a Member of the Hexameric Arylphorin Protein Family.** *J Mol Biol* **389**, 74-89 (2009).

[10] Suloway, C.; Pulokas, J.; Fellmann, D.; Cheng, A.; Guerra, F. *et al.* **Automated molecular microscopy: the new Leginon system.** *J Struct Biol* **151**, 41-60 (2005).

[11] Lander, G. C.; Stagg, S. M.; Voss, N. R.; Cheng, A.; Fellmann, D. *et al.* **Appion: an integrated, database-driven pipeline to facilitate EM image processing.** *J Struct Biol* **166**, 95-102 (2009).

[12] Roseman, A. M. **FindEM--a fast, efficient program for automatic selection of particles from electron micrographs.** *J Struct Biol* **145**, 91-9 (2004).

[13] Rindskopf, D. **An introduction to the bootstrap - Efron,B, Tibshirani,RJ.** *J Educ Behav Stat* **22**, 245-245 (1997).

[14] O'Mahony, F. C.; Nanda, J.; Laird, A.; Mullen, P.; Caldwell, H. *et al.* **The use of reverse phase protein arrays (RPPA) to explore protein expression variation within individual renal cell cancers.** *Journal of visualized experiments : JoVE* (2013).

[15] Kemmerling, S.; Ziegler, J.; Schweighauser, G.; Arnold, S. A.; Giss, D. *et al.* **Connecting mu-fluidics to electron microscopy.** *J Struct Biol* **177**, 128-34 (2012).

[16] Jain, T.; Sheehan, P.; Crum, J.; Carragher, B.& Potter, C. S. **Spotiton: a prototype for an integrated inkjet dispense and vitrification system for cryo-TEM.** *J Struct Biol* **179**, 68-75 (2012).

5 Connecting µ-fluidics to electron microscopy

The following section has been published in:

The Journal of Structural Biology 177, 128-134 (2012)

(doi: 10.1016/j.jsb.2011.11.001)

I contributed to the experiments validating the developed methodology in the context of complex biological samples such as cell lysates.

Connecting µ-fluidics to electron microscopy

Simon Kemmerling[1], Jörg Ziegler[1], Gabriel Schweighauser[1], Stefan A. Arnold[1], Dominic Giss[1], Shirley A. Müller[1], Philippe Ringler[1], Kenneth N. Goldie[1], Nils Goedecke[2], Andreas Hierlemann[2], Henning Stahlberg[1], Andreas Engel[1,3], And Thomas Braun[1,*]

1 Center for Cellular Imaging and NanoAnalytics (C-CINA), Biozentrum, Universität Basel, Basel, Switzerland

2 Bio Engineering Laboratory (BEL), Department of Biosystems Science and Engineering (D-BSSE), ETHZ, Basel

3 Department of Pharmacology, Case Western Reserve University, Cleveland, USA

*Corresponding Author: Thomas.braun@unibas.ch

Keywords: Electron Microscopy, Microfluidics, Single-molecule Analysis, Mass and Shape, Systems Biology

5.1 Abstract

A versatile methodology for electron microscopy (EM) grid preparation enabling total content sample analysis is presented. A microfluidic-dialysis conditioning module to desalt or mix samples with negative stain solution is used, combined with a robotic writing table to micro-pattern the EM grids. The method allows heterogeneous samples of minute volumes to be processed at physiological pH for structure and mass analysis, and allows the preparation characteristics to be finely tuned.

5.2 Introduction

Systems Biology aims to quantify the molecular elements of a biological system, to determine their interactions and to integrate this information into network models.[1] The development of comprehensive models requires experimental information about the spatial and temporal arrangements of the network components as well as their structure, a challenge that required a multi-resolution approach and the combination of different techniques.[2,3] Cryo-electron tomography (cryo-ET) is the ultimate technique to reveal the spatial organisation of protein structures and macromolecular complexes in single cells.[4,5] Currently cryo-ET is restrained by several limitations, such as the size of the cell that can be analysed (maximum diameter of ~2 µm),[6] and by problems in data segmentation and in the template matching required for protein recognition (restricted to relatively large protein complexes).[7] Indeed, many target structures can only be recognised if labelled with electron-dense markers[8], which, despite recent progress,[9] often involves harsh preparative treatment of the cells. Furthermore, while ET delivers structural and spatial information, correlation of these with other methods such as mass spectroscopy (MS)[10] is difficult. A complementary approach is to physically lyse the cells and to subsequently write the entire sample onto electron microscopy (EM) grids for structure analysis by transmission EM (TEM), or mass analysis by scanning TEM (STEM). Ultimately, the use of microfluidic techniques offers the potential to analyse a single cell by making it possible to investigate protein ultrastructures and membrane fragments in lysates[11].

Here we present a lossless sample deposition method for EM (Figure 5-1), which allows the handling of minute sample volumes and immobilization of the total sample content on EM grids to obtain, for example, the full cell inventory. This methodology is combined with a microfluidic sample-conditioning module. The constellation provides a new staining technique for heavy metal salts (negative stain) for TEM as well as specific desalting for mass measurements by STEM.

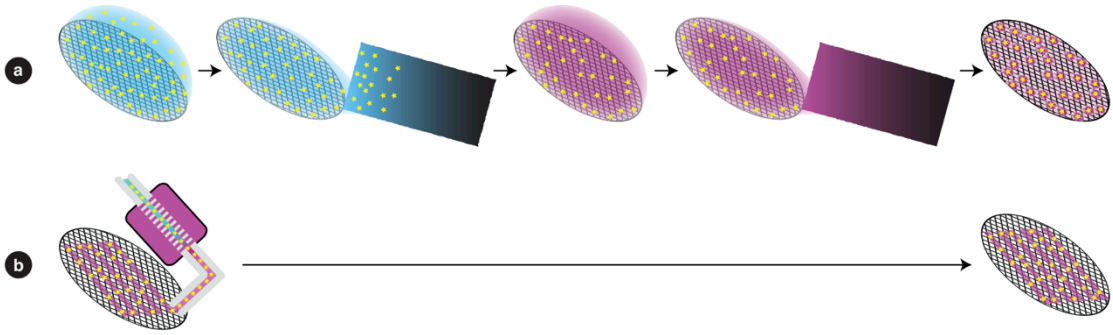

Figure 5-1: *Principles of negative staining for EM. (a) Classical negative staining by hand: The sample is absorbed to the carbon film of an EM grid and the grid is blotted to remove the excess sample solution. The absorption time and the specific absorption properties of the sample components determines the fraction of the sample that is immobilized. A wash and blot cycle sometimes follows (not shown). The grid is then incubated with the negative stain solution of choice, followed by another blotting step to remove excess stain solution. The grid is left to air-dry before investigation in the electron microscope. With this method only a specific sub-fraction of the sample is immobilized on the grid. (b) The here developed microfluidic negative staining approach: A very small amount (0.1-0.3 µl) of stain-mixed sample is applied to the grid via a nozzle of 50 µm inner diameter. The grid is then air-dried without any blotting. With this method the entire sample is immobilized on the grid. Additionally, the micro-precision of the writing process allows a meander-type micro-pattern of stained sample to be created on the carbon film.*

5.3 Materials and methods

5.3.1 Stain preparation

The reservoir of the sample-conditioning module (Figure 5-2a) was filled with different commonly used negative stains prepared in the following way: *Phosphothungstic acid ($PTA_{7.0}$)*: Sodium-phosphotungstate tribasic hydrate (Riedel-de Haen, Switzerland) was dissolved in double-distilled water (ddH_20) to give a 1% or 2% (w/v) final concentration. The pH of the aqueous solution was adjusted to 7.0 using 1M potassium hydroxide; *Ammonium molybdate ($AM_{6.5}$)*: Ammonium molybdate (Aldrich, Switzerland) was dissolved in ddH_20 to give a aqueous solution with a final concentration of 0.5% (w/v) at pH 6.5; *NanoVan® ($NV_{8.0}$)*: The 2% ready to use methylamine vanadate (Nanoprobes, USA) solution at pH 8.0 was diluted with ddH_20 to give a final concentration of 1% (w/v*); NanoW® ($NW_{6.8}$)*: The 2% ready to use methylamine tungstate (Nanoprobes, USA) solution at pH 6.8 was diluted with ddH_20 to give a final concentration of 1% (w/v); *Uranyl acetate ($UA_{4.5}$)*: Uranyl acetate was dissolved in ddH_20 to give a final concentration of 0.25% (w/v) at pH 4.5; *Buffered uranyl acetate ($UA_{7.0}$)*: To prepare UA at pH 7, the above 0.25% (w/v) uranyl acetate solution was mixed with an equal volume of a 20 mM oxalic acid solution. The pH was adjusted using 3% ammonium hydroxide, added slowly while stirring.[12] This resulted in a 0.12 % UA solution at pH 7.0.

5.3.2 Test samples

Several samples were used for the initial tests and as a proof of concept: The chosen test samples apoferritin (AF; from equine spleen; Sigma, Switzerland) and tobacco mosaic virus (TMV; kindly supplied by Ruben Diaz-Avalos, New York Structural Biology Center, USA) are well characterized, and TMV is used as a standard for mass calibration in scanning transmission electron microscopy (STEM). The used test-samples were composed as follows: (1) A mixture of 0.05 mg/ml AF and 0.1 mg/ml TMV in phosphate buffered saline pH 7.4 (PBS; P4417, Sigma-Aldrich, Switzerland). (2) 0.05 mg/ml AF in PBS. (3) 0.1 mg/ml TMV in quartz-ddH_20. (4) Baby Hamster Kidney (BHK) cell lysate in PBS (see next section).

5.3.3 BHK cell culture and lysis

Attached Baby Hamster Kidney (BHK21; ECACC 85011433) cells were grown for 48h in a polystyrene T75-flask containing 30 ml of DHI-5 medium (see end of section) at 37° C, 100% air humidity, and 5% CO_2. To harvest the cells the medium was removed and the flask was washed with 7 ml of PBS. To detach the cells from the flask surface, 3 ml of trypsin-EDTA were added and the cells were incubated for 5 min at 37° C. Afterwards, 7 ml of DHI-5 medium were added and the detached cells were mixed using a pipet. 0.5 ml of the cell suspension was left in the flask and again incubated with 30 ml of fresh media for 48 h to obtain the next batch. The rest of the cell suspension was centrifuged twice and washed with PBS (48xg, 2min). The pellet was dissolved in 2ml of PBS. In an Eppendorf tube 200 µl of this cell suspension were further diluted with 800 µl of PBS and the cells were lysed by sonification for 2 min at 25 kHz while cooling.

DHI-5 medium is a mixture of DME (Dulbecco`s Modified Eagels Medium; D6171, Sigma, Switzerland), HamF12 (Nutrient Mixture F-12Ham; N8641, Sigma, Switzerland), and IMDM (Iscove`s Modified Dulbecco`s Medium, I3390, Sigma, Switzerland) media (1:1:2), supplemented with 5% FCS (Fetal Bovine Serum, E7524, Sigma, Switzerland) and complemented with non essential amino acids (MEM Non essential amino acid solution, M7145, Sigma, Switzerland), L-glutamine (L-Glutamine Solution, G7513, Sigma, Switzerland) and Vitamins (RPMI1640 Vitamins Solution, R7256, Sigma, Switzerland).

5.3.4 Microfluidic setup

Samples were specifically treated and then deposited on carbon films covering 200 and 400 mesh Ni-TEM grids or on the special grids used for mass measurement (see below). This was achieved using a custom-built modular microfluidic setup (Figure 5-2a) consisting of a syringe pump, a 10-port 2-position valve, a custom-built sample conditioning module, a custom-built hand-over module, with functionalized nozzle, xyz-stage and several HPLC consumables (fused silica capillaries, PTFE tubing and connectors; BGB-analytic, Switzerland). The whole system is driven by the syringe pump (KDS210; Ismatec SA, Switzerland) and the sample is injected via a sample loop on the valve (Valco

10-port 2-position valve; BGB-analytic, Switzerland). All electronic components of the apparatus are controlled by a LabView-based custom-made software system (supplemental Figure 5-6), which features a macro language for flexible automation by coordination of the different modules. On request we will provide the software and the construction plans.

5.3.5 Sample-conditioning module

The sample-conditioning module consists of a custom-build reservoir that holds about 5 ml of solution (dialysis reservoir); either stain solution (for negative stain TEM) or 100 mM ammonium acetate prepared using quartz-ddH_20 (desalting). About 10-12 cm of a 13 kDa cut off cellulose fiber (Spectra/Pro® microdialysis fibers ID=200 µm; Spectrum Laboratories, USA) that holds 3-4 µl of sample at one time spans this reservoir. When the sample is pumped through this conditioning module at a rate of 2 µl/min, the dialysis time is about 2 min.

5.3.6 Hand-over module and grid preparation

The hand-over module deposits sub-microlitre sample volumes on EM grids by contact writing and can be programmed to automatically prepare a series of grids. The Ni-TEM grids are held in place by magnets and their carbon films are activated with atmospheric pressure helium cold-plasma (piezobrush® PZ1, Polyscience AG Switzerland) immediately before sample application. Initial tests showed that a 4 sec treatment at a distance of 1 cm from the plasma source gives comparable results to the conventional glow discharge,[13] without destruction of the carbon film. A fully controllable micro-mechanical device (Physik Instrumente xyz micro-precision translation stages; Dyneos AG, Switzerland) brings a thin nozzle that is connected by micro-capillaries to the sample-conditioning module, in close proximity to the EM grid (Figure 5-2b). After liquid contact, the grids are moved under the nozzle with sub-micrometer precision to create a micro-pattern of the sample on carbon in the form of a thin wet film. In this way 0.1-0.3 µl of stained or specifically desalted sample are 'written' on the grid, which is then air-dried. The degree of wetting obtained can be tuned by modifying the plasma treatment, and the writing can be optimized for the sample by adjusting the writing parameters. A defined combination of grid hydrophobicity (defined by plasma treatment parameters), writing speed, and surface tension of the applied solution (can be changed by the addition of ethanol traces), allowed a continuous line about 13 mm long and about 200 to 300 µm wide to be written (Figure 5-2c).

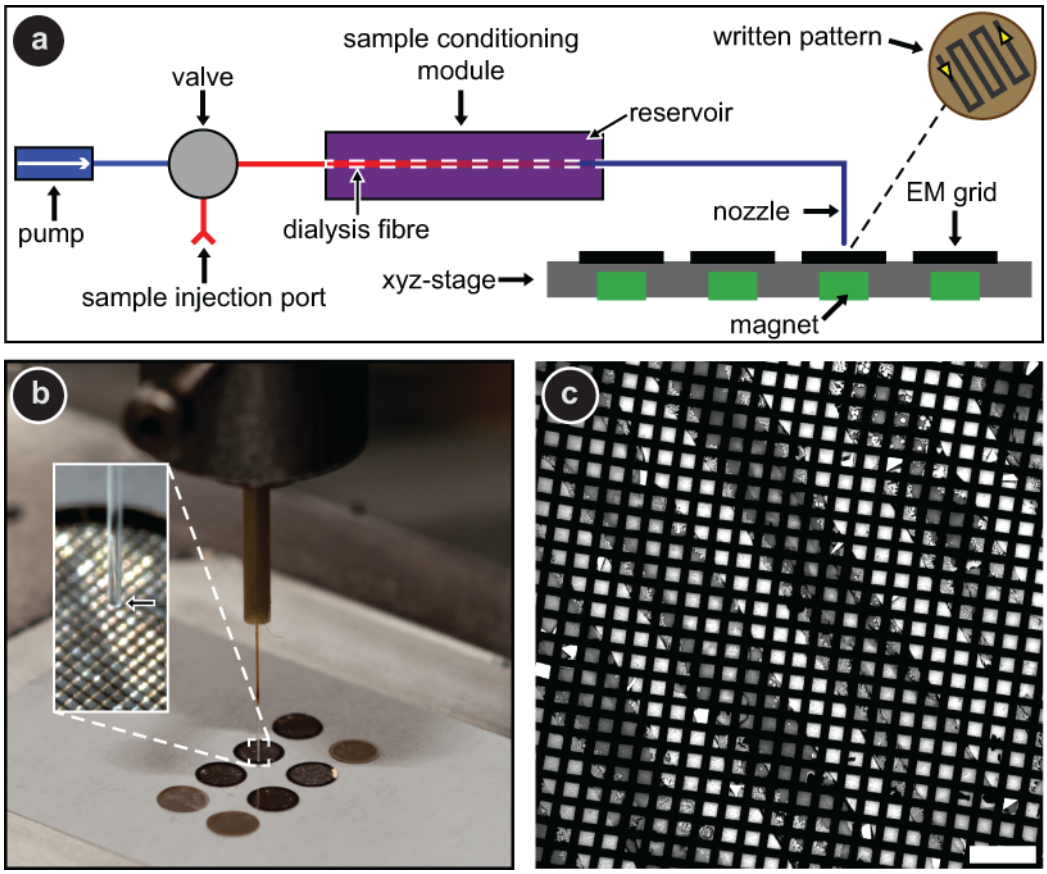

Figure 5-2: *Sample-conditioning module and micro-patterning device. (a) Schematic representation of the main components and the meander-type writing pattern. (b) Nozzle positioned above an EM grid on the xyz-stage. Inset: enlarged view; the arrow indicates the nozzle tip. (c) TEM image of a micro-patterned grid showing a section of the six 200-300-µm-wide lines of a $PTA_{7.0}$ stained sample (diagonal dark grey lines) written on an EM grid (black) and the empty carbon film in between (light grey). Scale bar: 200 µm.*

5.3.7 Nozzle preparation

Commercially available fused silica capillaries (Polymicro) were used to make the nozzles. These were processed in the following way to optimize the liquid handling and direct the fluid onto the EM grids. The first 0.5-1.0 cm of the polyimide coating of the fused silica capillaries was stripped away using hot chromosulfuric acid.[14] Afterwards, the nozzle was extensively rinsed with ddH_20 to remove all traces of the acid. The fused silica was then cleaned by successively dipping the capillaries into ddH_20, ethanol and acetone for 10 min while shaking. Subsequently, the fused silica surface was activated by a 1 min treatment with cold atmospheric pressure helium plasma (piezobrush® PZ1, Polyscience AG, Switzerland). Immediately after plasma treatment the capillary tips were dipped into a silanization solution (~5% dimethyldichlorosilane in heptane; Silanization Solution 1, 85126, Fluka, Switzerland) for 1 hour and baked at 90° C for 4 hours. The stripped and silanized capillaries have an internal nozzle diameter of 50 µm.

5.3.8 Scanning Transmission Electron Microscopy

A Vacuum Generators (East Grinstead, U.K.) HB-5 STEM interfaced to a modular computer system (Tietz Video and Image Processing Systems) was used. All samples were prepared on thin carbon films spanning gold sputtered, carbon-coated, 200-mesh-per-inch, gold-plated copper grids.[15] The aim was to determine whether samples leaving the microfluidics setup were clean and suitable for mass evaluation. After extensive rinse cycles for maintenance of the set-up, the sample dialysis reservoir was filled with quartz-ddH_2O. A stock solution of TMV in quartz-ddH_2O was then passed through the conditioning module (micro-dialysis time of 2 min) and written to STEM microscopy grids by the hand-over module. The control grid, which also served as mass standard, was manually prepared in the conventional manner, i.e., a 5 µl droplet of the same TMV stock was adsorbed to a STEM grid, blotted and washed on 8 droplets of 100mM ammonium bicarbonate solution prepared with quartz-ddH_2O, blotting after each step. All grids were allowed to air-dry. Series of digital 512 X 512 pixel, dark-field images were recorded from the grids at an acceleration voltage of 80 kV and a nominal magnification of 200,000x. The recording dose used varied between 290 and 635 electrons/nm^2. The images were evaluated with the MASDET program package as described previously.[16] All mass-per-length (MPL) data were corrected for beam-induced mass-loss. The results from the control grid (mass standard) gave the instrumental scale factor, which was correspondingly applied to all measurements. The MPL data from the test grid were binned into a histogram and described by a Gaussian curve. The average MPL and standard deviation (SD) were also calculated and compared to the expected value of 133 kDa/nm^2,[15] and to the SD of the control grid results, respectively.

5.4 Results

The apparatus enables micro-patterning of EM grids with stained or desalted samples. It consists of two main units, (a) a sample-conditioning module for staining or desalting (or an inline combination of both), and (b) a hand-over module for micro-patterning the sample onto the grids (Figure 5-2a). The instrument is designed for a prospective degree of automation and controlled by custom-written software (Supplemental Figure 5-6). In the first step the sample is conditioned using the micro-dialysis principle. This method was chosen because it is easy to integrate and because of its multiple application potential. In this sample-conditioning module, the sample flows through a cellulose fibre capillary (13 kDa cut-off) that extends through a reservoir of either negative stain solution or a volatile buffer (e.g., ammonium acetate or ammonium bicarbonate) in quartz double-distilled water (ddH_2O). Dialysis occurs as the sample liquid flows through the chamber, to either add the negative stain solution or remove undesired salts. The sample flow rate defines the dialysis time and can be adapted in a range from sec to min. Liquid contact writing is then used to deposit the sample on EM grids supporting a thin carbon film that was rendered partially hydrophilic by activation with an atmospheric pressure helium cold-plasma. This treatment replaced the conventional glow discharge

technique.[13] The piezo-driven plasma generation was chosen, as it is easier to integrate in an automated setup. The hand over unit is a micro-mechanical positioning device that brings a thin nozzle in close proximity to the grid. After liquid contact has been established, the grid is moved under the nozzle at sub-micrometer precision to create a meander-type micro-pattern of the sample on its carbon film (Figure 5-2b and 2c). When this is finished, the nozzle is quickly moved up and down as the next grid is positioned (the time required is operator defined; minimum 0.5 sec). At present, a series of 26 grids can be written in sequence.

We have tested this new grid preparation method with a range of commonly used negative stains,[17] namely phosphotungstic acid at pH 7.0 ($PTA_{7.0}$), ammonium molybdate at pH 6.5 ($AM_{6.5}$), NanoVan at pH 8.0 ($NanoV_{8.0}$), NanoW at pH 6.8 ($NanoW_{6.8}$), and uranyl acetate at pH 4.5 ($UA_{4.5}$) and pH 7.0 ($UA_{7.0}$), and compared the results with grids prepared by conventional negative staining/blotting methods. Due to the effective staining behaviour of this method only half or even less (2 min micro-dialysis against 0.5% -1%) of the stain solution concentrations normally applied were used. A mixture of tobacco mosaic virus (TMV) and apoferritin (AF) in phosphate buffer system (PBS; 10 mM phosphate buffer, 2.7 mM KCl, 137 mM NaCl, pH 7.4) was employed to investigate the staining quality (Figure 5-3 left column, and Supplementary Figure 5-7), while complete cell lysates of baby hamster kidney (BHK) cells allowed the staining behaviour for heterogeneous samples to be assessed (Figure 5-3 right column, and Supplementary Figure 5-8). UA, one of the most commonly used negative stains employed in conventional negative stain EM, caused sample aggregation in our new method at both, pH 4.5 and pH 7.0 (Supplementary Figure 5-9) and was not investigated further. Uranyl formate was not considered for testing, as a similar fixative effect as for UA has been reported.[17] The other stains examined gave excellent results for both test samples. When used at significantly lower concentrations than in classical staining methods, these stains provided good contrast in the EM and clearly revealed structural details. With the exception of $UA_{4.5}$, all of the stains were stabilized at physiological or close to physiological pH. When BHK cell lysates were examined in an analogous procedure, ultrastructural details, such as membrane fragments packed with proteins, filaments and individual proteins were all clearly resolved in the TEM with no sign of aggregation (Supplementary Figure 5-10).

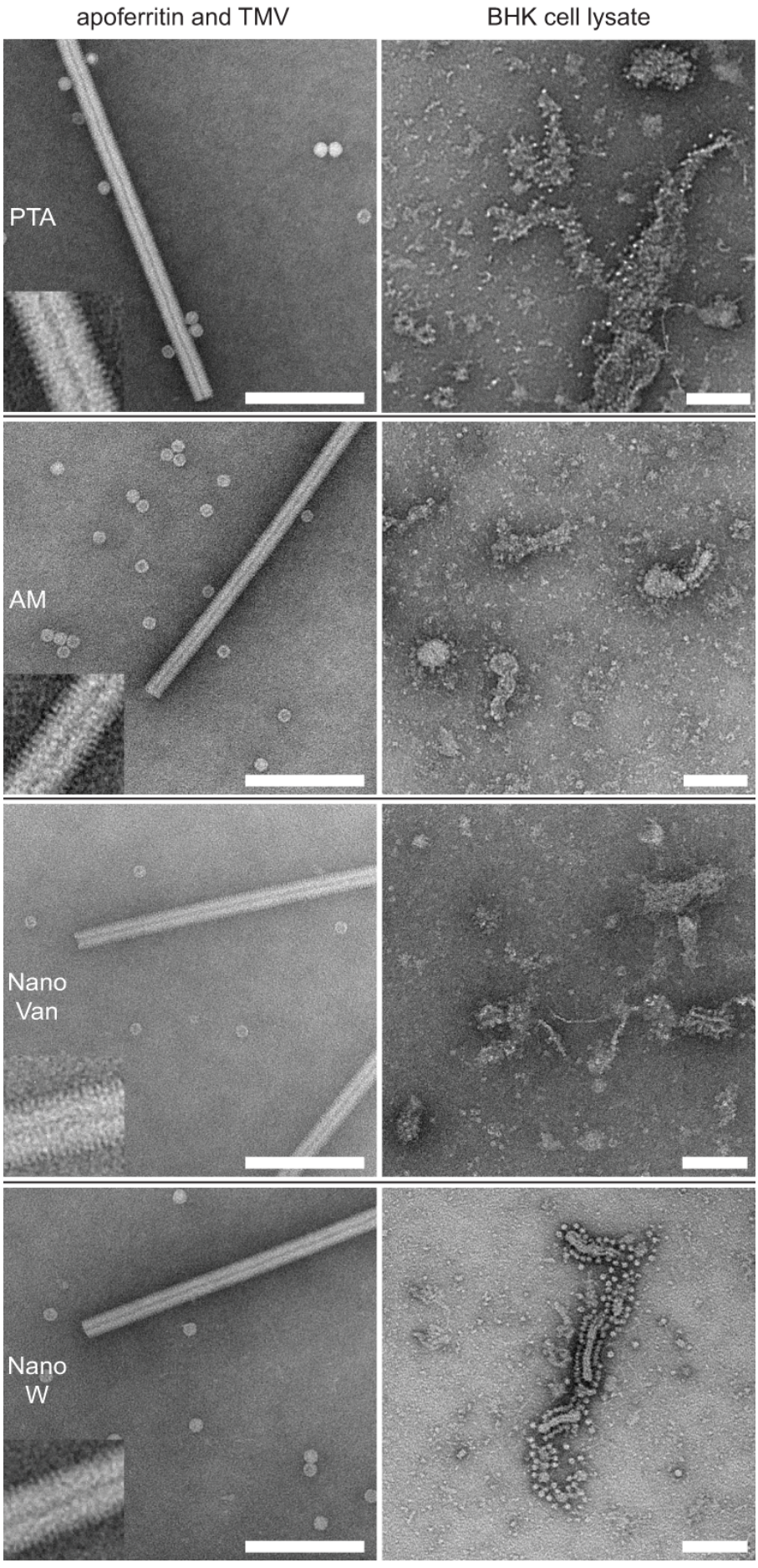
apoferritin and TMV
BHK cell lysate
PTA
AM
Nano
Van
Nano
W

Figure 5-3: *Gallery of TEM images. This selection shows TEM images of the two test samples prepared with the setup and different stains. (Left column) Mixture of AF and TMV. For all negative stains the central channel and the 23Å repeat of TMV and the sub-structure of the AF is visible. (Right column) BHK cell lysate showing typical membrane structures with integrated membrane proteins that exhibit the shape of ATPases. (Rows) Samples in PBS were conditioned with 1% $PTA_{7.0}$, 0.5% $AM_{6.5}$, 1% $NanoV_{8.0}$, and 1% (left) or 2% (right) $NanoW_{6.8}$. Scale bars: 100 nm; insets depict three-fold enlarged regions of the TMV. (for more images see Supplementary Figs. 2 and 3).*

A STEM mass measurement achieves an accuracy of 5 – 10% depending on the sample and, working from an image, directly links the mass data to shape information.[11] Initial tests made with TMV clearly showed that the modular microfluidic setup is capable of preparing the stringently clean grids required for these measurements (Figure 5-4a). The carbon film of the written, air-dried grids of TMV in quartz-ddH_2O dialysed against quartz-ddH_2O was clean. Further, the mass-per-length measured for TMV was within 1.5% of that measured for the control grids, which were manually prepared in the conventional way and imaged in the same data acquisition session (Figure 5-4b). Mass measurements require the removal of all non-volatile buffer components.[15] The classic way to do this specific desalting is to wash the grid several times with quartz-ddH_2O or a volatile buffer, e.g., ammonium acetate or bicarbonate, directly after sample adsorption. With the new grid preparation method, the required desalting is achieved before adsorption by dialysis. To avoid drastic pH changes and sample aggregation (Supplementary Figure 5-11), micro-dialysis can be done against a volatile buffer, which allows the pH to be kept as close as possible to physiological values at all stages. Changes in the lateral aggregation of TMV after dialysis against ammonium bicarbonate illustrate the effect, and document the efficiency of the sample–conditioning module (Supplementary Figure 5-11).

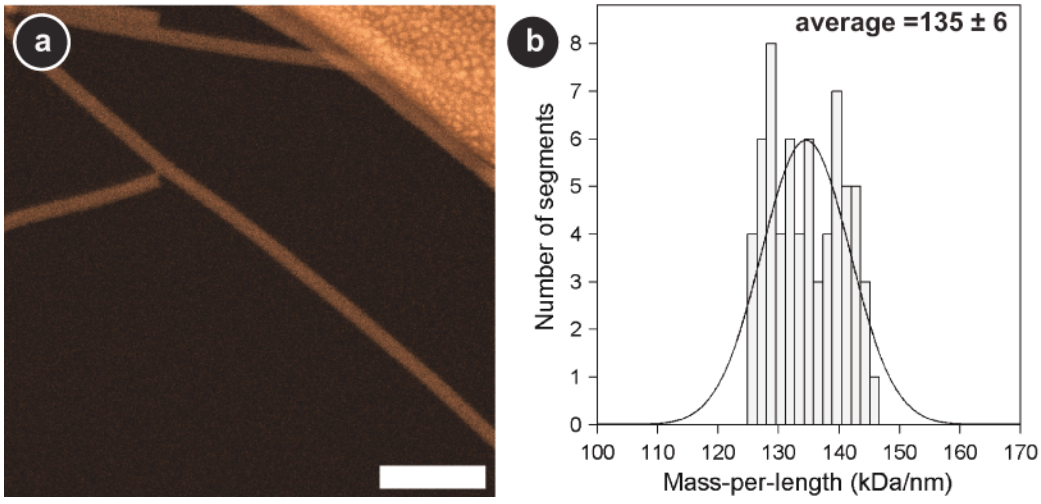

Figure 5-4: *Mass measurement of TMV by STEM to test the preparation quality and cleanliness delivered by the microfluidic setup. (a) STEM dark-field image of unstained, air-dried TMV written on a STEM microscopy grid for mass measurement. TMV (0.1 mg/ml) in quartz-ddH_2O was dialysed against quartz-ddH_2O for 2 min in the sample preparation module and written on the grid. The thin carbon film beneath the TMV rods is clean (uniform dark regions). A small segment of the gold-sputtered, perforated thick carbon*

layer supporting this film is also visible (bright irregular region upper right). (b) Mass-per-length histogram of correspondingly written TMV. After scaling according to the mass standard, the determined average mass-per-length, 135 ± 6 kDa/nm, is within 1.5% of the expected value, 133 kDa/nm. Further, the standard deviation of the data set is comparable to that of the mass standard, ± 4 kDa/nm, which was prepared in the conventional way (see Materials and Methods). Scale bar: 100 nm.

5.5 Discussion

Negative stain TEM is a standard method used in most electron microscopy laboratories involved in biology or biomedicine. In classical negative staining techniques for EM, a drop of sample (3 – 7 µl) is applied to the EM grid, which is then washed and stained. Each step is followed by a blotting procedure to remove excess liquid (**Fig. 1a**). Consequently, only a fraction of the sample and the stain remains on the grid. The amount of sample remaining depends on the adsorption, washing and blotting times, is often not reproducible, and the relative particle densities on the grid may be distorted by preferential adsorption of specific sample sub-fractions. Instead, our newly developed method adds the stain via dialysis prior to immobilization on the EM grid. Only 0.1-0.3 µl of the stain-mixed sample are required and no washing or blotting steps are involved (Figure 5-1b). This allows a much higher proportion (close to 100%) of the initial sample to be deposited on the EM grid, so that the true relative ratios between the different sample constituents are maintained (Supplementary Figure 5-12). Moreover the stain density is controlled by the heavy metal concentration in the reservoir and the flow rate and can be easily tuned (Figure 5-5).

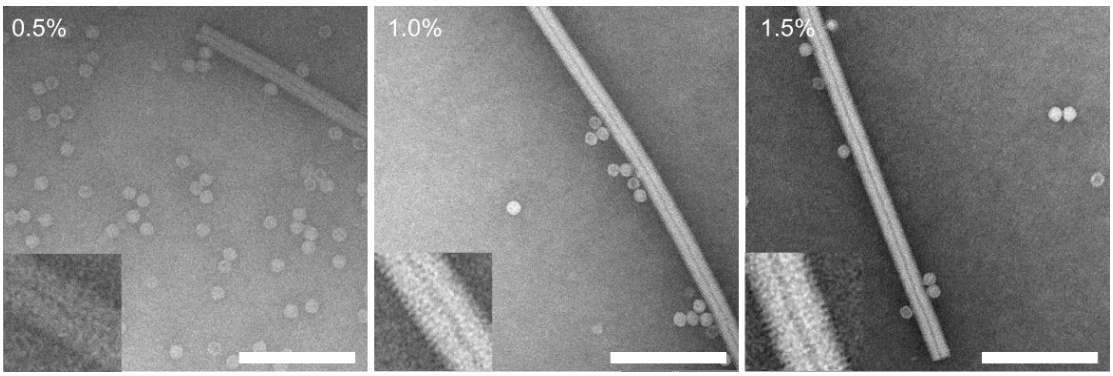

Figure 5-5: *Fine-tuning of the stain density: Representative images of samples conditioned with different $PTA_{7.0}$ concentrations , clearly showing the different stain densities. This demonstrates that easy and reproducible stain density fine-tuning is possible to adapt too different samples or to reveal different details of the same sample. Combined with several applicable stains with distinct properties this offers the potential to individually optimize the staining for a certain sample or certain sample details. The mixture of AF and TMV in PBS was conditioned with 0.5%, 1% or 1.5% of $PTA_{7.0}$ Scale bars: 100nm; insets depict three-fold enlarged regions of the TMV.*

In our hands, the automated procedure is more reproducible than manual staining, especially for „difficult" stains such as AM, nanoW and PTA. This new

method without any blotting or washing steps provides good contrast even for stains with weak electron scattering properties; the contrast is significantly higher than that achieved manually. Furthermore, the stain seems to be homogenously distributed around the particles, a fact that might be important for subsequent data analysis steps, such as alignments. Both, the contrast and the stain distribution attained with low scattering stains, may be favourably influenced by the preincubation of the protein complexes before adsorption to the grid surface as the stain has more time to penetrate the fine structures of the proteins. However, the resolution still appears to be limited by the grain size of the stain. Visually, AM seems to exhibit an excellent balance between stain grain size, contrast and "dynamic range" (Supplementary Figure 5-10c). Moreover, their tolerance to phosphate buffers, the most frequently used buffers in biochemistry and cell biology, and the possibility to adapt their pH makes AM and PTA applicable to a broad spectrum of samples.

In the future, the hand-over module will be developed to allow grid preparation for higher resolution techniques such as cryo-EM where the ice thickness is a critical, contrast-determining property. To this end, the grid temperature will be kept at the thaw point to avoid evaporation or condensation of the liquid during writing. Subsequently, the grid will be shot into liquid ethane. Alternatively, it will be freeze-dried to allow improved mass and shape measurements by STEM.

The microfluidic sample preparation platform presented here has the potential to become an important tool not only for systems biology but also for EM in general, which demands reproducible, quantitative sample grid preparation and assessment. The possibility of micro-patterning EM grids will allow a more systematic and convenient analysis of complex samples in the future. Combined with microfluidic methods for cell lysis, protein separation and labelling, this method for total cell content analysis for structure and mass offers the potential to optimally complement other experimental system biology techniques such as MS[18] and ET.[19,20] For this particular application, the raw images must be analyzed by feature matching methods[7,19,21] to obtain quantitative information. To aid the analysis, a visual library will be constructed containing the projections of *a priori* target molecules. The raw data images recorded from samples prepared in a lossless manner will be segmented by a hierarchical algorithm,[22,23] and the various particles present classified according to their size and shape. Shape matching will also allow the link to be made between negative stain and STEM images, combining the higher resolution and high contrast of the TEM projections with the mass obtained from unstained samples by STEM. Finally, cross-correlation techniques will be used to assign the TEM projections to the most probable match in the visual library.[19]

The outlined automated sample preparation technique opens the way for a new visual proteomics approach. Ultimately it will allow the total content of a single cell or miniscule tissue region to be examined by EM. It will then become possible to assemble complete ultrastructural libraries from cells or tissues. The method will make the structural study of the various cellular components on the single molecule level possible. We foresee the method as a valuable tool to study complex biological systems, complementing other systems-biological methods.

5.6 Supplementary Material

5.6.1 Screenshot of the LabView-based control software

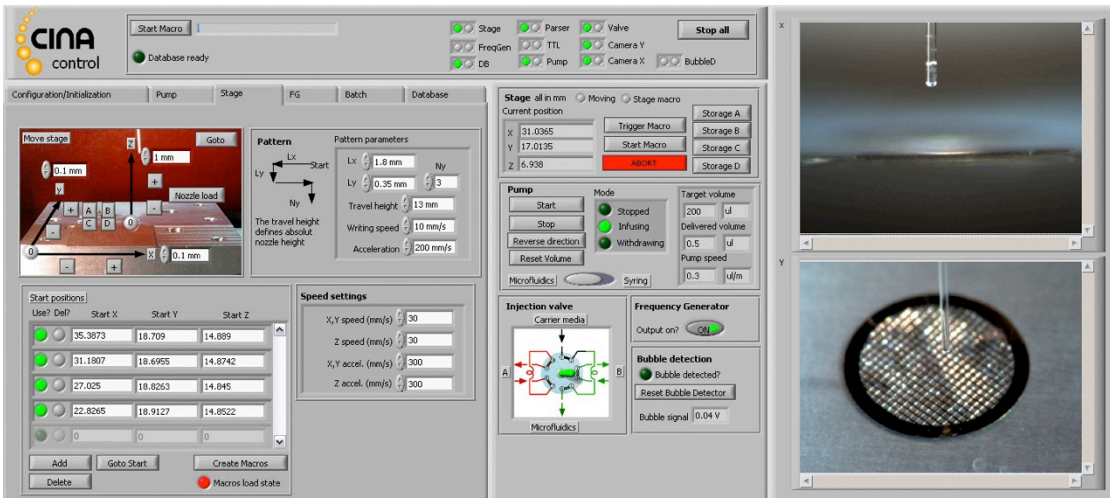

Figure 5-6: *Graphical user interface of the LabView-based control software: This self-written software allows all setup components to be controlled and examined. It shows the status of all components and two cameras installed at different angles deliver live images of the nozzle and the grid being processed, respectively. The parameters controlling the components can either be set individually or via a macro language that was integrated to facilitate automation.*

5.6.2 Gallery of negatively stained test samples

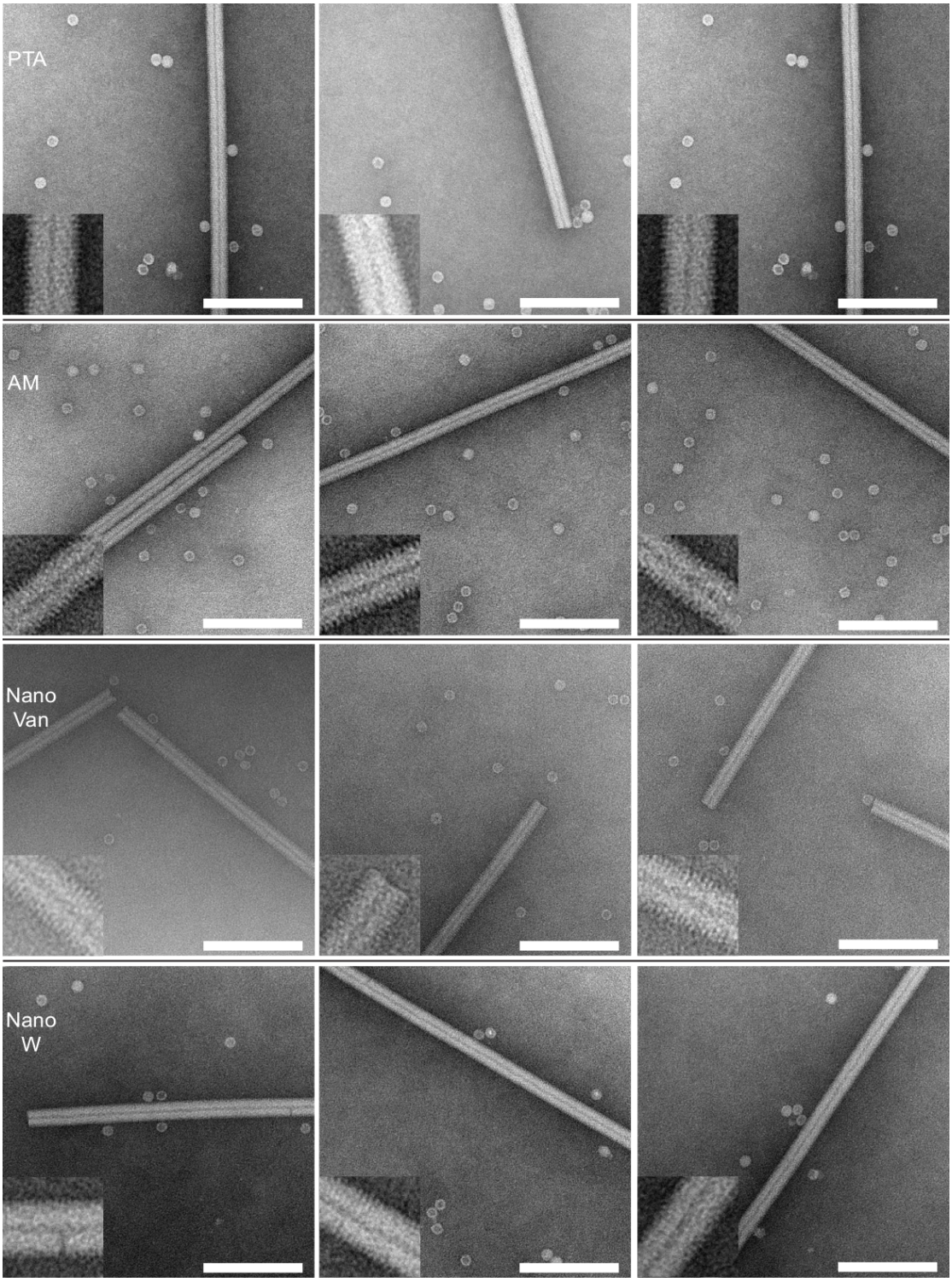

Figure 5-7: *Further examples of negatively stained TMV and AF samples. For all four stains the ultrastructure of TMV and AF is well preserved and the surrounding background shows a smooth fine grain. Samples were conditioned with 1% $PTA_{7.0}$, 0.5% $AM_{6.5}$, 1% $NanoV_{8.0}$, and 1% $NanoW_{6.8}$. Scale bars: 100 nm; the insets depict three-fold enlarged regions of the TMV.*

5.6.3 Gallery of negatively stained BHK lysate

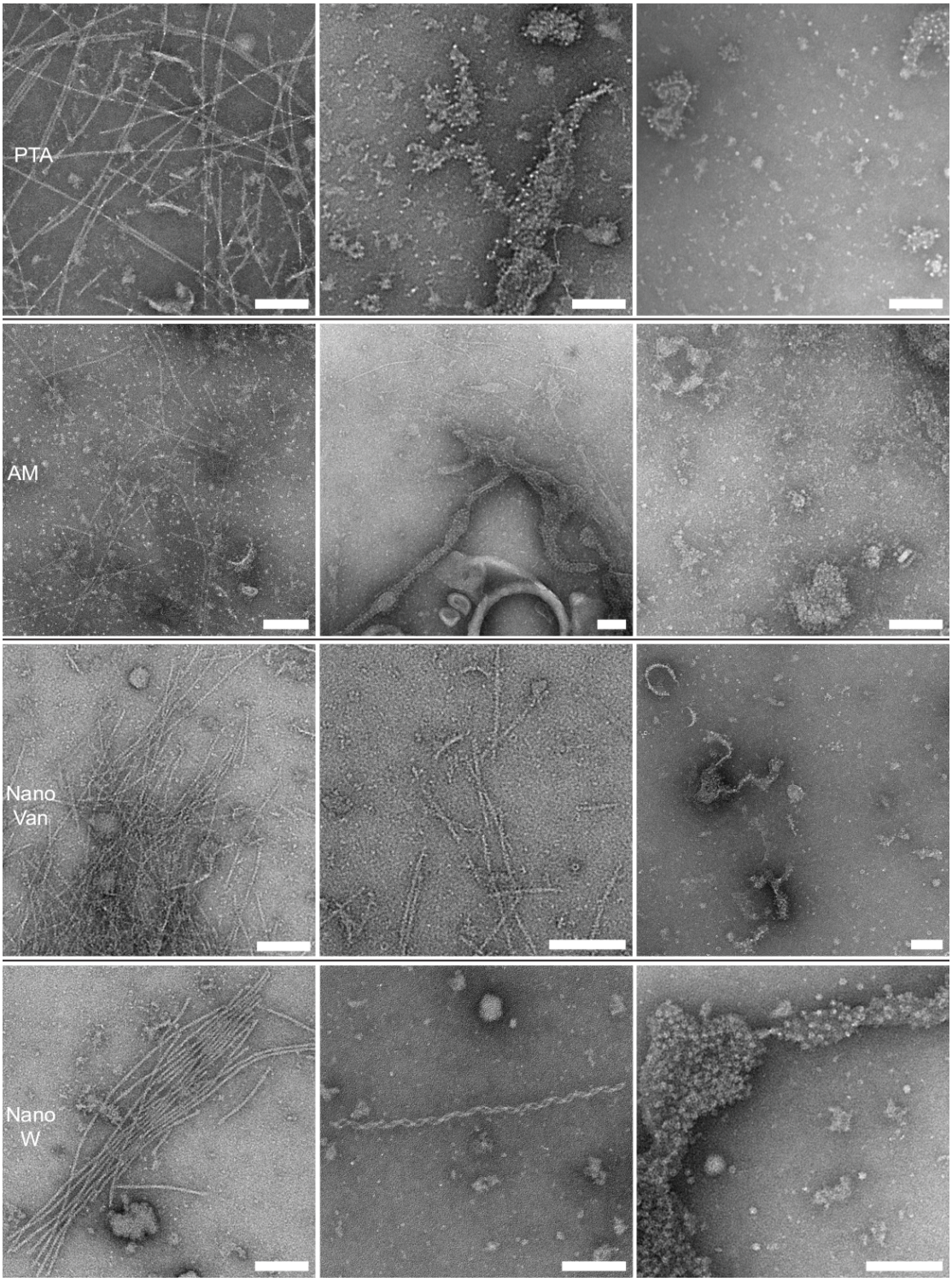

Figure 5-8: *Further examples of negatively stained BHK lysate for the four different stains, revealing structures resembling actin filaments (e.g. top left) and protein-packed membranes (e.g. top center). Samples were conditioned with 2% $PTA_{7.0}$, 0.5% $AM_{6.5}$, 1% $NanoV_{8.0}$, and 2% $NanoW_{6.8}$. Scale bars: 100 nm.*

5.6.4 UA staining results

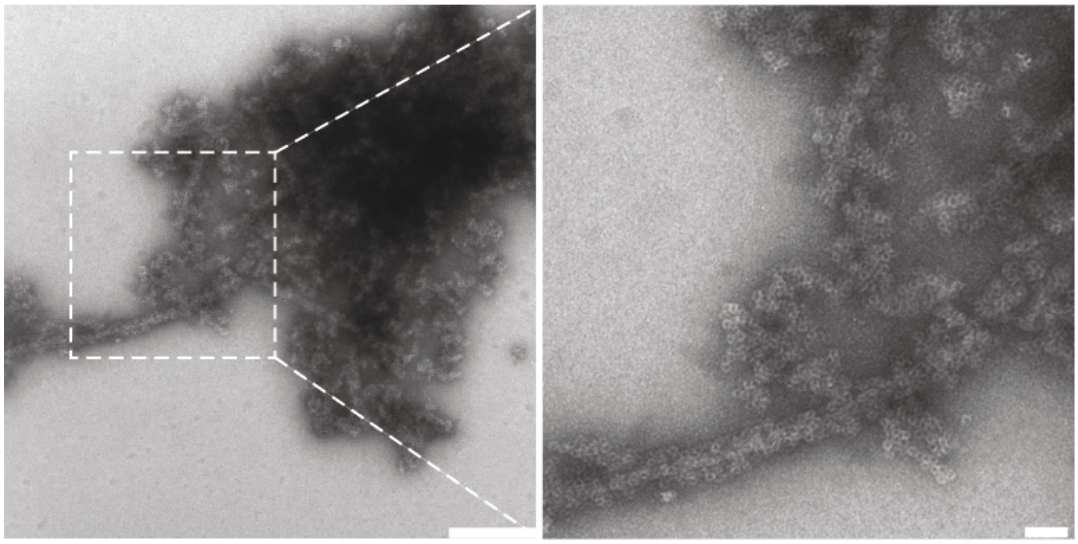

Figure 5-9: *UA staining results. A TEM image of aggregated TMV and AF conditioned with 0.25 % $UA_{4.5}$. An enlarged view of the marked region is shown on the right. Other experiments showed, that there is serious precipitation when $UA_{4.5}$ is mixed with the sample at concentrations above 0.5 % and dried down on the grid (data not shown), even if the buffer does not contain phosphate; the sample was in HEPES or ddH_2O. Decreasing the UA concentration to 0.25% or below prevented the formation of precipitates, but the fixation property of UA caused sample aggregation when stain and sample were mixed prior to immobilization on the grid. Furthermore, buffering the UA solution at a concentration of 0.25% or below at pH 7 could not prevent this sample aggregation. Scale bars: (left) 250 µm; (right) 50µm.*

5.6.5 Images of BHK cell lysate demonstrating the absence of aggregation

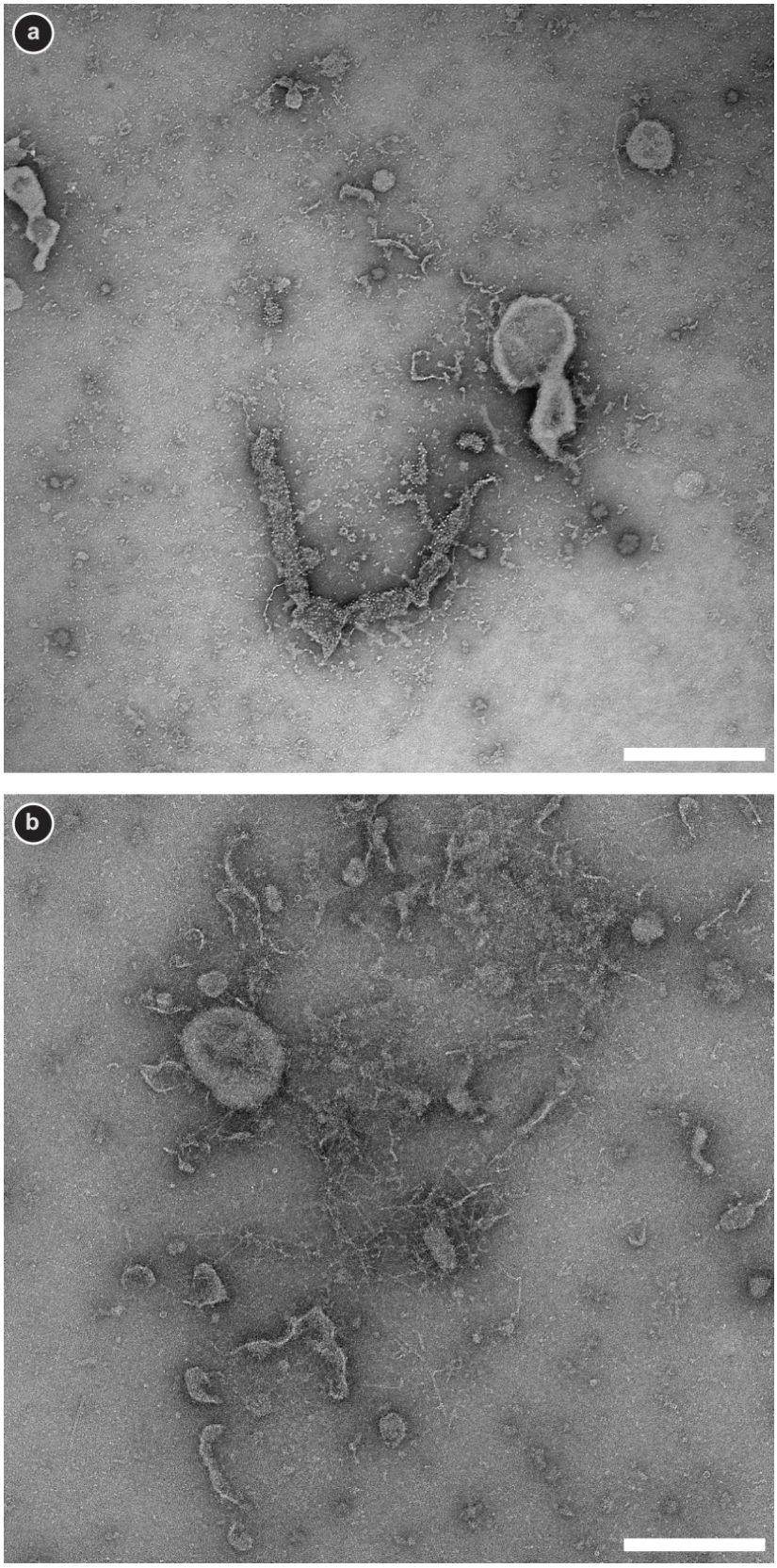

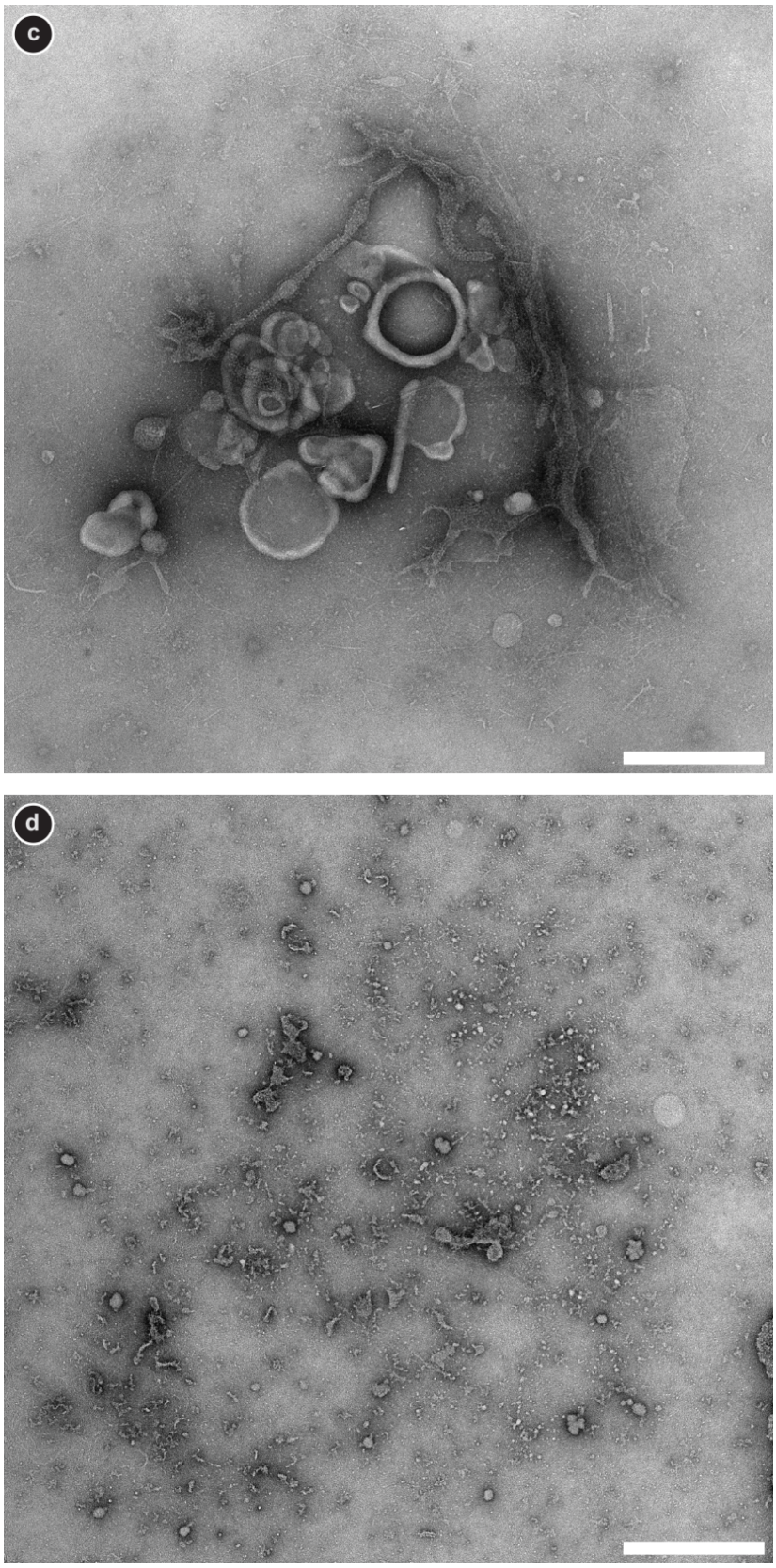

Figure 5-10: *Images of BHK cell lysate demonstrating the absence of aggregation. The overview images show soluble proteins, membrane patches and filaments; there is no sign of aggregation. The sample in PBS was conditioned with (a) 2% $PTA_{7.0}$. (b) 0.5% $AM_{6.5}$. (c)1% $NanoV_{8.0}$. (d) 2% $NanoW_{6.8}$. Scale bars: 500 nm.*

5.6.6 TMV preparation for STEM

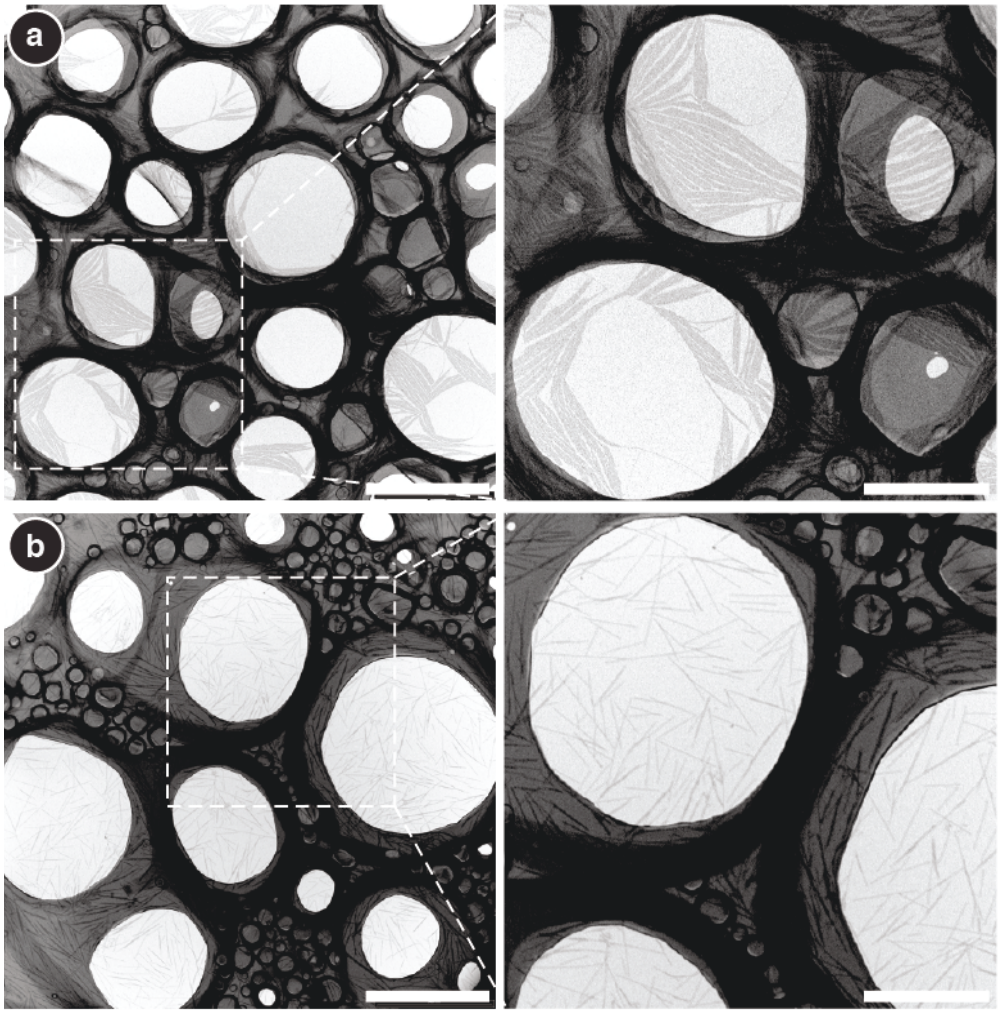

Figure 5-11: *TEM images of unstained TMV written on STEM grids after passage through the sample preparation module: (a) TMV in quartz-ddH_20, after micro-dialysis against quartz-ddH_20. The rods tend to aggregate, which would hinder mass determination; only a few are well separated from their neighbors. (b) TMV in quartz-ddH_20, after micro-dialysis against 100 mM ammonium bicarbonate buffer. The rods are homogeneously distributed over the grid and generally well separated. The marked change in aggregation shows that conditioning was effective. The results illustrate that even robust samples like TMV benefit from solutions that are buffered close to physiologic pH. Scale bars: (left column) 500 µm; (right column) 250 µm.*

5.6.7 Comparison of manual and automated grid preparation

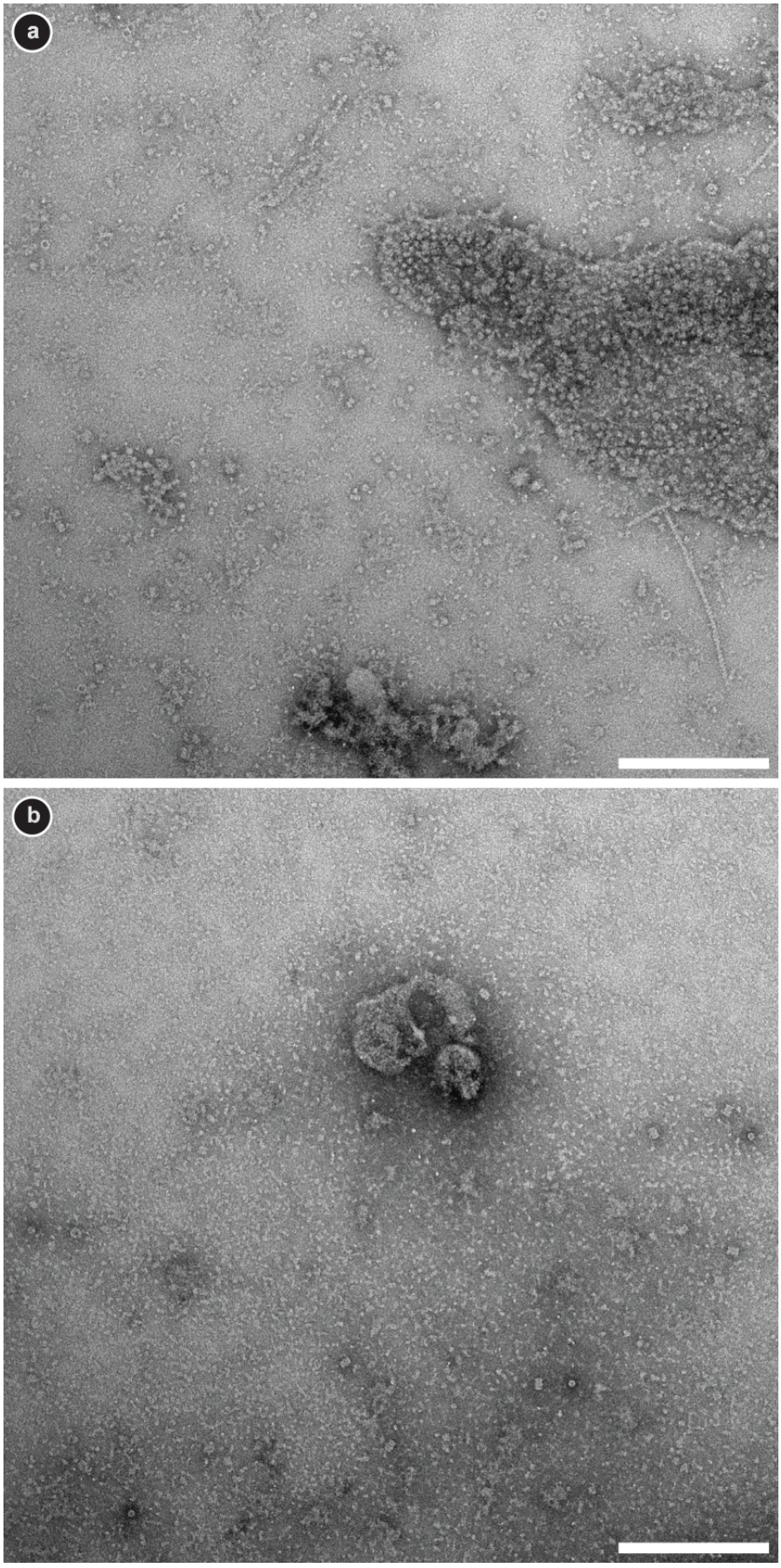

Figure 5-12: *Comparison of manual and automated grid preparation. Representative overview images of lysate from heat-shocked (46°C for 60min) BHK cells. (a) Prepared with the setup and conditioned with 1% NanoW$_{6.8}$. (b) Manually prepared (1 min sample adsorption followed by four wash steps of 5 sec) and stained with 2% NanoW$_{6.8}$ (two times 5 µl of stain for 10 sec). Besides the heat-shock proteins that can be observed with both preparation methods the setup preparation method reveals more sample constituents. Large "protein packed" membrane patches as well as filaments are abundant and clearly visible with structural details. These components were not observed when the grids were prepared by hand. Scale bars: 200 nm.*

5.7 References

[1] Aderem, A. **Systems biology: its practice and challenges.** *Cell* **121**, 511-513 (2005).

[2] Aloy, P.& Russell, R. B. **Structural systems biology: modelling protein interactions.** *Nature Reviews Molecular cell biology* **7**, 188-97 (2006).

[3] Kherlopian, A. R.; Song, T.; Duan, Q.; Neimark, M. a.; Po, M. J. *et al.* **A review of imaging techniques for systems biology.** *BMC systems biology* **2**, 74-74 (2008).

[4] Ben-Harush, K.; Maimon, T.; Patla, I.; Villa, E.& Medalia, O. **Visualizing cellular processes at the molecular level by cryo-electron tomography.** *Journal of cell science* **123**, 7-12 (2010).

[5] Lučić, V.; Förster, F.& Baumeister, W. **Structural studies by electron tomography: from cells to molecules.** *Annual review of biochemistry* **74**, 833-65 (2005).

[6] Leis, A.; Rockel, B.; Andrees, L.& Baumeister, W. **Visualizing cells at the nanoscale.** *Trends in Biochemical Sciences* **34**, 60-70 (2009).

[7] Bohm, J.; Frangakis, A. S.; Hegerl, R.; Nickell, S.; Typke, D. *et al.* **Toward detecting and identifying macromolecules in a cellular context: template matching applied to electron tomograms.** *Proceedings of the National Academy of Sciences of the United States of America* **97**, 14245-14250 (2000).

[8] Nickell, S.; Kofler, C.; Leis, A. P.& Baumeister, W. **Perspectives A visual approach to proteomics.** *Nature Reviews Molecular Cell Biology* **7**, 225-230 (2006).

[9] Kireev, I.; Lakonishok, M.; Liu, W.; Joshi, V. N.; Powell, R. *et al.* **In vivo immunogold labeling confirms large-scale chromatin folding motifs.** *Nature Methods* **5**, 311-313 (2008).

[10] Aebersold, R.& Mann, M. **Mass spectrometry-based proteomics.** *Nature* **422**, 198-207 (2003).

[11] Engel, A. **Assessing Biological Samples with Scanning Probes.** *Single Molecule Spectroscopy in Chemistry, Physics and Biology* **96**, 417-431 (2010).

[12] Hayat, M. A. *Principles and Techniques of Electron Microscopy.*

Biological Applications, 4th ed.; Cambridge University Press: Cambridge, 2000.

[13] Aebi, U.& Pollard, T. D. **A glow discharge unit to render electron microscope grids and other surfaces hydrophilic.** *Journal of electron microscopy technique* **7**, 29-33 (1987).

[14] Matthewson, M. J.; Kurkjian, C. R.& Hamblin, J. R. **Acid stripping of fused silica optical fibers without strength degradation.** *Journal of Lightwave Technology* **15**, 490-497 (1997).

[15] Müller, S. A.; Goldie, K.; Burki, R.; Haring, R.& Engel, A. **Factors influencing the precision of quantitative scanning transmission electron microscopy.** *Ultramicroscopy* **46**, 317-334 (1992).

[16] Krzyzánek, V.; Müller, S. A.; Engel, A.& Reichelt, R. **MASDET-A fast and user-friendly multiplatform software for mass determination by dark-field electron microscopy.** *Journal of Structural Biology* **165**, 78-87 (2009).

[17] Bremer, a.; Henn, C.; Engel, a.; Baumeister, W.& Aebi, U. **Has negative staining still a place in biomacromolecular electron microscopy?** *Ultramicroscopy* **46**, 85-111 (1992).

[18] Picotti, P.; Bodenmiller, B.; Mueller, L. N.; Domon, B.& Aebersold, R. **Full dynamic range proteome analysis of S. cerevisiae by targeted proteomics.** *Cell* **138**, 795-806 (2009).

[19] Forster, F.; Han, B. G.& Beck, M. **Visual Proteomics.** *Methods in Enzymology, Vol 483: Cryo-Em, Part C: Analyses, Interpretation, and Case Studies* **483**, 215-243 (2010).

[20] Barcena, M.& Koster, A. J. **Electron tomography in life science.** *Seminars in Cell & Developmental Biology* **20**, 920-930 (2009).

[21] Penczek, P. A.& Huang, Z. **Application of template matching technique to particle detection in electron micrographs.** *Journal of Structural Biology* **145**, 29-40 (2004).

[22] Coudray, N.; Buessler, J. L.; Kihl, H.& Urban, J. P. **Multi-scale and first derivative analysis for edge detection in TEM images.** *Image Analysis and Recognition, Proceedings* **4633**, 1005-1016 (2007).

[23] Adiga, U.; Baxter, W. T.; Hall, R. J.; Rockel, B.; Rath, B. K. *et al.* **Particle picking by segmentation: A comparative study with SPIDER-based manual particle picking.** *Journal of Structural Biology* **152**, 211-220 (2005).

6 General discussion

6.1 Validation of the established methodologies

The motivation for the development of the protein isolation method (see chapter 2 and 3)[1] was two fold: on one hand, the traditional methodologies employed to investigate large, dynamic multimolecular protein complexes come with some intrinsic drawbacks which the presented method aims to overcome. On the other hand, in the long run the interactome of single cells should be investigated to avoid biological noise. To this end, concepts that reduce the complexity of single-cell lysates must be found to facilitate the analysis of such samples. The presented methodology was designed for being easily down scalable in respect to volumes and concentrations while conserving its functionality, thereby accessing the realms of single-cell processing.

Traditional methods used in proteomics often rely on gel electrophoresis and mass spectrometry.[2,3] Analytes thereby typically undergo exhaustive purification procedures prior to their analysis, based on gel filtration, affinity and size exclusion chromatography, immunoprecipitation, chemical crosslinking and genetic engineering to introduce affinity tags. The state of a protein, in terms of its composition and structure, can be extremely difficult to maintain throughout a purification process. This is especially true for large, dynamic multimolecular protein complexes often composed of weakly interacting constituents. The presented isolation method uses the benefits of magnetic beads combined with photocleavable linkers for mild and very specific isolation of minute volumes of endogenous protein complexes. The approach utilizes antibodies to capture the target proteins, at the cost of being dependent on the availability of the required affinity molecule and its specificity. In return, endogenous proteins can be studied, i.e. targets are formed *in vivo* and represent a true native state, as no tag must be introduced which might affect the fidelity of a complex. The method yields samples of high purity, in particular for a one-step purification method, and allows protein binding partners constituting a complex to be labelled; both facilitates sample interpretation during subsequent TEM analysis. Exploiting the single particle detection limit of TEM, the relative occurrence and the composition of different protein subcomplexes formed around a common central protein can be investigated. The presence of heterogeneous subcomplexes indicates different cellular functions to be associated with a particular subcomplex and is thus important to understand and extremely difficult to assess with classical analysis methods available. Thus the developed protein isolation method combined with single particle TEM provides an elegant way to rapidly probe and characterize protein complexes. It can provide initial structural information of targets prior to time consuming large-scale protein purification and complex hybrid approaches for analysis.[4] Moreover, proof-of-concept experiments revealed that the amount of isolated protein is dependent on the target protein concentration in the processed cell lysate. This finding ultimately gives access to quantitative studies on protein abundances in cell lysates. At the current stage the developed methodologies for protein isolation and quantification can not compete with traditional methods used in quantitative proteomics, e.g. mass spectrometry,[3] because of the time consuming data acquisition associated with quantitative TEM. Yet, after future

refinements and developments (see below and chapter 7), it will be possible to measure the state of protein complexes from single cells and in reasonable time, thereby creating the prerequisites for quantitative and qualitative proteomics at the single cell level and entering a field typically hard to access for present biophysical and biochemical methods.

To our knowledge, this is the first time where the suitability of single particle TEM for protein quantification was demonstrated. Consequently, the fundamentals of protein quantification by single particle TEM were investigated and a method for efficient concentration measurements proposed (chapter 4). The findings implied that notably picomolar to nanomolar protein concentrations can be accurately measured using the presented techniques and protocols. In contrast, many traditional methods routinely used for protein quantification, such as absorbance-based measurements, encounter difficulties when operated with such low concentrations. The presented method relies on the reproducible adsorption and distribution of proteins to the carbon surface of TEM grids. In general, TEM grid preparation is expected not to be reproducible when prepared by hand and as a result quantitative information on a sample to be distorted. This statement is in strong contradiction to the presented results.

At the current state, the major disadvantage of the presented isolation method appears to be the intrinsically low particle concentrations on the TEM preparations produced. Although single particle analyses were successfully demonstrated, the investigation of more complex samples is expected to be extremely time consuming. The low particle concentrations are the result of the low concentrated eluates yielded by the presented method and of the inefficient grid preparation protocol employed. Possible solutions to increase the concentration of the isolated proteins are discussed in chapter 7.2.1. However, a robust methodology is desired to deposit low volume samples in an efficient and unbiased manner to TEM grids in order to process single-cell extracts or, as described above, target structures that are specifically isolated from relatively few cells for TEM analysis. Classical preparation techniques for TEM involve washing and blotting steps, thereby wasting about 99.5% (depending on the physiochemical properties of the protein and the grid preparation protocol, see chapter 4) of the proteins in the applied solution. Furthermore, the selective nature of protein adsorption to the grid surface hinders quantitative conclusions on the occurrence of constituents, e.g. in the cell lysate to be drawn. To overcome these issues, an alternative approach for sample conditioning and deposition to various sample carriers was developed and validated (chapter 5).[5] This approach uses microdialysis to, e.g. desalt or negatively stain a sample prior to its transfer to TEM grids. Rapid motorized-stages and syringe pumps ensure the dispensing and spreading of sub-microliter volumes to the sample carriers. Subsequent air-drying of deposited samples avoids selective adsorption of proteins to the support and eliminates the need for washing and blotting steps. This concept showed to be methodologically very sound and was successfully applied to purified proteins and heterogeneous samples such as batch cell lysates. Various negative stains were evaluated, all of which provided very reproducible staining of high quality and more homogenous distribution compared to grids prepared by hand. In contrast to the widely used negative stain uranyl acetate, the tested stains proofed to be tolerant to phosphate

buffers, hence allowing protein structures sensitive to buffer conditions to be processed close to physiological pH conditions. In addition staining characteristics can be finely tuned. Furthermore, initial experiments demonstrated that sample preparations for subsequent STEM analysis were competitive to those routinely prepared by hand and mass determinations can be done.

The proposed isolation method was expected to profit a lot from a technique allowing for an efficient and unbiased transfer of proteins to TEM grids. Consequently, the isolation setup was connected to the modules for sample conditioning and deposition. However, initial tests still yielded grid preparations with inherently low concentrated particles, which was attributed to the loss of the low sample amounts that occurred during the transfer and processing steps. This loss was caused by, e.g. nonspecific adsorption of proteins to the capillary walls. Although some modifications of the setup, such as the drastic reduction of transfer paths and utilizing surface passivation of capillaries could improve the yield of processed protein to some extend, a future hybrid setup is envisaged to follow a different concept. I.e. rather than the serial connection of the different modules, the fusion of the individual processing methodologies into a single module is desired.

The complexity of the interactome has to be tackled with hybrid approaches. In this respect, the motivation for the development of a novel approach to single-cell visual proteomics is to provide an alternative and complementary method to characterize the proteome and to correlate the acquired data to those of other techniques used in single-cell proteomics. While a global qualitative and quantitative visual analysis of the entire proteome still requires a lot of efforts and developments, the methodologies acquired during the course of this thesis will ensure that quantitative targeted proteomics by qTEM is soon in the realms of possibility.

6.2 Protein isolation in the context of single cells

The visual analysis of the entire proteome of a single eukaryotic cell using negative stain TEM is a challenging task. This especially applies for the identification of the individual protein species constituting the proteome. At the cost of loosing most of the cellular context, the simplest solution to facilitate protein identification is to follow a targeted proteomics approach where specific structures are isolated from the crowded cell lysate to reduce the sample's complexity.

The presented methodologies for protein isolation, sample conditioning and deposition are ready to be applied for the processing of single-cell lysates. A detailed description of a feasible hybrid setup fusing all the techniques relevant for quantitative targeted proteomics of single cells by TEM is given in chapter 7.2.2. Due to the low copy numbers of protein species present in a single eukaryotic cell and the inherent low sample volumes, the main challenge will be to minimize sample loss and protein dilution during processing, as dilution has a massive negative impact on isolation and transfer efficiencies. The design of the presented isolation methodology already accounts for these difficulties; the

usage of magnetic beads and microcapillary techniques offers the simple miniaturization of the setup in the sense of volumes and concentrations to meet the requirements for single-cell processing. However, even for the unlikely case where 100% of a target protein species are successfully isolated and homogenously distributed on a TEM grid more than 100 images must be collected on average to detect a single protein (assuming hundred thousand proteins adsorbed to the grid and imaged at a pixel size of 0.40 nm). This estimation emphasizes that new ways for efficient data acquisition and analysis must be found when dealing with targeted visual proteomics of single cells. For example, isolated proteins could be deposited on the TEM grid only at specific positions to induce a higher particle concentration. Complementary, automated image acquisition and processing will be required. Finally, new detectors[6] permitting higher frame rates compared to conventional CCD cameras used in the electron microscopy field might offer to scan the grid surface in a very efficient and rapid fashion.

6.3 References

[1] Giss, D.; Kemmerling, S.; Dandey, V.; Stahlberg, H.& Braun, T. **Exploring the Interactome: Microfluidic Isolation of Proteins and Interacting Partners for Quantitative Analysis by Electron Microscopy.** *Analytical chemistry* **86**, 4680-4687 (2014).

[2] Aebersold, R.& Mann, M. **Mass spectrometry-based proteomics.** *Nature* **422**, 198-207 (2003).

[3] Ong, S. E.& Mann, M. **Mass spectrometry-based proteomics turns quantitative.** *Nature chemical biology* **1**, 252-62 (2005).

[4] Rudashevskaya, E. L.; Sacco, R.; Kratochwill, K.; Huber, M. L.; Gstaiger, M. *et al.* **A method to resolve the composition of heterogeneous affinity-purified protein complexes assembled around a common protein by chemical cross-linking, gel electrophoresis and mass spectrometry.** *Nature protocols* **8**, 75-97 (2013).

[5] Kemmerling, S.; Ziegler, J.; Schweighauser, G.; Arnold, S. A.; Giss, D. *et al.* **Connecting mu-fluidics to electron microscopy.** *Journal of structural biology* **177**, 128-34 (2012).

[6] Li, X. M.; Mooney, P.; Zheng, S.; Booth, C. R.; Braunfeld, M. B. *et al.* **Electron counting and beam-induced motion correction enable near-atomic-resolution single-particle cryo-EM.** *Nature methods* **10**, 584-+ (2013).

7 Conclusions and outlook

7.1 Aim and scope of this thesis

The aim of this thesis was to pave the way for quantitative targeted proteomics of single cells by transmission electron microscopy (TEM). To this end, a novel microfluidic-based method for the quantitative isolation of protein complexes from minute volumes of cell lysates has been developed. In addition, the suitability of single particle TEM for protein quantification has been reported for the first time and the fundamentals of quantitative TEM established. Furthermore, a novel methodology for the preparation of high quality negative stain TEM samples from minute sample volumes of complex biological mixtures was developed. Already now these procedures are promising tools for the fast isolation and labelling of protein complexes or aggregates from cell lysates, the quantitative analysis of proteins by TEM, and for negative stain single particle TEM in general. Future developments aim to improve some aspects of the individual methods and to combine them with a recently developed module for single cell lysis,[1] ultimately enabling the qualitative and quantitative analysis of the heterogeneity of protein complexes from individual cells.

7.2 Future developments

7.2.1 Rapid isolation of protein complexes for cryo-TEM

Structural information employing negative stain TEM is very limited, i.e. to about 2 nm,[2] yet, near atomic resolution is required to fully understand the role of a complex or the working mechanism of a channel. Cryo-TEM can provide near atomic resolution of protein complexes[3] but also requires relatively high protein concentrations for optimal grid preparation. Hence, to date the developed isolation method is dedicated to negative stain single particle TEM as only low concentrated samples of purified proteins are produced. Future developments aim to increase the concentration of the eluted target structures, ultimately enabling cryo-sample preparation and thus, providing an elegant way to rapidly probe the structure of a protein complex without the need of large-scale protein purification using traditional methods. Three options are considered to increase the protein concentration: First, downscaling of the capillary diameter and the length of the magnetic bead plug will lead to a locally increased concentration of immobilized target proteins. Second, prior to photocleavage, the bead plug is encapsulated using air or oil droplets (following two-phase microfluidics) to avoid dilution during the elution process. Third, the resulting low-volume eluate is deposited on a TEM grid using a hand-over approach similar to that described in chapter 5, followed by plunge-freezing of the grid (currently under testing).

7.2.2 Towards quantitative targeted proteomics of single cells

Future developments aim to combine the developed protein isolation method with an approach for the lysis of single eukaryotic cells to reduce the complexity

of the revealed proteome and thereby facilitate the subsequent visual analysis by TEM. For this purpose, a new setup is under construction that will also accommodate long-term cell culturing and live-cell imaging for the correlation of light- and electron microscopy. The basic idea of this concept is described in the following. At first an individual cell from the culture is selected for TEM analysis, e.g. upon a stimulus that triggered a fluorescence signal. The targeted cell is then lysed using electroporation and the revealed proteome aspirated into a capillary. In a second step, a small amount of magnetic beads that are conjugated to affinity molecules via photocleavable linkers, are aspirated and incubated with the cell lysate. The total sample volume will be at the order of 15 nL. Subsequently the beads are trapped via external magnets and the non-immobilized proteins either discarded or processed for TEM analysis. After washing, the bead plug is illuminated with UV-light and the released targets are transferred to the conditioning module and subsequently dispensed on TEM grids. To avoid dilution during sample transfers, a two-phase microfluidic approach might be demanded. Because of the low copy numbers of a particular protein species from a single cell, the concentration of isolated protein on a TEM grid is expected to be inherently low. In this respect, the protein eluate should be deposited only on a defined small area of the TEM grid to induce a local progressive concentration of proteins.

7.2.3 Nanobeads

The usage of novel magnetic nanoparticles can significantly improve the presented isolation methodology, facilitate its integration for the processing of single cell lysates, or might also offer a completely new approach for quantitative targeted proteomics by TEM.

To date, the presented isolation method relies on superparamagnetic beads of 1 µm in diameter. This dimension necessitates the removal of these beads from conjugated target proteins using photocleavage since the comparatively large beads would cover proteins in TEM. Therefore, the usage of smaller magnetic particles, i.e. of 10 – 20 nm in diameter, would firstly, eliminate the need for a photocleavage step and secondly, provide an intrinsic electron dense label for the isolated target structures. Though, such small magnetic particles are difficult to manipulate using magnetic field gradients since the magnetic force acting on a magnetic bead scales with the third power of the bead radius while the drag force exerted by the fluid surrounding the bead scales simply with the bead radius. I.e. a compromise for the bead dimensions between suitability for TEM and accessibility for magnetic manipulation must be found. Novel magnetic nanobeads of down to 30 nm in diameter are made of metals and thus offer a much higher magnetization than those beads used in our studies. These nanobeads are routinely used to purify target structures from e.g. rats blood[4] or water[5] but are still too large for TEM analysis and whether a reduction of the bead diameter maintains the magnetic accessibility of beads is up to be investigated. A possible solution could be the introduction of additional micrometer-sized superparamagnetic beads, which would locally increase the magnetic field gradients. This procedure for field enhancement is similar to the integration of soft magnetic composites on microfluidic channels.[6]

Another application of magnetic nanobeads could be the very simple high-throughput isolation of target structures from single cell lysates directly on TEM grids. This approach could look as follows: First, a suspension of nanobeads conjugated to affinity molecules, e.g. antibodies, is added to a carbon coated TEM grid together with the lysate of a single cell containing the target structures. After incubation, a magnetic field gradient is applied, pulling the beads together with the targets down to the carbon film. Subsequently, washing steps are applied to remove cell lysate from the immobilized nanobeads. Finally the grid is negatively stained (or frozen) and the field gradient removed. To some extend, this isolation approach is similar to that of affinity-grids,[7,8] but might offer a much higher isolation efficiency and purity. Due to the applied field gradient every nanobead is expected to become immobilized on the carbon surface leading to much higher protein concentrations compared to those of grids prepared by hand. Furthermore, negative staining can be done directly on the grid; thus, the hand-over and the conditioning module as presented in chapter 5 are not required, resulting in a very efficient low-tech high-throughput protein isolation and labelling method for TEM.

7.3 Future applications

The protein isolation method developed during the course of this thesis is dedicated to hypothesis-driven biology. Hence, prior knowledge about a target is required to perform an experiment. Once a protein constituting a multimolecular protein complex can be targeted, the heterogeneity of such a complex can be studied. Though, protein complexes are often composed of weakly interacting proteins and the targeting of an individual protein using genetic engineering to introduce affinity tags might be very challenging and disturb the fidelity of a complex. For such complexes being difficult to handle using traditional purification methods, such as the human Mediator complex[9] or inflammasomes,[10] the proposed method can offer initial qualitative and quantitative information in short time. Upon the integration of cryo-sample preparation and improvement of resulting protein concentrations, the methodology might even rule out classical methods used for protein purification to some extend.

With the completion of the proposed setup for protein isolation from individual cells, hypothesis-driven experiments can be performed at the single cell level, e.g. the heterogeneity of a multimolecular protein complex formed around a common targeted bait protein can be studied qualitatively and quantitatively. The individuality of this diversity is eventually assessed by comparing the measurement to those of other cells that are known to be in the same or different state.

The procedure outlined above allows many biological questions to be addressed that are of great relevance for human society and extremely difficult to tackle with biophysical methods currently available. For example, the prion-like spreading of protein aggregations through the nervous system, closely linked to many neurodegenerative disorders[11] such as Alzheimer's disease

(amyloid-β and tau protein)[12] and Parkinson's disease (α-synuclein),[13] can be investigated. To date the detailed molecular mechanism of how these aggregations of misfolded proteins propagate from one cell to another remains elusive. Furthermore evidence rises that different structural forms of aggregations might lead to different phenotypical disorders, such as Lewy body disease or Parikinson's disease. To address these questions, we designed initial experiments that allow the spreading mechanism as well as the structural information of the involved aggregations to be detected and monitored at the single cell and single molecule level in a spatial and temporal fashion. In these experiments minimalistic neuronal tissues are built using fetal human mesencephalic cell line (LUHMES, lund human mesencephalic) that is differentiated to form neurite networks with dendrites and axons. Employing the proposed single-cell protein isolation setup described above, it will be possible to perform "seeding" experiments, where for example a diseased cell is placed inside the "healthy" cell culture. Live-cell imaging will allow to monitor the development and morphology of the network and to select individual cells at specific time points or upon a fluorescence trigger for the extraction of protein aggregates and subsequent structural analysis at the single molecule level using TEM.

7.4 References

[1] Kemmerling, S.; Arnold, S. A.; Bircher, B. A.; Sauter, N.; Escobedo, C. *et al.* **Single-cell lysis for visual analysis by electron microscopy.** *J Struct Biol* **183**, 467-73 (2013).

[2] Ohi, M.; Li, Y.; Cheng, Y.& Walz, T. **Negative Staining and Image Classification - Powerful Tools in Modern Electron Microscopy.** *Biological procedures online* **6**, 23-34 (2004).

[3] Liao, M. F.; Cao, E. H.; Julius, D.& Cheng, Y. F. **Structure of the TRPV1 ion channel determined by electron cryo-microscopy.** *Nature* **504**, 107-+ (2013).

[4] Herrmann, I. K.; Schlegel, A.; Graf, R.; Schumacher, C. M.; Senn, N. *et al.* **Nanomagnet-based removal of lead and digoxin from living rats.** *Nanoscale* **5**, 8718-8723 (2013).

[5] Rossier, M.; Schreier, M.; Krebs, U.; Aeschlimann, B.; Fuhrer, R. *et al.* **Scaling up magnetic filtration and extraction to the ton per hour scale using carbon coated metal nanoparticles.** *Sep Purif Technol* **96**, 68-74 (2012).

[6] Ichikawa, N.; Katsuyama, Y.; Nagasaki, Y.& Ichiki, T. **Microfluidic devices integrated with permalloy micropatterns for bead-based assay.** *Roy Soc Ch*, 384-386 (2005).

[7] Kelly, D. F.; Dukovski, D.& Walz, T. **Monolayer purification: A rapid method for isolating protein complexes for single-particle electron microscopy.** *P Natl Acad Sci USA* **105**, 4703-4708 (2008).

[8] Yu, G. M.; Vago, F.; Zhang, D. S.; Snyder, J. E.; Yan, R. *et al.* **Single-step antibody-based affinity cryo-electron microscopy for imaging and structural analysis of macromolecular assemblies.** *J Struct Biol* **187**, 1-9 (2014).

[9] Taatjes, D. J. **The human Mediator complex: a versatile, genome-wide regulator of transcription.** *Trends in biochemical sciences* **35**, 315-22 (2010).

[10] Broz, P.& Monack, D. M. **Molecular mechanisms of inflammasome activation during microbial infections.** *Immunol Rev* **243**, 174-190 (2011).

[11] Goedert, M.; Clavaguera, F.& Tolnay, M. **The propagation of prion-like protein inclusions in neurodegenerative diseases.** *Trends in neurosciences* **33**, 317-25 (2010).

[12] Clavaguera, F.; Lavenir, I.; Falcon, B.; Frank, S.; Goedert, M. *et al.* **"Prion-like" templated misfolding in tauopathies.** *Brain pathology* **23**, 342-9 (2013).

[13] Masuda-Suzukake, M.; Nonaka, T.; Hosokawa, M.; Oikawa, T.; Arai, T. *et al.* **Prion-like spreading of pathological alpha-synuclein in brain.** *Brain : a journal of neurology* **136**, 1128-38 (2013).

8 Scientific output

Peer-reviewed publications:

- **D. Giss**, S. Kemmerling, V. Dandey, H. Stahlberg & T. Braun (2014). Exploring the interactome: microfluidic isolation of proteins and interacting partners for quantitative electron microscopy. *Anal Chem*, 86(10), 4680-7.
- S. Kemmerling, J. Ziegler, G. Schweighauser, S. A. Arnold, **D. Giss**, S. A. Mueller, P. Ringler, K. N. Goldie, N. Goedecke,, A. Hierlemann, H. Stahlberg, A. Engel & T. Braun (2012). Connecting µ-fluidics to electron microscopy. *J Struct Biol*, 177, 128-134.

Conference proceedings:

- **D. Giss**, S. Kemmerling, V. Dandey, H. Stahlberg & T. Braun (2013). Microfluidics to isolate untagged proteins from cell extracts for visual analysis by electron microscopy. *Proceedings of the 17th International Conference on Miniaturized Systems for Chemistry and Life Sciences (MicroTAS)*, Freiburg, Germany, pp. 1785-1787, ISBN 978-0-9798064-6-9.

To be submitted:

- **D. Giss**, H. Stahlberg & T. Braun (2014). Protein quantification by single particle transmission electron microscopy. *To be submitted to the Journal of Structural Biology*.

Oral and poster presentations:

- International Biophysics Congress (IUPAB) 2014, Brisbane (AUS).
- 7th European Summit for Clinical Nanomedicine and Targeted Medicine (CLINAM) 2014, Basel (CH).
- Swiss NanoConvention 2014, Brugg (CH).
- The 17th International Conference on Miniaturized Systems for Chemistry and Life Sciences (MicroTAS) 2013, Freiburg (DE).
- Swiss NanoConvention 2013, Basel (CH).
- 10th NCCR Structural Biology Symposium 2012, Zuerich (CH).
- SystemsX PhD Student Retreat 2011, Kandersteg (CH).

9 Acknowledgment

The work presented in this thesis would not have been possible without the support of many colleagues.

First of all, I want to thank Prof. Henning Stahlberg for giving me the opportunity to do this PhD program in his laboratory and for his advice and support during my thesis.

Further I would like to thank Prof. Roderick Lim for being my co-referee and Prof. Andreas Hierlemann for his participation in my PhD advisory committee.

I would like to express my deep appreciation to Dr. Thomas Braun for being an excellent supervisor, guiding and supporting me throughout this thesis, his patience and being always available for fruitful discussions and inputs.

Very importantly I would like to thank all the past and current colleagues working on the single-cell visual proteomics project: Simon, Stefan, Benjamin, Andrej, Gabriel, Jan, Nora and Christoph.

Special thanks go to Dr. Shirely Mueller for her help with manuscript writing and sharing her knowledge and expertise.

I would also like to acknowledge Sebastian Scherer and Benjamin Bircher for adjuvant inputs and discussions. Further thanks go to Philippe Ringler, Alexandra Graf, Mohamed Chami and Ken Goldie for sharing their expertise on electron microscopy and sample preparation. I am grateful to Bill Anderson and Venkat Dandey for their support with T12.

Finally I am deeply grateful to all my colleagues at C-CINA for providing an excellent, friendly and relaxed working atmosphere, for all the good times we have had together, for exciting lunch breaks and funny Thursday evenings.